Proceedings Book

Humboldt Kolleg

« Advancements in Nanotechnology and Microelectronics (ANM'09) »

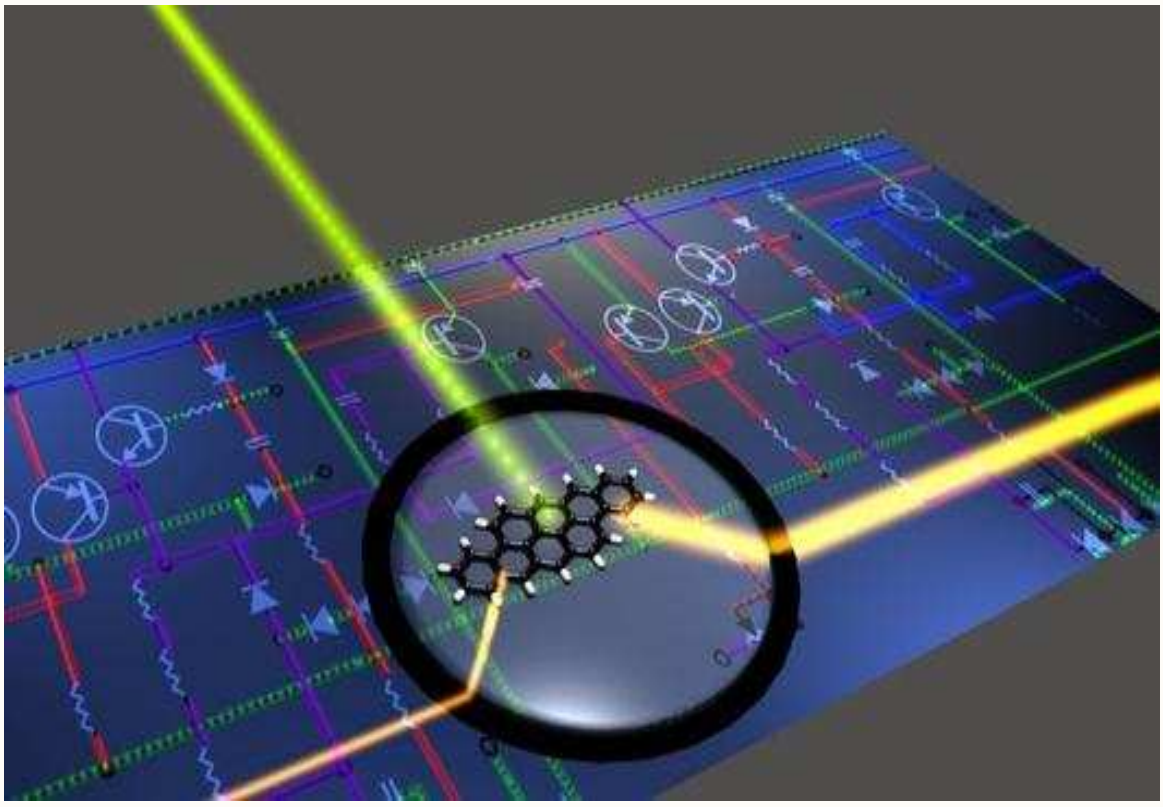

Edited by

Prof. Dr. Michael J. Schöning ***Prof. Dr. Adnane Abdelghani***

Tunisia, November, 13&14, 2009

Welcome Address

Dear Colleagues,

Welcome to the first Humboldt Kolleg in “Advancements in Nanotechnology and Microelectronics” (ANM’09) in Tunisia, sponsored by the "Alexander von Humboldt" foundation. The ANM’09 multi-disciplinary scientific program includes "hot" topics in the fields of "Nanotechnology and Microelectronics" ranging from "Bio/Micro/Nano Materials and Interfacing" aspects, "Chemical and Bio-Sensors", "Magnetic and Superconducting Devices", "MEMS and Microfluidics" over "Theoretical Aspects, Methods and Modelling" up to the important bridging "Academics meet Industry".

We are really most indebted to all members of the Scientific Committee and Gereral Chairs for Joint Sessions and to all speakers and chairmen, who have dedicated invaluable time and efforts for the realisation of this event.

On behalf of the Organizing Committee, we are cordially inviting you to join the conference and hope that your stay will be rewarding and enjoyable.

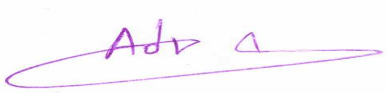

Prof. Dr. Michael J. Schöning
Institute of Nano- and Biotechnologies,
Aachen University of Applied Sciences

Prof. Dr. Adnane Abdelghani
National Institute of Applied Science and Technology

Gammarth, November 13th, 2009

Preface

Nanotechnology implies the creation of functional materials, devices and systems through control of matter on the nanometer length scale (1-100 nanometers) as well as the exploitation of novel phenomena and properties (physical, chemical, biological, mechanical, electrical, etc.) at this length scale. Nanotechnology has emerged as one of the most exciting research areas in the last decade as researchers have improved the abilities to image biomolecules, and to model, control and manipulate matter and devices at small dimensions.

On the other hand, microelectronics is related to the study and manufacturing of electronic components which have to be very small (usually, in the lower micrometer-scale) and reliable. Microelectronics is almost a generic term and subsumes areas as diverse as communication, information technology, data processing, process control, nano-electronics and photonics, but also interfaces sensorics and nanotechnology. Because of its immense economic impact and commercial potential, almost all the developing countries are gradually aspiring to adopt nanotechnology and microelectronics R&D strategies. But at the same time, they are also desperately in need of quickly comprehending the full implications of the level of nanotechnology and microelectronics presently required by them within the nation and forecasted for the years ahead in terms of its capabilities, limitations, viability, economics and infrastructural requirements by undertaking a pragmatic analysis in totality. The main concepts and aims of the first “Humboldt Kolleg” in Tunisia are, therefore:

-To strengthen the network between junior researchers and the “Alexander von Humboldt (AvH)” program.

-To encourage junior researchers and young scientists to apply for post-doc positions within the AvH foundation.

-To amplify the knowledge about the advancements in both (bio-)nanotechnology and microelectronics in developing countries.

-To disclose the high interdisciplinarity between physicists, chemists, (micro-)biologists and engineers for modern research aspects.

-To show the impact of nanotechnology and microelectronics for industrial requests (start-up and spin-off).

General Chairs

L. Schultz, IFW-Dresden, GER
S. Ben Ahmed-INSAT, TN
E. Sackmann-LMU, GER
K. Karrai-LMU, GER

Program Chairs

A. Abdelghani-INSAT, TN
M. J. Schöning-INB, GER

Scientific Committee

E. Sackmann-LMU, GER
K. Karrai-LMU, GER
M. J. Schöning-INB,GER
L. Schultz, IFW-Dresden, GER
A. Abdelghani-INSAT, TN
Nico F.De Rooij-Samlab, CH
N. Jaffrezic-Renault-UCBL, FR
H. Said-IPEST, TN
M. Boussaid-INSAT, TN
A. Selmi- FSM, TN
L.Vonna-ICSI, FR
C. Heywang-CPMOH, FR
H. Ben Ghoslen-FSS, TN
M. Ellouze-FSS, TN
K. El-Araby, Egypt
M. S-Rahal, Algeria
H. Ben Hamida-STM, TN
W. Touayar-INSAT, TN
W. A.Badawy, Egypt
S. Ben Saoud-INSAT, TN
M. A. Maaref-INSAT, TN
F. Ben.Ammar-INSAT, TN
S. Lakhdar-LMU, GER
T. Ktari-INSAT, TN
S. Helali-IPEST, TN
M. Marrakchi-ISBAT, TN
J. Ghommam-INSAT, TN

Local Organizing Committee

A. Abdelghani-INSAT, TN
A. Selmi- FSM, TN
H. Ben Ghoslen-FSS, TN
M. Ellouze-FSS, TN
S. Chatti, INRAP, TN
I. Trabelsi, CERT, TN

Main Topics

The topics of the conference will include, but will not be limited to, the following topics:

- Nanodevices and Nanomaterials: Issues and challenges
- Microsensors and Microsystems
- Photonic Gap Material and their Applications
- Biosensors and Bioelectronics
- New conducting polymers for Microelectronics devices
- Physic of Biomembranes , carbon nanotubes and DNA BioChips
- New technology of Quantum Optics
- Renewal Energy and Photovoltaic cells
- Micro-and Nanoparticles for drug delivery
- Scanning Near Field Optical Microscopy Techniques (AFM, STM, SNOM)
- Nanometrology
- Modeling & analysis and Embedded systems
- Design & test of integrated circuits
- Nanotechnology in robotics
- Biomaterials and Biophotonics

Table of Contents

Keynote Speakers

Orals Communications

OC 7: Dr. A.-F. Lehlooh
Low temperature Mössbauer spectroscopy study of macromolecular complexes of polycarbosilazane coordinated of mixed valence Fe(II-III) chlorides

OC 8: Dr. H. M. El Ghanem
AC and DC electrical conductivity measurements of polyaniline-doped with copper(1)X salts, {Cu(1)X (X= Cl, Br,I_2)} as a potential gas sensor

OC 9: Dipl.-Ing. P. Kirchner'
Investigation of a thin-film calorimetric gas sensor for H_2O_2 detection in industrial processes

OC 10: Dr. S. Chatti
Novel biomaterials based on sugar diols: syntheses, characterization and application

OC 11: Dr. I. Trabelsi
Wastewater treatment by using nanofiltration: case study of a Tunisian touristic resort

OC 12: Dr. J. Ghommam
Passivity-based synchronization of complex dynamical networks

OC 13: Dr. M. C. Zaghdoudi
Use of mini heat pipes including axially capillary microgrooves for electronics cooling

OC 14: Dr. N. Fourati
Chemical and biological detection investigations using shear horizontal surface acoustic wave sensor

OC 15: Dr. I. Hafaiedh
Functionalized gold nanoparticles for impedimetric immunosensors

OC 16: Prof. A. Selmi
Giant magnetoresistance: fundamentals and applications

OC 17: Dr. H. Mahjoub
Dynamic wave scattering and rheological investigations on a temperature-sensitive hydrocolloidal system of silice-particles

OC 18: Dr. F. Lakrad
Effect of a high-frequency actuation on the pull-in instability in MEMS

OC 19: Prof. M. Sekkal-Rahal
Conformational study of sulphated carrabiose molecule by DFT methods

OC 20: Dr. M. Ellouze
Structure and magnetic properties of fine particle $La_{0.7}Ca_{0.3}MnO_3$ prepared by mechanic synthesis method

OC 21: Dr. S. Ameur
Metal deposition on conductive and semi-conductive modified surfaces

Posters Communications

P1: M. Ezzdini, S. Rekaya, R. Hamila, F. Saidi, L. Sfaxi, and H. Maaraf, Plasma-assisted MBE growth of Ga (As, N) materials: growth conditions and optical properties

P2: S. Mnasri, S. Abdi-Ben Nasrallah, N. Sfina, and M. Said, Magnetic properties in $Cd_{1-x}Mn_xTe$ diluted magnetic semiconductor quantum wells

P3: A. Cherif, and A. Kanoun,Up-conversion fluorescence dynamics in Er^{3+}/Yb^{3+} co-doped tellurite glasses

P4: S. Bellon, M. Anger-Leroy, R. Daniel, W. Buchmann, F. Gonnet, N. Jarroux, and. Ch. Frydman, Hyphenation of surface plasmon resonance imaging to matrix-assisted laser desorption ionization mass spectrometry by on-chip MALDI-MS analysis

P5: W. Ouerghui, J. Martinez-Pastor, J. Gomis, M. A. Maaref, D. Granados, and J. M Garcia, Carrier tunneling in quantum rings

P6: A. Triki, M. Guicha, M. Ben Hassen, and Z. Fakhfakh, Dielectric studies of natural fibre reinforced composites for automotive applications

P7: S. Ben Afia, M. Triki, S. Jaziri, and H. Belmabrouk, Band offset calculations of diluted magnetic heterostructure ZnMnSe/ZnSSe

P8: F. Saadallah, S. Abroug, and N. Yacoubi, Photothermal measurements of non-radiative lifetime of doped GaSb

P9: H. Khmissi, L. Sfaxi, L. Bouzaïene, F. Saidi, and H. Maaref, Effect of carriers transfer behaviour on the optical properties of InAs quantum dots embedded in AlGaAs/GaAs heterojunction

P10: H. Ben Fredj, S. Helali, Z .Sassi, N. Jaffrezic-Renault, L. Vonna, and A. Abdelghani, Conductor polymers for biosensor applications

P11: A. H. Hamzaoui, K. Farah, F. Hosni, A. Mejri, and H. Ben Ouada, Formation of silver nanoparticles in ion-exchanged silicate glass by thermal annealing

P12: K. Daoudi, M. Oueslati, A. Selmi, and T. Tsuchiya, Excimer-laser assisted metal-organic deposition of manganite thin films for bolometric applications

P13: A. Abdellatif, H. Rahmouni, M. Baazaoui, S. Zemni, and K. Khirouni, Study of electrical properties of $La_{0.67}Ba0_{.33}Mn_{1-x}Fe_xO_3$ pervoskites

P14: K. Farah, A. H. Hamzaoui, F. Hosni, A. Mejri, and H. Ben Ouada, Effect of gamma irradiation and thermal annealing on the nanocluster formation in silver ion-exchanged silicate glass

P15: A. Labidi, A. Bejaoui, C. Lambert-Mauria, K. Aguir, and M. Maaref, Electrical investigation of WO_3 thin layers for ethanol and acetone vapors detection

P16: A. Ltaief, N. Chehata, and A. Bouazizi, Organic nanocomposites for photovoltaic applications

P17: M. B. Mejri, M. Marrakchi, H. Baccar, S. Helali, M. Aouni, M. Hamdi, N. Jaffrezic-Renault, and A. Abdelghani, Electrochemical impedance spectroscopy for specific detection of *Enterovirus*

P18: M. Ghrib, T. Ghrib, N. Yacoubi, A. W. Kolsi, and H. Ezzawia, Study of aluminum alloys in nanocrystalline grain syntethises by mechanical milling high energy and consolidated the room temperature and high pressure

P19: N. Sellami, A. Melliti, A. Sahli, M. A. Maaref, C. Testelin, and R.Kuszelewiez, The effect of the excitation density and of the temperature on the photoluminescence circular polarization of AlInAs/AlGaAs quantum dots

P20: N. Mecirdi, Z. Benamara, and B. Akkal, Electrical characterization of InN/InP heterojunction with quantum effect

P21: A. Direm, H. Boussekine, and N. Benali-Cherif, Phase determination with direct methods

P22: H. Boussekine, A. Direm, and N. Benali-Cherif, 2-méthylanilinium nitrate

P23: M. Driss, A. Kerbouche, and N. Oumrani, Study of the behavior of mortars based of cements composed toward the attacks of acids waters

P24: M. Haddoug, G. Gaaliche, and W. Boujarra, Physical design kit pre-layout and post-layout validation

P25: S. Dhahri, L. Kabbai, A. Zitouni, K. Torki, and R. Tourki, A low power ASIC design of a FSS motion estimator for H.264AVC

P26: T. Soltani, A. Gharbi, J. P. Marcerou, and H. T. Nguyen, Microscopic observations and dielectric behavior showing a demixing phenomenon in chiral tilted smectics liquid crystals

P27: S. Dabbous, T. Ben Nasrallah, A. Amlouk, K. Boubaker, M. Amlouk, and S. Belgacem, A new 3D abacus as a tool for phothovoltaic-thermal (PV-T) binary and ternary semiconductors scaling

P28: T. Ghrib, M.S. Ben Kraîem, N.Yacoubi, A. Cheikhrouhou, and C. Bordel, Study of the ferromagnetic transition of a nanoscale samples by the PTD technique

P29: Y. Benmimoun, S. Flazi, A.Tilmatine, and O. Rabah, Study and realization of an electric process to fight against harmful insects « KAHRATRAP »

P30: Y. Bergaoui, J. M. Fougnion, C. Zerrouki, N. Fourati, and A. Abdelghani, Shear horizontal surface acoustic wave sensors for specific and non specific streptavidin-anti streptavidin recognition

P31: R. Hadef, Two-dimensional imaging of nanoscale particles sizes

P32: S. Helali, H. Baccar, and A. Abdelghani, Electrochemical study of horseradish peroxidase biosensor based on functionalised magnetic beads and polypyrrole film

P33: Z. Zaâboub, B. Ilahi, L. Sfaxi, H. Maaref, B. Salem, V. Aimez, and D. Morris, Tuning InAs/GaAs quantum dot's emission wavelength by ion implantation and subsequent annealing

P34: I. Saïdi, K. Sellami, and K. Boujdaria, Calculation of exciton energy levels in III-V self-assembled quantum dots

P35: H. Rahmouni, R. Jemai, N. Kallel, A. Selmi, and K. Khirouni, Electrical study of Ti doped $La_{0.7}Sr_{0.3}MnO_3$

P36: N. Issaoui, N. Rekik, B. Oujia, and M. J. Wójcik, Infrared lineshapes of hydrogen bonds within the linear response theory

P37: H. Rahmouni, R. Jemai, N. Kallel, A. Selmi, and K. Khirouni, Electrical study of 30% Cr doped $La_{0.7}Sr_{0.3}MnO_3$ material by impedance spectroscopy

P38: B. Azeza, L. Sfaxi, R. Mghaieth, and H. Maaref, Growth of GaAlAs multilayers on porous Si by molecular beam epitaxy for the photovoltaic applications

P39: M. H. Hadj Alouane, B. Ilahi, H. Maaref, B. Salem, V. Aimez, D. Morris, A. Turala, P. Regreny, and M. Gendry, Effect of phosphorus ion implantation-induced intermixing on the optical properties of self-assembled InAs/InP quantum sticks

P40: J. Chermiti, F. Aouni, M. Ben Ali, and N. Jaffrezic-Renault, Numerical modelling of micro-sensors electrical behavior for biomedical and environmental applications

P41: N. Mehnane, F. Badi, M. Reda Aced, H. Abid, and N. Sekkal, The electronic properties of Ga(As,N) ternary and superlattice (SL) systems

P42: R. Bchir, A. Bardaoui, M. Machhout, R. Chtourou, and H. Ezzaouia, Design and optimization of a 1.55 µm waveguide based on Silicon planar photonic crystals

P43: K. Issa, M. Hjiri, B. Azeza, R M'ghaieth, and H.Maaref, Stimulated emission in silicon's nonacristals

P44: O. Touayar, Z. Ben Achour, and N. E. Sifi, Investigation of the electrical properties, stability and metrological characteristics of ZnO/PS/c-Si photodiode (SiPZ) used as a transfer standard in the visible spectral range

P45: S. Helali, A. Abdelghani, N. Jaffrezic-Renault, P. N. Trikalitis, C. E. Efstathiou, and M. I. Prodromidis, On-site monitoring of fish spoilage using vanadium pentoxide xerogel modified interdigitated gold electrodes

P46: Y. Salah, and R. Tourki, Real-time scheduling for networks-on-chip using TDM virtual circuit and RTOS policies

P47: A. Oudir, M. Mahdouani, R. Bourguiga, F. Pardo, and J. L. Pelouard, Influence of the heterojunction bipolar transistor's geometry on its microwave behaviour

Program

Friday, November 13, 2009

08.00-09.00: Registration

09.00-09.20: Opening Session

Prof. S. Ben Ahmed, The Director of the INSAT, Tunisia
Prof. A. Abdelghani (Humboltianer), INSAT, Tunisia

09.25-09. 35: Welcome Address on behalf of the President of the Alexander von Humboldt Foundation, held by Prof. Ludwig Schultz

09.35-09.40 : Alexander Von Humboldt : Network for the future

Session 1: "Bio/Micro/Nano Materials and Interfacing"

Chairman: Prof. Michael J. Schöning

-Understanding cell adhesion by application of smart supported membranes, Prof. Erich Sackmann, LMU, Germany (**Keynote**)
-Biophotonics solutions to explore the bio-nano world, Dr. Chiraz Frydman, HORIBA Scientific, France (**Keynote**)

10.30-11.00: Group Photo / Coffee Break

Chairman: **Dr. Fafa Ben Hatira**

-Iminium activation in organocatalysis: a look inside the "black-box", Dr. Sami Lakhdar (Humboltianer), LMU, Munich
-Porous silicon layers as a promising new technology in solar energy: conversion and optoelectronics, Prof. Waheed A. Badawy, (Humboltianer), Egypt
-Novel biomaterials based on sugar diols: syntheses, characterization and application, Dr. Saber Chatti (Humboltianer), INRAP, Tunisia

-Dynamic wave scattering and rheological investigations on silicon nanoparticles, Dr. Hasna Mahjoub, INSAT, Tunisia

-Metal deposition on conductive and semi-conductive modified surfaces, Dr. Sami Ameur, IPEST, Tunisia

12.30-13.15: Poster session

13.15-15.00: Lunch

Session 2: "Chemical and Bio-Sensors"

Chairman: Dr. S. Lakhdar (Humboltianer)

-Semiconductor-based field-effect devices: selected examples for chemical and biological sensing, Prof. Michael J. Schöning, Aachen University of Applied Sciences, Germany (**Keynote**)

-Liberation of nanoencapsulated proteins and their proteolysis monitored by a conductometric biosensor, Prof. Nicole Jaffrezic-Renault, LSA-Lyon1, France (**Keynote**)

16.00-16.30: Coffee break / Poster Session

Chairman: Dr. Majda-Rahal Sekkal (Humboltianer)

-Functionalized gold nanoparticules immobilization for impedimetric immunosensors application, Dr. Imene Hafaiedh, IPEST/UCB-Lyon1, Tunisia

-Artificial membranes of functionalized hemicyanines used for selective cation detection, Dr. C. Heywang (Humboltianer), Bordeaux, France

-Chemical and biological detection investigations using shear horizontal surface acoustic wave sensor, Dr. Najla Fourati, CNAM, Paris, France

-Investigation of a thin-film calorimetric gas sensor for H_2O_2 detection in industrial processes, Patrick Kirchner, Aachen University of Applied Sciences, Germany

-AC and DC electrical conductivity measurements of polyaniline-doped with copper(1)X salts, {Cu(^{1})X (X= Cl, Br,I_2)} as a potential gas sensor, Dr. H. M. El Ghanem, Jordan University of Science and Technology, Jordan

Saturday, November 14, 2009

09.30-10.30:

Session 3: "Magnetic and Superconducting Devices"

Chairman: Dr. C. Heywang (Humboltianer)

-Riding on magnetic fields - the miraculous world of superconductor-, Prof. Ludwig Schultz, IFW-Dresden, Germany (**Keynote**)

-Giant magnetoresistance: fundamentals and applications, Prof. Abderrahman Selmi (Humboltianer), FSM, Tunisia

-Structure and magnetic properties of fine particle La0.7Ca0.3MnO3 prepared by mechanic synthesis method, Dr. M.Ellouze (Humboltianer), FSS, Tunisia

10.30-11.00: Coffee break / Poster Session

Session 4: "MEMS and Microfluidics"

Chairman: Prof. Abderrahman Selmi (Humboltianer)

-Use of mini heat pipes including axially capillary microgrooves for electronics cooling, Dr. Chaker Zaghdoudi, INSAT, Tunisia

-Growth and stability of water microstructures on patterned substrates: aspect ratio vs surface chemistry – toward microfluidic applications, Dr. Laurent Vonna (Humboltianer), ICS- Mulhouse, France

-Effect of a high-frequency actuation on the pull-in instability in MEMS, Dr. Faouzi Lakrad, University Hassan II-Casablanca, Morocco

12.15-13.00: Poster Session
13.00-15.00: Lunch

Session 5: "Theoretical Aspects, Methods and Modelling"

Chairman: Prof. Khaled Karrai (Humboltianer)

-Passivity-based synchronization of complex dynamical networks, Jawher Ghommam, INSAT, Tunisia
-MPSoC performance modeling using SDFG: SW to HW task migration, Dr. Imed Bennour, FSS, Tunisia
-Advancement on the biomechanical modeling of the spine, Dr. F. Ben Hatira, INSAT, Tunisia
-Conformational study of sulphated carrabiose molecule by DFT methods, Prof. M. Sekkal-Rahal (Humboltianer), Sidi-Bel-Abbes, Algeria
-Low temperature Mössbauer spectroscopy study of macromolecular complexes of polycarbosilazane coordinated of mixed valence Fe(II-III) chlorides, Dr. A.-F. Lehlooh (Humboltianer), Yarmouk University, Jordan

16.20-16.45: Coffee Break / Poster Session

Session 6: "Academics meet Industry"

Chairman: Dr. **Ismail Trabelsi** (Humboltianer)

-Instrumentation to explore the nano-world: a path from the university to the industry, Prof. K. Karrai (Humboltianer), Attocube Systems AG, Germany (**Keynote**)
-Wastewater treatment by using nanofiltration: case study of a Tunisian touristic resort, Dr. Ismail Trabelsi (Humboltianer), CERTE, Tunisia
-Different ways to strengthen scientific cooperation between Germany and the Maghreb, Prof. Abdelhadi Soudi (Humboltianer), President of the "Alexander Von Humboldt North African Alumi Association"

17.45-18.15: **Selection of "Best poster presentations"**

18.30: Closing Session

Keynote Speakers

Keynote 1- Understanding cell adhesion by application of smart supported membranes

Erich Sackmann
Physics Department E22. Technical University of Munich, Germany
sackmann@ph.tum.de

Abstract:
The study of cell adhesion shows, in an impressive way, how cells use the laws of physics to explore their environment and adjust their material properties to fulfil their multiple biological functions. At the same time it shows that it is possible to understand the function of complex living material on the basis of the physics of soft materials.

In order to achieve this goal it is necessary to establish more and more realistic model systems and to study the physical properties of such models, wild-type cells and mutants in parallel. A further benefit of such studies could be the discovery of new strategies to design technical materials with novel properties.

In recent years, substantial progress has been made by theoretical modelling, and the development of mimetics of cell and tissue surfaces on electro-optical devices by application of the concept of designing composite membranes on polymer cushion by self assembly. This studies show that cell adhesion is controlled by lock-and-key forces mediated by cell surface receptors, a phalanx of (short and long range) non-specific (generic) interactions and, last but not least, membrane elasticity.

Further progress was based on the application of reflection interference contrats microscopy and dynamic image analysis allowing to study cell substrate contact with lateral resolution of 1 nm and height resolution of 5 nm. Magnetic tweezer method allows measurements of adhesion forces and force induced control of then adhesion dynamics.

References:

[1] Bausch, A. R., W. Moller and E. Sackmann (1999)."Measurement of local viscoelasticity and forces in living cells by magnetic tweezers." Biophysical Journal **76**(1): 573-579.

[2] Bausch, A. R., F. Ziemann, A. A. Boulbitch, K. Jacobson and E. Sackmann (1998).
"Local measurements of viscoelastic parameters of adherent cell surfaces by magnetic bead microrheometry."Biophysical Journal **75**(4): 2038-2049.

Keynote 2- Riding on magnetic fields - the miraculous world of superconductors

Ludwig Schultz [1,2,3]

[1] Leibniz Institute for Solid State and Materials Research Dresden, IFW Dresden, GERMANY
l.schultz@ifw-dresden.de
[2] TU Dresden, Institute of Materials Science, GERMANY
[3] evico GmbH Dresden, GERMANY

Introduction: At present different concepts for magnetic levitation are discussed. The conventional system is the Transrapid, which is now regularly running between Shanghai Airport and Shanghai Centre. Our approach is a passive superconducting magnetically levitated system, which uses bulk superconductors cooled only to liquid nitrogen temperature. At low temperatures, superconductors do not only carry the electrical current without any resistance, but are also able to freeze in a magnetic field of any configuration. By this, they act as permanent magnets, but with a magnetic remanence, which is, for example for massive YBaCuO material, by far larger than that of ferromagnetic permanent magnets. The ability to freeze in a magnetic field can be used for completely new applications. In the presentation, this will be demonstrated for different types of superconducting magnetically levitated trains, which can either be in an upright position, in a hanging position, see figure 1, or moving along a wall without any mechanical contact. With regard to scaling-up, the SupraTrans project will be presented.

Figure 1: Superconducting model railway on a magnetic track

Superconductors: Superconductors are characterized by an abrupt loss of electrical resistivity and by specific magnetic properties below a critical temperature T_c. In comparison with the low temperature superconductors as they were known until 1986, the high-temperature superconductors (HTS) discovered thereafter require much less cooling since the critical temperature of the HTSC is above the temperature of liquid nitrogen (-196°C). It is a specific feature of solid superconducting materials that they can pin the magnetic flux to a great extent, see figure 2. This pinning effect is a result of the fact that an applied superconducting current loops which are generated during cooling the material below its superconducting transformation temperature.

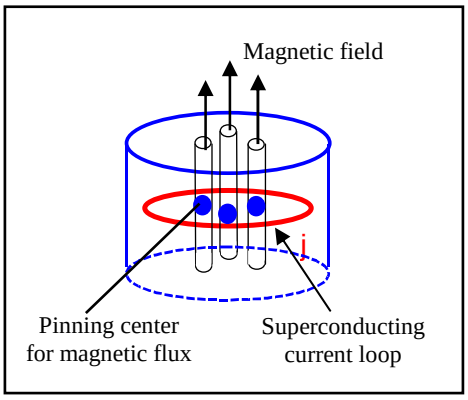

Figure 2: “Pinning effect”

SupraTrans project: The SUPRATRANS technology uses the flux pinning in melt textured massive YBCO to stabilize the lateral and vertical position of the vehicle on top of the magnetic track. This self-stabilization is the main advantage of the superconductive levitation in comparison to the already used Transrapid –technology, which needs an electronic control system to keep a constant distance between the train and the track

References:

[1]L. Schultz, O. de Haas, P. Verges, C. Beyer, S. Roehlig, H. Olsen, L. Kuehn, D. Berger, U. Noteboom, U. Funk, Superconductively levitated transport system - The SupraTrans project, IEEE Trans. Applied Superconductivity 15 (2005) 2301-2305.
[2]S. Gruss, G. Fuchs, G. Krabbes, P. Verges, G. Stoever, K.-H. Mueller, J. Fink, L. Schultz, Superconducting bulk magnets: Very high trapped fields and cracking, Appl. Phys. Lett. 79 (2001) 3131-3133.
[3]L. Schultz, G. Krabbes, G. Fuchs, W. Pfeiffer, K.-H. Mueller, Superconducting permanent magnets and their application in magnetic levitation, Z. Metallkunde 93 (2002) 1057-1064

Keynote 3- Instrumentation to explore the nano-world: a path from the university to the industry

K. Karrai
Attocube Systems AG, Munich, Germany.

Abstract:
Knowledge resulting from fundamental research topics is often decades ahead of potential applications. The long time separating typically early results stemming from basic research and industry involvement is often a source of disconnection between the two worlds. In several situations however it is very suitable and even possible to involve an industrial activity at a very early stage of research should the scientist awareness be raised and addressed in time. Here a per sonal case study is presented, describing how "attocube systems AG", originally a university spin-off company active in instrumentation for nanotechnologies, bridges the gap between the two worlds. The personal point of view is presented by a university researcher with a recent and active exposure to the world of industry.

Keynote 4- Semiconductor-based field-effect devices – towards nano-structured surfaces

Michael J. Schöning[1,2]
[1] Aachen University of Applied Sciences, Jülich Campus, Institute of Nano- and Biotechnologies (INB), Ginsterweg 1, 52428 Jülich, GERMANY, m.j.schoening@fz-juelich.de
[2] Research Centre Jülich GmbH, Institute of Bio- and Nanosystems (IBN-2), 52425 Jülich, GERMANY

Introduction: Silicon-based field-effect devices are being on of the basic structural elements in a new generation of chemical and biological micro- and nanosensors. The reason therefore is that they provide several advantages such as small size and weight, fast response time, possibility of an on-chip integration to realize sensor arrays, high robustness, low fabrication costs, etc. Their fields of application reach from medicine and process control over biotechnology, environmental monitoring, food and drug industries up to defence and security requirements.

Among the multitude of concepts discussed in literature, bioelectronic devices with the possibility of a direct electronic readout of the biologically induced signal on the chip as well as functional hybrid nano-biosystems based on nanostructured surfaces or interfaces are two new promising strategies. Here, both the sensitivity and selectivity of the biological systems connected to semiconductor circuitries might be increased. This paper is focusing on recent developments at the INB creating "nanostructured" surfaces for a new class of functional hybrid nano-biosystems.

Experimental results: 1) Nanocrystalline (NCD) diamond has been recognized as a promising transducer material for bio-/chemical sensing due to its outstanding electrochemical properties, superior chemical inertness and biocompatibility. Capacitive EDIS (electrolyte-diamond-insulator-semiconductor) field-effect structures with O-terminated NCD films are discussed for multi-parameter detection (pH, penicillin) as well as for the label-free electrical monitoring of adsorption and binding of charged macromolecules (e.g., polyelectrolyte multilayers).

2) Recently, functionalized gold nanoparticles (NP) have been used to enhance the electrochemical and photometric sensor features. Key experiments exemplified the use of Au-NP-functionalized hybrid nano-biosystems for ion-sensing with bare as well as enzyme-modified Au-NP. The amplification of the biosensor signal will be discussed. Alternatively, the assembly of carbon nanotubes (CN) into nanostructured thin films deposited by the layer-by-layer technique offers the possibility of incorporating single-walled CN together with polyamino-amide (PAMAM) dendrimers for bio-/chemical sensing. Those field-effect devices display enhanced biosensor performance.

3)Coupling of bio-computing systems with electronic chips is highly promising because of the complexity of biological materials and their unique properties such as selectivity of biocatalyzed reactions and specificity of biorecognition processes. Logic gates defined by enzyme-catalyzed reactions can serve as starting point for complex biocomputing networks. Using Si field-effect structures, enzyme-based "OR—Rest" and "And—Reset" logic gates have been realized and activated by different combinations of bio-/chemical input signals. The corresponding output signals result in pH changes due to the particular enzymatic reaction.

Acknowledgements: The author thanks M.H. Abouzar, M. Bäcker, J. Gun, K. Haenen, E. Katz, M. Krämer, O. Lev, A. Poghossian, J.R. Siqueira Jr., P. Wagner for discussion and technical support, the "MIWFT des Landes NRW", the "BMBF", the "Alexander von Humboldt Stiftung", and the "DAAD-CAPES" foundation for financial support.

References:

[1]Poghossian, A. and Schöning, M.J. (2006), Silicon-based chemical and biological field-effect sensors, in *Encyclopedia of Sensors*, American Scientific Publishers, Stevenson Ranch, Vol. 9, pp. 463-534.

[2]Poghossian, A. and Schöning, M.J. (2007), Chemical and biological field-effect sensors for liquids – a status report, in *Handbook of Biosensors and Biochips*, John Wiley & Sons, Ch. 24, pp. 1-17.

[3]Poghossian, A., Ingebrandt, S., Offenhäusser, A. and Schöning, M.J. (2009) Feld-effect devices for detecting cellular signals *Seminars in Cell & Development Biology*, 20, 41-48.

[4]Schöning, M.J. and Poghossian, A. (2002) Recent advances in biologically sensitive field-effect transistors (BioFETs), *Analyst*, 127, 1137-1151.

Schöning, M.J. (2005) „Playing around" with field-effect sensors on the basis of EIS structures, LAPS and ISFETs, *Sensors*, 5, 126-138.

[5]Schöning, M.J. and Poghossian, A. (2008), Detection of charged macromolecules by means of field-effect devices (FEDs): possibilities and limitations, in Electrochemical Sensors, Biosensors and Their Biomedical Applications, Elsevier, Ch. 7, pp. 187-212.

Keynote 5- Identification of biomolecules captured by surface plasmon resonance using MALDI mass spectrometry

S. Bellon[2,1], W. Buchmann[3], F. Gonnet[3] and R. Daniel[3], C. Frydman[1,2]

[1] HORIBA Scientific, France
Chiraz.frydman@horiba.com
[2] GENOPTICS Bio Interactions, France
[2] Université d'Evry-Val-d'Essonne, Laboratoire Analyse et Modélisation pour la Biologie et l'Environnement, France

Introduction: SPRi (Surface Plamson Resonance imaging) allows thermodynamic analysis of biomolecular interactions, and may be advantageously used for ligand-fishing of captured biomolecules on immobilized receptors. Mass spectrometry is a powerful tool for structural characterization and identification. Therefore, the combination of SPR and MS into one concerted procedure is of a great interest for functional and structural analysis within the fields of proteomics, drug-discovery, diagnostic, and bio-security

Method: For that purpose, we have used a SPR-sensor surface biochip in a micro-array format. The biochip gold surface was functionalized by a self-assembled monolayer of polyethylene oxide carrying a NHS group reacting with primary amines. This functionalization allowed to immobilize the bio-molecular receptors in an active state and to avoid nonspecific adsorption. The validation of the system was performed by measuring antigens-antibodies interactions by SPR, and by MALDI detection of the retained antigens directly from the biochip. MALDI matrix was directly dropped on the biochip and mass spectra were obtained from distinct spots. Using this biochip, the transfer in the MS apparatus consecutive to a SPR experiment was simple. In addition, it required no intermediate treatment that could lead to sample loss and/or contaminations.

Resulat: Two types of antibodies were arrayed by coupling to NHS functionalized biochip gold surface (SPRi-slide^{TM}): Anti-β-lactoglobulin and Anti-ovalbumin. The SPR experiments were performed using an ammonium acetate running buffer (MS compatible). Lysine solution was first injected to react with the free remaining active NHS groups of nonarrayed surface. The biochip was then ready for specific analyte capture. A mixture of proteins (β-lactoglobulin and ovalbumin) diluted in the running buffer was injected and analyte capture was followed in real time.

After SPR experiments, the biochip was removed and inserted directly in an appropriate MALDI-MS plate holder. Finally MALDI matrix was dropped specifically on each spot.

The representative mass spectra obtained from the protein-bound antibody array showed multiply charged protein ions corresponding to the specific antigen, without any trace of non-specific binding. The quantity of proteins retained specifically as determined from SPR measurement was enough to obtain good quality mass spectra. Mass spectra were also acquired from underivatized portion of the chip, allowing the control of the absence of non-specific binding of proteins.

The SPRi/MALDI-MS combination on an array platform is a powerful tool for affinity separation and subsequent identification of compounds from complex solutions. The biochip developed in this work, namely the SPRi-slide^{TM}, was easily transferable from SPR apparatus to the MALDI-MS plate, and direct MS analysis was directly carried out on micro-array biochip. High-throughput multiplexed analysis with spatial resolution is permitted with this array platform.

Innovative aspect: Ligand fishing by SPR and subsequent MALDI-MS identification of the retained ligands have been carried out from the same surface..

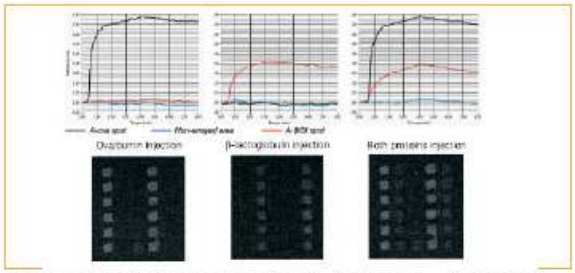

Figure 1: Antibody / protein interaction (— A-ova spot, — A-βλGl spot, — Non-arrayed area)

References:

[1]Bellon, S. and Buchmann , W. (2009) Hyphenation of Surface Plasmon Resonance Imaging to Matrix-Assisted Laser Desorption Ionization Mass Spectrometry by On-Chip Mass Spectrometry and Tandem Mass Spectrometry Analysis Anal. Chem Received for review May 25, 2009. Accepted July 29,2009.

Keynote 6- Liberation of nanoencapsulated proteins and their proteolysis monitored by a conductometric biosensor

M. HNAIEN[1], E. RUFFIN[2], F. LAGARDE[1], C. BORDES[1], S. BRIANÇON[2], N. JAFFREZIC RENAULT[1*]

[1] Université de Lyon, F-69622, Lyon, France; Université Lyon 1, Villeurbanne; LSA, UMR 5180, CNRS, CPE, 43 bd du 11 novembre, 69100 Villeurbanne, France

[2] Université de Lyon, F-69622, Lyon, France; Université Lyon 1, Villeurbanne; LAGEP, UMR 5007, CNRS, CPE, 43 bd du 11 novembre, 69100 Villeurbanne, France

* nicole.jaffrezic@univ-lyon1.fr

Introduction: In this work, BSA was used as a model protein in microencapsulation process by multiple emulsion-solvent extraction/evaporation method. The polymer used to encapsulate BSA was poly (ε-caprolactone) (PCL). This polymer was selected for its biodegradable character, its in-vitro stability and its low degradation rate. Moreover, PCL degradation does not generate an acid environment unlike poly (lactic-acid) (PLA) and poly (glycolic-acid) (PGA) polymers by hydrolysis of ester bonds **(**Sinha, 2004**)**. The enzymatic biosensor based on proteinase K (Hnaien, 2009) was used to monitor the BSA release kinetics and to evaluate the conformation of protein encapsulated .

Results and Discussion:

BSA release kinetics from PCL microspheres was followed by Bradford analysis (Figure 1). PCL microspheres displayed a classical two-stage release profile characterized by a very high initial release ("burst effect" or 38% released after 4 hours) followed by a plateau (Quaglia, 2005)**.** At the end of experiment (72 hours), the percentage of protein released was about 83%.

The BSA release kinetics from PCL microspheres was also determined using the conductometric biosensor (Figure 1). After 24 hours, a stable conductivity was observed, confirming the results obtained by the Bradford method. Nevertheless, Figure 2 shows that the ratio conductivity/BSA concentration strongly varied with time. In the first 5 hours, a very high conductivity/concentration ratio was observed and it sharply decreased from 13 to 7.5 $\mu S.mg^{-1}.L$. The mean value of this ratio 10.2 $\mu S.mg^{-1}.L$ indicates that the protein was mainly non native during the five first hours of release and it corresponds to proteins remained at the surface of microparticles where it underwent a denaturation. In the second part, the conductivity/concentration ratio decreased and stabilized at about 5.5 $\mu S.mg^{-1}.L$ after 24 hours. This value corresponds to a mixture of solvent-denaturated BSA and of native BSA protected by the microparticles.

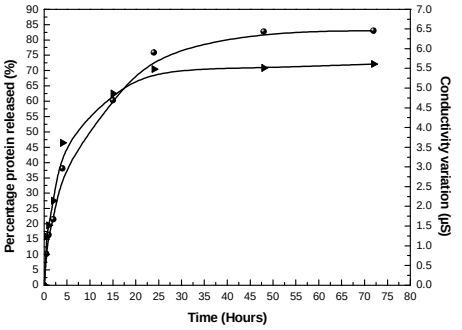

Figure 1: BSA release kinetics from microsphere determined by Bradford method (—●—) and conductometric biosensor (—▶—).

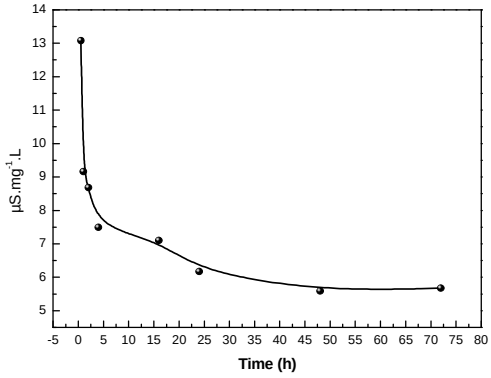

Figure 2: Ratio conductivity/protein concentration as a function of release time.

References:

[1] Hnaien M., Hassen W. M., Abdelghani A., Cotte S., Leonard D., Bessueille F., Jaffrezic-Renault N., Electrochemistry Communications 11, 165 (2009)

[2]Quaglia F., Ostacolo L., Nese G., De Rosa G., Immacolata La Rotonda M., Palumbo R., Maglio G., Macromol. Biosci. 5, 945 (2005).

[3] Sinha V. R., Bansal K., Kaushik R., Kumria R., Trehan A., International Journal of Pharmaceutics 278, 1 (2004).

Orals Communications

OC1- Artificial membranes of functionnalized hemicyanines used for selective cation detection

C. Grauby-Heywang[1], P. Batat[1], N. McClenaghan[2] and G. Jonusauskas[1]

[1]Centre de Physique Moléculaire Optique et Hertzienne, UMR CNRS 5798,
Université Bordeaux 1, Bordeaux, FRANCE
ch.heywang@cpmoh.u-bordeaux1.fr
[2] Institut des Sciences Moléculaires, Université Bordeaux 1, Bordeaux, FRANCE

Introduction: Hemicyanines (Figure 1) are fluorescent compounds, which can be functionalized with various chemical groups, such as crowns able to coordinate cations, and hydrophobic chains essential to organize them into Langmuir monolayers and Langmuir-Blodgett (LB) films. These artificial membranes have been the subject of numerous investigations (Abraham et a., 2008; Niidome et al., 2000; Rajesh et al. 2007). In this work, our goal is to elaborate such membranes in order to develop systems for selective cation detection. Their potential applications cover various domains, such as biology or environment. Barium and calcium cations have been chosen because of their diameter as compared to the size of the crown: calcium fits perfectly with the size of the crown, whereas barium is too voluminous to fit into.

Content: Both cations (concentrations in the 0-10 mM range) induce a spectacular change of the π-A isotherm of the hemicyanine dye, as compared to the one obtained with pure water (Figure 1), suggesting different types of organization. In the case of Ba^{2+}, a strong plateau appears. Ba^{2+} being too large to fit into the crown, it could be coordinated by two neighboring dye molecules. The plateau would be due to the regular organization of these "sandwich"-like aggregates induced by compression. The presence of Ca^{2+} provokes a clear shift of the isotherm to lower mean molecular areas, but we do not observe any plateau. These results show that Ca^{2+} is also able to interact with the hemicyanine, likely by coordinating into the crown, because of its lower diameter.

Monolayers have been transferred onto planar support at a surface pressure of 25-30 $mN.m^{-1}$. In the case of LB films transferred from pure water, two main absorption bands are observed around 475 nm ("visible" band) and 270 nm, corresponding to the $S_0 \rightarrow S_1$ and $S_0 \rightarrow S_n$ transitions of the dye, respectively. The presence of a blue-shifted shoulder on the side of the "visible" band reveals also the presence of H-aggregates. The presence of cations, even at low concentration, prevents partially aggregation. Fluorescence emission spectra of LB films show the presence of a band in the near infrared due to dye

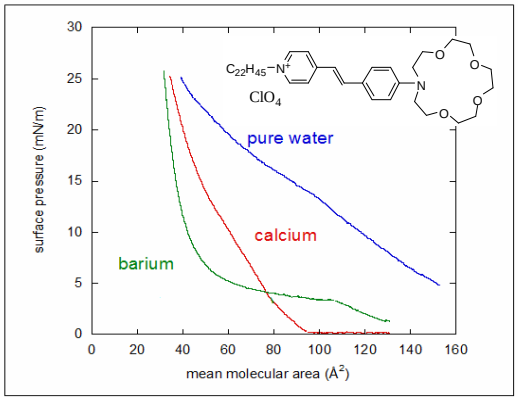

monomers and a strongly red-shifted one, which could be

Figure 2: chemical structure and π-A isotherms of the hemicyanine studied in this work.

due to hemicyanine-cation complexes. Fluorescence microscopy performed on LB films confirm the presence of red, large and homogenous areas. At last, time-resolved fluorescence experiments using a streak camera and picosecond excitation show a multicomponent relaxation of our samples, suggesting the presence of different species in LB films.

Conclusion: The different behavior of our samples in the presence of Ba^{2+} or Ca^{2+} is encouraging, our goal being to detect selectively their presence.

References:

[1] Abraham, E., Grauby-Heywang, C., Selector, S. and Jonusauskas, G. (2008) Characterization of hemicyanine LB films by picosecond time resolved fluorescence. *J. Photochem. Phobiol. B*, 93, 44-52.
Niidome, Y., Ayukawa, H. and Yamada, S. (2000) Effects of aliphatic tails on monolayer structures of hemicyanine dyes at the air-water interface as studied by in situ SHG measurements and surface pressure-area isotherms. *J. Photochem. Phobiol. A*, 132, 75-80.
[2] Rajesh, K., Sharath Chandra, M., Hirakawa, S., Kawamata, J. and Radhakrishnan, T.P. (2007) Polyelectrolyte templating-strategy fort he fabrication of multilayer hemicyanine LB films showing enhanced and stable second harmonic generation. *Langmuir* 23, 8560-8568.

OC2- Growth and stability of water microstructures on patterned substrates: aspect ratio vs surface chemistry – toward microfluidic applications

L. Vonna and H. Haidara

Institut de Science des Matériaux de Mulhouse, 15 rue Jean Starcky BP2488, 68057 Mulhouse Cedex, France
laurent.vonna@uha.fr

In industrial applications the control of the length and stability of liquid microstructures are required in many fields such as inkjet printing, microfluidics… Various strategies have been proposed in order to produce surfaces with chemical and topographical patterns leading to well-defined fluid morphologies (microcontact printing, photolithograpy…). For all of these systems, the prescribed surface properties emerge from the fine tuning of the aspect ratio of both the topography and chemical surface pattern, as well as the relative surface tension of the system (liquid vs substrate).

The aim of this study is to define the critical length scales for the stability of water microstructures condensing on a micropatterned substrate. Non-wetting microdomains of varying size (4µm to 128µm) and surface density were imprinted on surfaces of different wettability in order to adjust the chemical contrast between the wetting and non-wetting domains. We were able to correlate the length and stability of the water channels with the size of the non-wetting domain and the chemical contrast (Figure 1). For the most wettable substrate, a continuum of stable water film was formed over large scales whatever the size of the microdomains (Figure 1c). It was possible in a second step to connect this continuum with droplets acting as reservoir for nanoparticles for example. Droplets of ethanol/water mixtures were used to generate Marangoni flows and transport the nanoparticules into the continuum. This approach points a possible set-up for microfluidic applications.

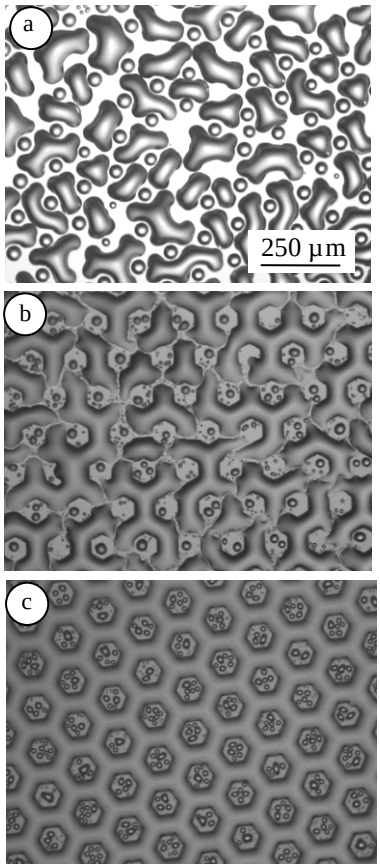

Figure 1: Water channels formed over substrates of increasing wetting contrast (from a to c). Diameter of the non-wetting domains is 64µm.

OC3- Iminium catalysis from physical organic chemist's point of View

Sami Lakhdar, Herbert Mayr

Department Chemie und Biochemie der LMU München Butenandtstr. 5-13, 81377 München, Germany
Sami.lakhdar@cup.uni-muenchen.de

Extensive studies of the reactions of carbocations and Michael acceptors with *n*-, σ- and π-nucleophiles have been shown that the rates of theses reactions can be described by eq. 1,[1] where electrophiles are characterized by the solvent-dependent nucleophilicity parameter *N* and the slope-parameter *s*.[2]

$$\log k_{20°C} = s(N+E) \qquad (1)$$

This type of reaction is involved in many organocatalytic reaction cycles, e. g., the iminium catalyzed reactions (Scheme 1).

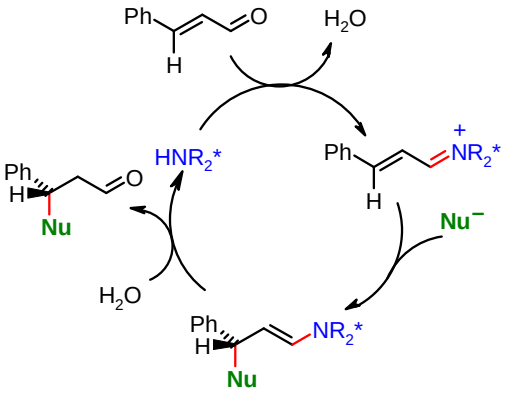

Scheme 1. Mechanism of Iminium Ion Catalyzed Additions of Nucleophiles

By studying the kinetics of several iminium ions with some reference nucleophiles, we have determined the *E* parameters of the iminium ions (Scheme 2). In this communication, we will show how these data can be employed for analyzing scope and selectivities of iminium.[3]

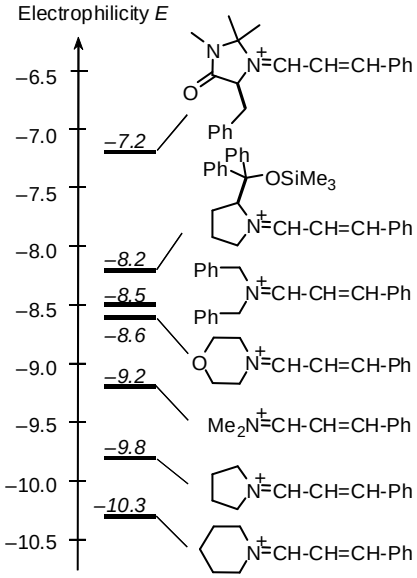

Scheme 2. Comparison of the Electrophilicities of Iminium Ions.

[1] a) H. Mayr, M. Patz, Angew. Chem. Int. Ed. Engl. **1994**, 33, 938–957. b) H. Mayr, T. Bug, M. F. Gotta, N. Hering, B. Irrgang, B. Janker, B. Kempf, R. Loos, A. R. Ofial, G. Remennikov, H. Schimmel, J. Am. Chem. Soc. **2001**, 123, 9500–9512. c) H. Mayr, B. Kempf, A. R. Ofial. Acc. Chem. Res. **2003**, 36, 66–77. d) H. Mayr, A. R. Ofial, Pure Appl. Chem. **2005**, 77, 1807–1821.
[2] a) S. Lakhdar, M. Westermaier, F. Terrier, R. Goumont, T. Boubaker, A.R. Ofial, H. Mayr. J. Org. Chem. **2006**, 71, 9088; b) S. Lakhdar , R. Goumont, F. Terrier, T. Boubaker, J.M. Dust and E. Buncel. Org. Biomol. Chem**., 2007**, 5, 1744; c) S. Lakhdar , R. Goumont, T. Boubaker, S. Kurbatov, F. Terrier. Chem. Eur. J. **2007**, 13, 8317.
[3] a) S. Lakhdar, T. Tokuyasu, H. Mayr. Angew. Chem. Int. Ed. **2008**, 47, 8723-8726; b) S. Lakhdar, R. Appel, H. Mayr. Angew. Chem. Int. Ed, **2009**, 48, 5034-503

OC4- Biomechanical analysis of a lumbar spinal unit based on a 3D finite element method

Fafa Ben-Hatira, PhD.[1,2], ,Zahira Nakhli[1], Kaouthar Saidane, PhD, [3], Abdelfatah Mrabet,M.D,Pr. [2]

[1] National Institut of Applied Sciences and Technologies, Tunisia.
[2] Tunisian group of spine and spinal cord Study and Research, Tunisia
[3] Group of Research in Sciences and Biomedical Technologies (GRSTB), Polytechnic School of Montreal, Canada.

Goals: The motivation of this numerical work is to present a 3D finite element model to reproduce the behavior of the biomaterial of a spinal human lumbar unit (bones,ligaments,..).

Methodology: A numerical three dimensionnal biomechanical model is presented to describe the mechanical beahavior of a complete functionnal human spinal unit. In deed, the biomaterial are described as system with mechanical properties related to with local properties. In particular, the bone is a composite tissue and its structural makes difficult the comprehension of the interactions between cellular elements, and mechanical properties.

In particular, the t	bf-res	utf8

The study of the behavior of human bones should take into account its cellular dimension and adopt a nanometric approch to give a right behavior law. In order to reach this goal, a preliminary work is done in the numerical model presented in this communication in order to establish the geometry of the different components of the lumbar unit with the appropriate mechanical properties. The originality of this work remains in using the finite element method to reproduce the behavior of a lumbar unit represented by five lumbar vertebreas, four intervertebral discs, the physiologic ligaments, medullar cone and the cauda equina. The entire structure of the components of a lumbar unit has been represented in this finite element model. A study on the behavior of the different biomaterial related to this lumbar unit will be presented to light out the problems of rupture of bones. Also, stresses in the discs and the bones under pure and complex loads have been investigated

Main results: The stresses on the vertebras and intervertebral discs, and the spinal cord are reported for simple compression, and a combined flexion with a preload of 500N. Critical values for these combined loads are given in this work.

Interpretation: The results show the details of the stresses undergone by the different component of the lumbar unit.

Keywords: Biomaterials, 3D finite element model, biomechanics of the human lumbar unit.

Some Results for Exctension

σmises for the disc &the bone

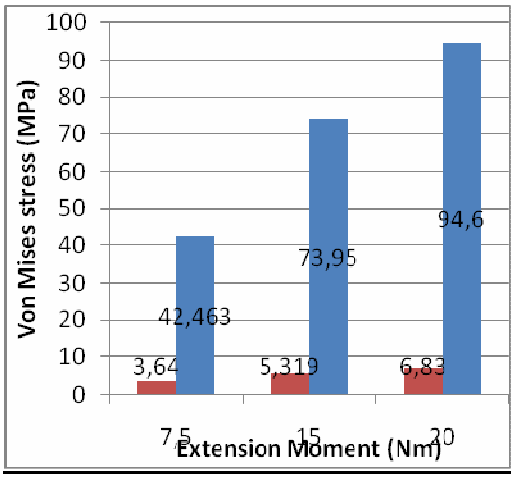

Equiv stress mises (Mpa)	*Shear Stress (Mpa) in the xy*

Results for the spinal cord

	plan
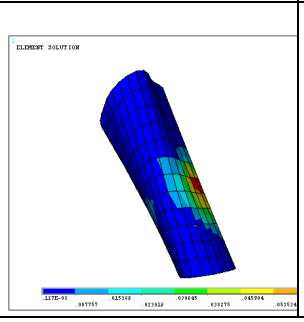	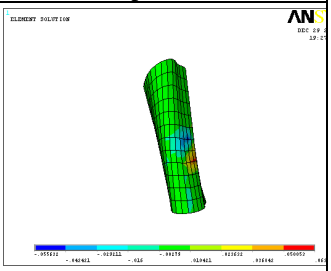

References:

1.BIOMECHANICAL PROPERTIES OF THE HUMAN SPINAL CORD AND PIA MATER, Edward L. Mazuchowski (1), Lawrence E. Thibault (2),(1) Department of Pathology,Wilford Hall Medical Center,Lackland AFB, Texas,(2) Biomechanics, Inc.,Philadelphia, PA, 2003 Summer Bioengineering Conference, June 25-29, Sonesta Beach Resort in Key Biscayne, Florida

2.Process of Lumbar Spinal Degeneration: Interrelationships Between DiscDegeneration and Facet Joint OsteoarthritisYuichi Kasai, Kenji Takegami, Koichiro Morishita, and Atsumasa Uchida *Mie University Faculty of Medicine, Tsu, Mie, Japan.*

3-Pression intra-discale L4-L5 in vivo au cours d'un traitement manipulatif, Horst MOLL*, Hans-Peter BISCHOFF*, Hans-Joachim WILKE**, Lutz CLAES**, Peter NEEF**, *Isny et **.Ulm, Allemagne, Revue de Médecine Vertébrale, 2005:17:12-

OC5- Porous silicon layers a promising new technology in solar energy conversion and optoelectronics

W. A. Badawy
Chemistry Department, Faculty of Science, Cairo University
12 613 Giza- Egypt
e-mail: wbadawy@cu. edu. eg
wbadawy50@hotmail.com

Abstract

Porous silicon layers on silicon represent a promising solar energy absorber that leads to large area solar cells and high solar conversion efficiency. An example of the improvement of the solar conversion efficiency can be seen from the results obtained by n-Si/oxide solar cells presented in the following Table:

Photovoltaic parameters of n-Si/oxide and n-Si/PSL/oxide solar cells under simulated solar spectrum (AM1) at 298K:

Photo voltic cell	J_{ph} mAcm^{-2}	V_{oc} mV	FF	η %
n-Si/SnO_2/M	29	550	0.57	9.1
n-Si/PSL/SnO_2/M	31	580	0.67	12.1
n-Si/TiO_2/M	29	590	0.61	1 0.4
n-Si/PSL/ TiO_2/ M	32	670	0.71	14.9
n-S//PSL//TiO_2-Ru(1%)/M	680	0.78	16.6	

The application of these layers in optoelectronics and their effective optical properties has found great interest. Fig. 1 presents the photoluminescence spectra measured by confocal microscope for p-Si samples after: Pt electroless deposition (A), Pt deposition and etching in 22 M HF/0.1 M $K_2Cr_2O_7$ (B) and Pt deposition and etching in 22 M HF/0.1 M $KBrO_3$.

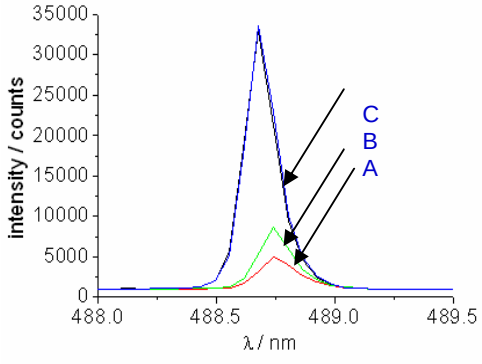

In this work porous silicon layers of definite pore structure have been prepared by stain etching of p-Si in aqueous hydrofluoric acid solutions containing different oxidizing agents. Nitric acid and potassium permanganate as oxidizing agents have shown promising effect. The electrical and electrochemical properties of the stain-etched films have been examined. The effect of etching time, oxidizing agent concentration and HF concentration on the main characteristics of the porous silicon layers was investigated and discussed. In this respect conventional electrochemical techniques and electrochemical impedance spectroscopy, EIS, have been used. The experimental data were fitted to theoretical data according to a proposed electronic equivalent circuit model. The morphology of the formed porous layers and their contaminations were investigated by the scanning electron microscopy, SEM, and energy dispersive x-ray, EDX, techniques. A scanning electron micrograph of the formed porous layer is presented in the following figure.

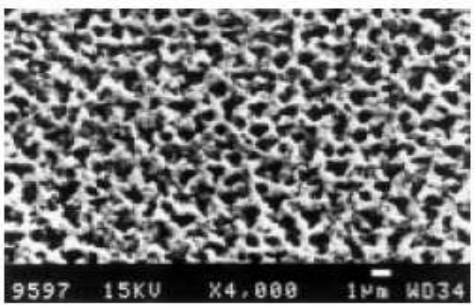

Fig. 2: SEM image of porous silicon when p-Si was etched in HF/HNO_3 solutions

The results have shown that porous silicon layers, PSL, with micro and nano pores were formed on p-Si when etched in HF/HNO_3 solutions. In $KMnO_4$ containing solutions a passive layer of K_2SiF_6 was formed inside the pores. The thickness of the passive layer was affected by the concentrations of both HF and $KMnO_4$. It reduces the effectiveness of the PSL in both the solar conversion process and also its electrical and optical characteristics.

OC6- MPSoC performance modeling using SDFG: SW to HW task migration

D. SEBAI[1], I. BENNOUR[2], A. JEMAI[1]
[1] LIP2 Laboratory, Faculty of Science at Tunis, Tunisia
[2] Faculty of Sciences at Monastir, Tunisia
imed.bennour@fss.rnu.tn

One of the major challenges that face MPSoC development is to estimate the performance of the final implementation early in the design process. This can help in making important design decisions before investing too much time in detailed implementations. Typically, the performance estimation is an important part of the Design Space Exploration (DSE), where different choices are investigated in order to determine the appropriate design trade-offs between the different conflicting objectives. Different choices of the underlying system architecture, the hardware/software mapping, and the chosen scheduling schemes will need to be evaluated. One of the DSE candidate solutions that designers may need to estimate is the migration of a SW task to a HW one. Indeed, designers must consider the consequences of the migration in precocious steps of the MPSoC design to estimate its gain compared to the pure SW solution.

This paper focus on the estimation of the gained performance when a given software task is moved to hardware. The main aim is to realize predictable performance on the system throughput before and after SW to HW migration. Throughput is a prominent and important constraint especially for embedded multimedia systems. We opt for a static estimation approach using the SDFG model to derive system throughput with analytical techniques. We use the SDFG to model the application, its mapping on a target platform, and the migration. Our work is based on the predictable design flow established by Sander Stuijk in 2007 at Eindhoven University of Technology.

The predictable design flow consists of thirteen steps which are divided over four phases: memory dimensioning, constraint refinement, tile binding and scheduling and NoC routing and schedulingm. The flow has been implemented as a tool named SDF^3. Every phase of the design flow takes a SDFG as entrance and produces a modified SDFG as output. The design decisions taken by each phase of the flow are modeled by adding new actors and edges to the initial SDFG of the application. The starting point of the flow is the SDFG of the application given by the designer. The modified SDFGs generated by different phases of the flow are successively the memory-aware SDFG, the resource-aware SDFG and the binding-aware SDFG.

This work starts by analysing the various impact of moving a task from SW to HW. The first migration impact that seems obvious is the remarkable decrease in the execution time of the hardware task compared to the software one. The second impact is on the workload of the rest of sw tasks remaining on the tile. If three tasks are executed on the same processor with a TDMA (time division multiple access) period of 100 time units. After migrating of one task the whole TDMA wheel size of the processor while be available for two tasks. The third impact is on the communication schemes that will be used to transfer data between the migrated task and the rest of tasks. The fourth inpact is that the moving of a SW task to HW may generate an extra load on communication network that badly affect the migration gain. The amont of the extra load depends on the initial mapping of the migrated task before the migration as well as the mapping of its communicating tasks and the sense of the communication: SW/HW, HW/SW and HW/HW. Figure 1 shows one of theses case where a SW/SW communication in a same tile is transformed to SW/HW.

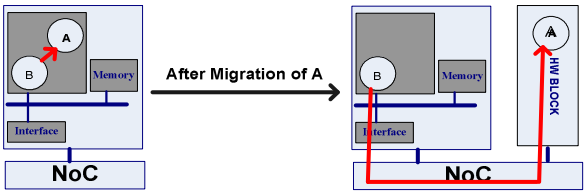

Figure 1. SH1 communication with A and B in the same tile before migration

We showed in this paper how each of these impacts can be modeled with SDFG in order to comput a lower bound on the system throughput. The proposed approach have been validaded on the MJPEG decoder as a case study.

References

[1]Sander Stuijk, 2007, Predictable Mapping of Streaming Applications on Multiprocessors", *thesis, Eindhoven University of Technology*.

OC7- Low temperature Mössbauer spectroscopy study of macromolecular complexes of polycarbosilazane coordinated of mixed valence Fe(II-III) chlorides

H. El-Ghanem[1], **A-F. Lehlooh[2]**, S. Mahmood[2]. , I. Arafa[3], A. Al-Rawas[4], A. Gismelseed[4]

[1] Department of Physics, Jordan University of Science and Technology, Irbid, JORDAN
[2]Department of Physics, Yarmouk University, Irbid 211-63, JORDAN
aflehlooh@yu.edu.jo
[3] Department of Chemistry, Jordan University of Science and Technology, Irbid, JORDAN
[4] Department of Physics, Sultan Qaboos University, Muscat, OMAN

Recently, an interest have been shown on polymers containing magnetic sites due to their advantages over classical magnetic materials, as it can be prepared with tunable magnetic properties [Lehlooh *et. al*. 2007]. A series of iron-polyethylenediaminecarbosilazane (PEDCSZ-Fe) chloride macromolecular complexes were prepared by the reaction of mixed valence Fe(II-III) chlorides with polyethylenediaminecarbosilazane matrix in toluene under inert atmosphere. The mixed valence macromolecular complexes composed of eight different ratios of (1:9, 2:8, 7:3, 4:6, 6:4, 7:3, 8:2 and 9:1). The preparation method of this system can be found in Lehlooh *et. al.* (2007) and the references within.

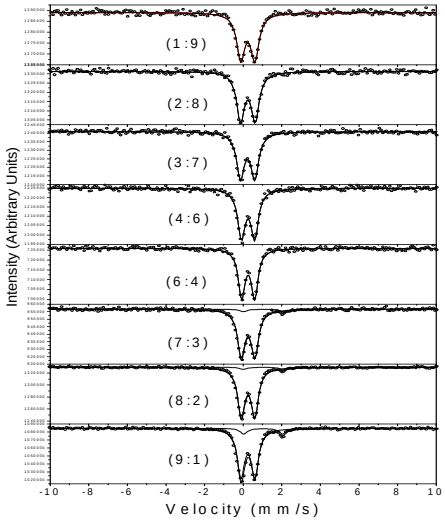

Figure 1: Room Temp. (RT) Mössbauer spectra.

The RT Mössbauer spectra of the PEDCSZ-Fe with mixed valences (Figure 1) show pure paramagnetic phases.This indicates that the samples have blocking temperature lower than RT, hence, the samples have a fine powder form. The paramagnetic phase has a quadrupole doublet with quadrupole splitting (QS_1~ 0.7 mm/s) in addition to a second quadrupole doublet with (QS_2 ~2.1 mm/s) which appears in those with (7:3, 8:2 and 9:1) ratios. The second quadrupole doublet is a characteristic of high spin Fe(II) phase. Its relative intensity is in disproportion with the ratios of Fe(II) in the samples. This indicates that part of Fe(II) has passed through a spin up transition. The spectra recorded at LN for some samples are shown in Figure 2. The spectra with low ratios (1:9 and 2:8) have paramagnetic behavior indicating that the samples have blocking temperatures smaller than LN, hence, having ultra fine particle sizes. The samples with higher ratios have broad magnetic splitting in addition the paramagnetic phase. The relative intensity of the magnetic component increases on behalf of the paramagnetic phase as the relative ratio of Fe(II) increases. The magnetic phase could be attributed to an iron oxide phase (Ferrihidrite) in ultra fine powder form as the Mössbauer parameters of the fittings revealed.

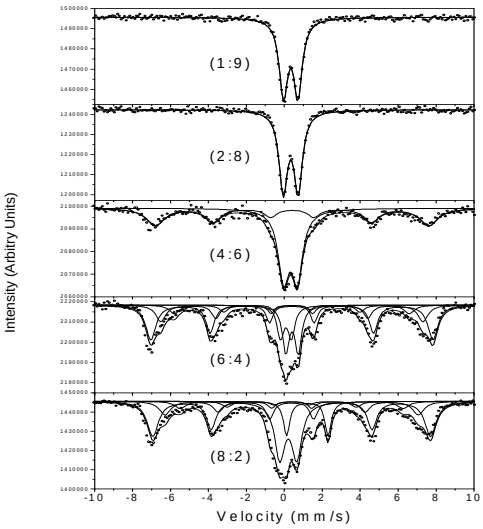

Figure 2: Liquid Nitrogen (LN) Mössbauer spectra.

References: Lehlooh A-F., El-Ghanem H., Arafa I. and Mahmood S. (2007) Mössbauer Spectroscopy Study of Macromolecular Complexes of Polycarbosilazane Coordinated with Fe(II), Fe(III) and Mixed Valence Fe(II-III) Chlorides, International Journal of Polymeric Materials, 56, 187-195.

.

OC8- AC and DC electrical conductivity measurements of poly-aniline-doped with copper(1)X salts, {Cu(1)X (X= Cl, Br,I_2)} as a potential gas sensor

H.M.El Ghanem[1], I.M. Arafa[2], M R Omari[1]

[1] Physics Department,, Jordan university of Science and Technology.
Irbid- Jordan, e-mail: hmel@just.edu.jo
[2] Applied chemistry department,, Jordan University of Science and Technology.
Irbid- Jordan.

Abstract:

Three sample sets of polyaniline-doped with copper (1) salts (Cl , Br and I_2) were prepared with different I_2 concentration. The bulk conductivity of all samples has been estimated from the I-V curves at room temperature before and after exposure to carbon monoxide (CO). It is found that the conductivity increased over 3-4 orders of magnitudes after exposure to CO. Furthermore, aging studies indicate that CO is physically attached to the polymer. The AC measurement includes; Impedance Z, phase angle θ, the real and the imaginary parts of the impedance, C_{exp} and tangent loss. The Cole-Cole plots of the real and imaginary components of the impedance for the three sets as shown in figure (1), indicate the large change in the bulk resistance (the diameter of the semi circle) before and after exposure to carbon monoxide.

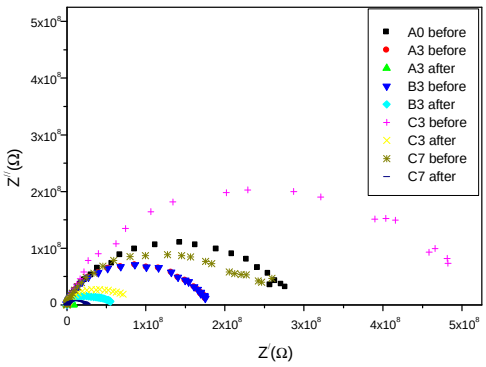

Figure 1. Cole-Cole plot of all samples before and after exposure to CO gas.

Maximum increase in the conductivity is recorded for sample C3 (2% I_2 concentration) as seen in table (1). This encourages us to claim that these samples may give cheep and sensitive sensors for CO dangerous gas.

The measured activation energies for all samples confirm that the source of electric conduction is electronic in nature. The dielectric response function confirms the appearance of well defined relaxation peaks, emphasizing the fact that cu-I_2 –CO complexes behave electrically as an RC network. The XRD and DSC measurements on these samples before and after exposure confirm the tendency of forming clusters of these complexes between the PANI chains.

Table 1: conductivity, bulk resistance and relaxation time to sample (C3, C7) before and after exposure to Carbon monoxide

.

Sample	C3 before	C3 after	C7 before	C7 after
Bulk resistance (Ω)	4.8×10^{8}	6.9×10^{7}	2.4×10^{8}	2.2×10^{7}
Relaxation time (sec)	1.285×10^{-2}	1.908×10^{-3}	5.859×10^{-3}	8.157×10^{-4}
Conductivity $(\Omega.m)^{-1}$	1.699×10^{-8}	9.747×10^{-8}	3.236×10^{-8}	22.818×10^{-8}

References:

[1] Arafa I. M., El-Ghanem H., and Al-Shalabi R., J.(2003), Formation, Characterization and Electrical Conductivity of Polycarbosilazane -Cu(II),-Ni(II) and -Cr(III) Chloride Metallopolymers Inorg. Organomet. Polym. 13 69.USA

[2]El Ghanem, H. M., Abdul Jawad, S., Aljundi, J., Afaneh, F., and Arafa, I.,(2003), Electrical properties of macromolecular complexes of coordinated polymers with mixed valence of Co(II) , Co (III) and Co (II-III) , Poly. Int. 52. Notherland.

OC9- Investigation of a thin-film calorimetric gas sensor for H_2O_2 detection in industrial processes

P. Kirchner[1,2], H. Spelthahn[1,2], A. Schneider[3], H. Henkel[3], P. Friedrich[4], J. Kolstad[5], M. J. Schöning[1,2]

[1]Institute of Nano- and Biotechnologies, Aachen University of Applied Sciences, Jülich, GERMANY
[2]Institute of Bio- and Nanosystems, Research Centre Jülich GmbH, Jülich, GERMANY
kirchner@fh-aachen.de
[3]von Hoerner & Sulger GmbH, Schwetzingen, GERMANY
[4]Aseptiksysteme & Foodtechnologie, Linnich, GERMANY
[5]Elopak, Spikkestad, NORWAY

Introduction: In the last decades, the microbial reduction of packages for food and beverages has become an important role in aseptic filling processes, especially to extend the shelf life of filled products. Therein, hydrogen peroxide vapour (HPV) is preferentially applied as decontaminant for aseptic packages compared to other chemicals, like formal dehyde and ozone. This is caused by the oxidising effect and the decomposition of HPV in environment-friendly products, namely water vapour and oxygen. In this process, the microbicidal efficiency of HPV depends thereby particularly on the H_2O_2 concentration that varies from 4 to 10% v/v. This correlation points out the requirement of a sensor system for the inline monitoring of the H_2O_2 concentration during the microbial reduction.

Experimental: In this work, a calorimetric gas sensor based on a differential set-up of a catalytically activated and a passivated temperature sensing element has been realised. If the sensor device is exposed to HPV, reaction heat can be determined as temperature difference between the active and passive sensor segment due to the exothermal decomposition of H_2O_2 on the catalyst. As temperature sensing elements, thin-film resistances were fabricated on chip level, which have been subsequently passivated with perfluoralkoxy. Manganese oxide has been examined as catalytically active material. In Fig. 1, a photography of the calorimetric gas sensor is presented.

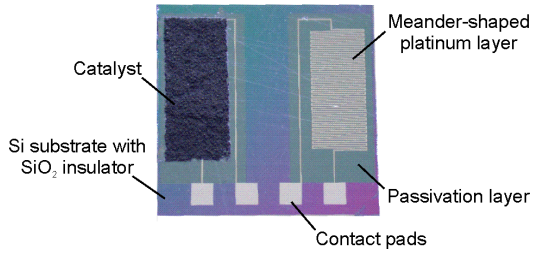

Figure 3: Thin-film calorimetric gas sensor for the H_2O_2 detection (chip size: 10 x 10 mm²).

Results and discussion: In a first sensor characterisation, the sensor signal in form of a temperature difference between the catalytically active and passive segment has been detected at a H_2O_2 concentration range of 0 to 8% v/v, shown in Fig. 2. Therein, the sensor device possesses a sensitivity of 0.57 °C/% v/v towards H_2O_2 and an accuracy of 0.11% v/v.

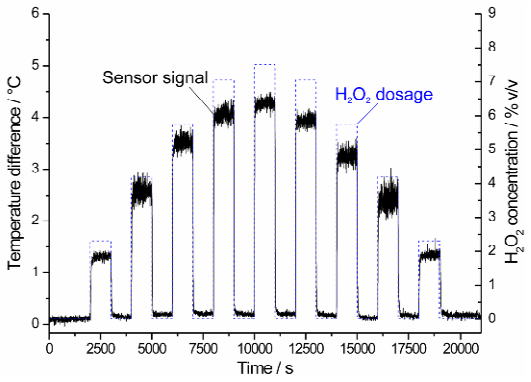

Figure 4: Temperature difference signal of the thin-film calorimetric gas sensor at various H_2O_2 concentrations.

Conclusion: A novel thin-film calorimetric gas sensor based on a differential set-up of catalytically activated and passivated thin-film resistances has been realised for H_2O_2 detection. In further steps, the sensor device shall be coupled on an RFID transmission system for inline monitoring of hydrogen peroxide in aseptic filling processes.

References:

[1] Cerny, G. (1992), Testing of aseptic machines for efficiency of sterilization of packaging materials by means of hydrogen peroxide, Packaging Technology and Science, 5, 77-81.

[2]Johnston, M.D., Lawson, S. and Otter, J.A. (2005), Evaluation of hydrogen peroxide vapour as a method for the decontamination of surfaces contaminated with Clostridium botulinum spores, Journal of Microbiological Methods, 60, 403-411.

OC-10 Novel biomaterials based on sugar diols: syntheses, characterization and application

S. Chatti[1], S. Mghirbi[1], H. Gorgi[1], H.R.Kricheldorf[2]

[1] Institut National de Recherche et d'Analyse Physico-chimique (INRAP),
Technopôle Sidi Thabet 2020 Sidi Thabet, Tunisia
saber.chatti@inrap.rnrt.tn
[2]Institut für Technische und Makromolekulare Chemie der Universität, Bundesstrasse 45,
D-20146 hamburg, Germany

Abstract:

Utilization of carbohydrate derivatives for biopolymers syntheses has been paid much attention not only because of the huge abundance of resources but also of the promising biodegradability and biocompatibility of them (Stross and Hemmer, 1991).

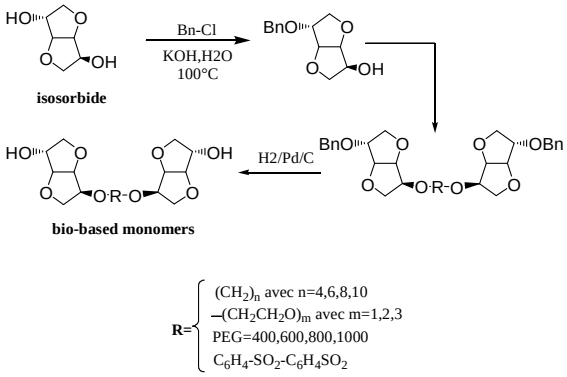

Figure 5: Synthesis of new diols from isosorbide

We have synthesed and characterized several bio-based sugar monomers (Chatti et al. 2000) (isosorbide and isomers) which can be used for the syntheses of novel biomaterials such as polycarbonates, polyesters, polyurethanes and poly(ether-sulfone)s (Chatti, 2006, 2009).

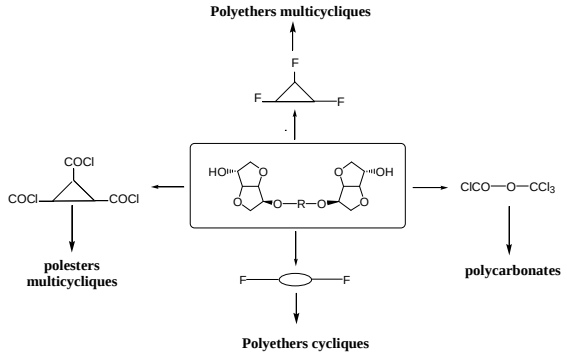

Figure 2: Biomaterials obtained by polycondensation of chirals diols with various difontionnalized agents

We have studied the influence of reaction conditions (reaction time, temperature, excess and stereochemistry of monomers) on the fraction of cyclic and linear chains of these biopolymers.

The resulting bio-based polymers has been characterized by NMR spectroscopy, MALDI-TOF mass spectrometry, SEC and DSC.

Sufficiently high molecular weights and glass transition temperature mean that such biopolymers could be useful as transparent engineering plastics, films and membranes (less sensitive to an attack of oil, gasoline and other organic solvent or liquid) and as bio-sensors (steroids, metals).

References

[1]Chatti, S.; Bortolussi, M. and Loupy, A. (2000) *Synthesis of diethers derived from dianhydrohexitols by phasetransfer catalysis under microwave.* Tetrahedron 2000, 56, 5877.

[2]Chatti, S.; Kricheldorf, H.R. and Schwarz, G.(2006) *Cyclic and Noncyclic Polycarbonates of Isosorbide (1,4:3,6-Dianhydro-D-glucitol).* Macromolecules, 39, 9064-9070, 2006.

[3]Chatti, S.; Hani, M. A.; Borhorst, K. and Kricheldorf, H.R. (2009). *Poly(ether-sulfone) of Isosorbide, Isomannide and Isoidide.* High Performance Polymers Journal, 21, 105-118, 2009.

[4]Stross, P. and Hemmer, R. (1991). Advances in *Carbohydrate Chemistry & Biochemistry*. 1991, 49, 93.

OC11- Wastewater treatment by using nanofiltration - case study of a Tunisian touristic resort

L. Gzara[1], I Trabelsi[2*]

[1]Laboratoire eau et technologie membranaire, CERTE, TUNISIA
Lassaad.gzara@certe.rnrt.tn
[2] Laboratoire de traitement et recyclage des eaux,CERTE, TUNISIA.
Ismail.trabelsi@certe.rnrt.tn, tél.79325 044 ; Fax79 325 802

Abstract: membrane treatment of wastewater of touristic resort is proposed. Initial chemical analyses of raw wastewater showed high content of COD and inorganic pollution. The use of nanofiltration following a pretreatment (coagulation or microfiltration), the obtained permeate meet easily Tunisian drinking water standard. The recovery rate was about 75%. The COD of conentrat was about 200 mgL-1 that can be directly discharged in sewer.

Introduction: Tunisia is one of the leading country in Tourism. The increasing local and foreign investment on hotel and touristic resort is well known. Consequently, an increase demand and consumption of fresh water along with discharge of wastewater need an integrated management through implementation of decentralised unit of wastewater treatment plant in this regard, a compact unit that treat wastewater by using advanced process such as nanomembrane is proposed. Infact, nanofiltration was choosen due to its energy saving (pressure less than 12 bar) and its high quality of permeate obtained that does not require any disinfection.

Materials and methods: All experiments in this study were run at labscale. The samples of wastewater were taken from a touristic resort located at borj Cedria that serve 3800 bed with a mean consumption of 20 000 m^3per month.About 80% of this amount is converted to wastewater and is deversed into sewer without any treatment nor any recycle. All parmeters such as COD, conductivity, pH, turbidity, nitrate, Mg, Ca, Cl, Na, and sulfate were measured according to standard methods.

	Raw wastewater	NF Permeate following coagulation	NF permeate following microfiltration
Conductivité (mS.cm^{-1})	1,61	1,33	1,35
pH	6,7	7,32	7,36
Turbidité (NTU)	14,93	0,487	0,195
DCO (mg.L^{-1})	76	8	36
[NH_4^+] (mg.L^{-1})	9,36	18	9,9
[NO_3^-- N] (mg.L^{-1})	25,2	25	19,6
Ca^{2+} (mg.L^{-1})	104	77	92
Mg^{2+}(mg.L^{-1})	65,61	24,56	24,19
Cl$^-$(mg.L^{-1})	1231,2	98,3	112,8
SO_4^{2-} (mg.L^{-1})	90,58	131,756641	29,62
Na^+ (mg.L^{-1})	231,08	154,88	191,44

Results and discussion:

The characteristics of wastewater along with its permeate through nanomembrane are given in table1. Type of pretreatment is keyrole in protection of nanofiltration membrane.As it is illustrated in table1 coagulation by addition $Al_2(SO_4)_3$ and microfiltration. The recovery rate and the main parameters of COD, turbidity and conductivity is given in figure1.

Table1: characteristics of raw wastewater and treated one by nanofiltration

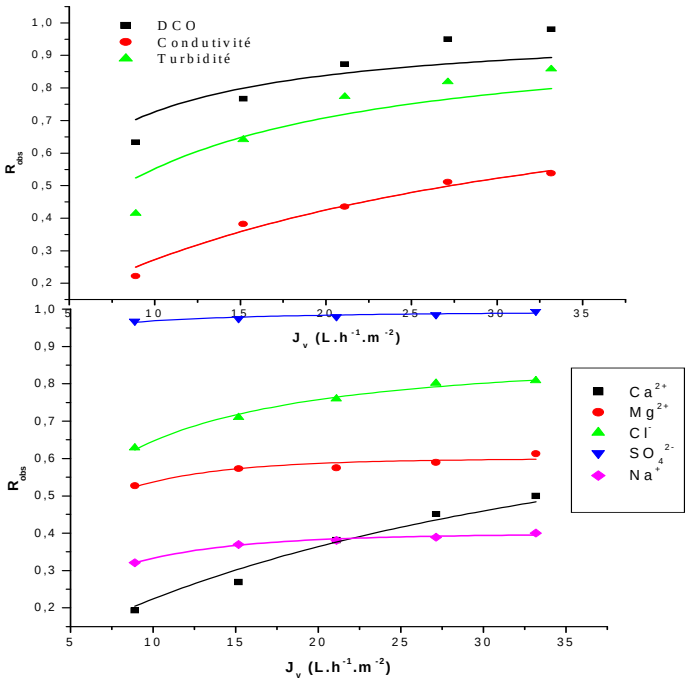

References:

[1] D. Bixioa, C. Thoeyea, J. De Koningb, D. Joksimovicb, D. Savicc,T. Wintgensd, T. Melin,Wastewater reuse in Europe, Desalination 187 (2006) 89.

OC12- Passivity-based synchronization of complex dynamical networks

J. Ghommam[1,2]

[1]Intelligent Control Design and Optimization of Complex Systems Unit,
Ecole Nationale d'Ingenieurs de Sfax, TUNISIA
Jawhar.ghommam@ieee.org
[2] Institut National des Sciences Appliquées et de Technologies, TUNISIA

Introduction: Complex networks are currently being studied across many fields of science and engineering (Strogatz, 2001), stimulated by the fact that many real systems, such as social, biological, electrical power grids,social and economic relations,etc can be described by models of complex network. Networks with different topological structures can be classified as regular networks,random networks,small-world networks,scale free networks,and evolving networks. Dynamic complex networks are typically nonlinear systems (Khalil, 2002) and the ubiquity of complex networks in science and technology naturally stimulates the study of the structure and behavior.

In this talk we will address the passivity of complex dynamical networks, including the possible presence of communication times delays and communication losses. We will consider a complex network with time delays, consisting of N identical coupled nodes, with each node being an n-dimensional system. This dynamical network is described by

$$\begin{cases} \dot{x}_i(t) = A_{\sigma_1} x_i(t) + B_{\sigma_2} x_i(t-\tau_{i1}) + f_i(t, x_i(t)) \\ \quad + E_i w_i(t) + \sum_{j=1}^{N} D_{ij} x_j(t-\tau_{i2}), \quad i = 1, \ldots, N, \\ z_i(t) = C_i x_i(t) \end{cases}$$

Passivity theory gives a framework for the design and analysis of control systems using an input–output description based on energy-related considerations. The main idea behind this is that many important physical systems have certain input–output properties related to the conservation, dissipation and transport of energy. This gives rise to the definition of passive systems which is very useful in the study and control of physical systems (Arcak, 2006).

Contribution: This talk will focus on providing some sufficient conditions for complex dynamical networks with and without delays in the states to be passive. Based on the passivity property and linearization, control and synchronization of the dynamical networks will also be addressed. An example for Chua'soscillator which state equations is given below

$$\begin{cases} \dot{x}_1 = \alpha(x_2 - x_1 - g(x_1)) \\ \dot{x}_2 = x_1 - x_2 + x_3 \\ \dot{x}_3 = -\beta x_2, \end{cases}$$

will be given to demonstrate the effects of time delays on dynamical networks and verify the effectiveness of the approach. An interested application for system synchronization is the coordination of multiple rigid body like autonomous vehicles where the presence of a human operator is potentially dangerous, unnecessary, or impossible. In many applications the vehicles must work cooperatively. We therefore exploite the frame work for passivity based synchronization of complex network to extend it to the case of cooperative control of autonomous underwater vehicles (Ghommam, 2008).

Figure 1: Photograph of the Cormoran AUV (ghommam, 2008)

References:

[1] Strogatz, S. H. (2001). Exploring complex networks.Nature,410, 268–276.
Khalil, H. K. (2002).Nonlinear systems(3rd ed.) Prentice Hall
[2] Arcak, M. (2006). Passivity as a design tool for group coordination. In Proc. 2006 American control conference.
[3]Ghommam, J. Calvo, O. Rozenfeld (2008), Coordinated path following for multiple underactuated AUVs, OCEANS 2008 - MTS/IEEE Kobe TechnoOcean, 2008

OC13- Use of mini heat pipes including axially capillary microgrooves for electronics cooling

J. Mansouri, S. Maalej, M.C. Zaghdoudi

Unité de Recherche Matériaux Mesures et Applications (MMA)
Institut National des Sciences Appliquées et de Technologies, TUNISIA
chaker.zaghdoudi@insat.rnu.tn

Introduction: Rapid growth in the use of internet and telecommunication services has created critical demands on the power required to energize this network. High speed access coupled with expanding needs for all modes of electronic communications have resulted in telecommunications systems that exhibit dramatic increases in power dissipation compared to previous systems. Thermal management of electronic components must therefore solve problems connected with the limitations on the maximum chip temperature with the requirements of the level of temperature uniformity. Heat pipes are not in general a low cost solution to the cooling problem, but it is most effective and has great potential as power levels and volume requirements increase. For these reasons, heat pipes have been applied up to now mainly in application with special working conditions and requirements such as in space thermal control, in aircraft devices, in traction drives, in audio amplifiers, in cooling of closed cabinets in harsh environmental conditions, etc.

The present study deals with the development of an enhanced Flat Mini Heat Pipe (FMHP) concept to be used for cooling high power dissipation electronic cards. Experiments are carried out in order to determine the thermal performance of such devices as a function of various parameters such as the heat input power, the heat sink temperature, and the tilt angle.

FMHP Fabrication: A FMHP, shown in Figure 1, which includes axial and rectangular capillary microgrooves, has been designed, manufactured, and tested. For comparison purposes, a solid heat sink that has the same size but more weight than the spreader is also tested. All of the test samples are made of the same copper and their dimensions are 100 mm length, 50 mm width, and 3 mm thickness. The FMHP body is manufactured in two halves. Manufacturing of FMHP begins with the capillary grooves being mechanically machined in the first half (2 mm thick) and the second half, which consists of a copper cover slip 1 mm thick , is bonded to the first half by an electron beam welding process. The heat pipe charging tube (2 mm diameter), from which the fluid working is introduced**, is** bounded to the heat pipe end by a classic welding technique.

Figure 6: Axial capillary microgrooves machined on a copper plate

Experimental Results: The experimental results are given in terms of heat source-sink temperature difference, T_{ev}-T_c and thermal resistance variations, R_{th}, as a function of the input heat flux rates, Q. The heat transfer improvement, obtained by comparing the heat pipe thermal resistance to the heat conduction thermal resistance of a copper plate having the same dimensions as the tested heat pipe, is given for different heat input flux rates and heat-sink temperatures (Fig. 2).

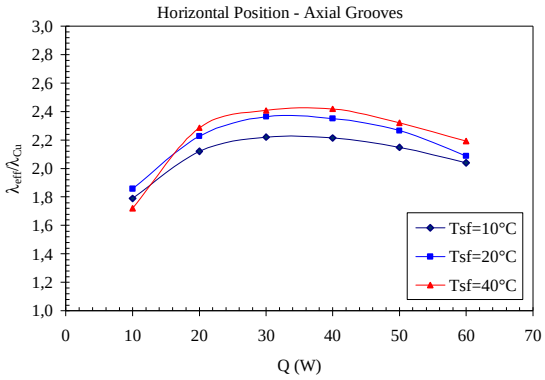

Figure 7: Variations of the ratio of the FMHP effective thermal conductivity to that of a copper plate with the input heat power, for different heat-sink temperatures

Conclusion: An experimental study is realized in order to determine the thermal performance of a FMHP with axially capillary microgrooves. The experimental results indicate that the heat transfer improvement depends on the heat flux rate, the heat sink temperature, the FMHP orientation, and the capillary structure. The FMHP thermal conductivity is higher than that of a copper plate having the same dimensions. The maximum heat transfer enhancement is about 250 %.

OC14- Chemical and biological detection investigations using shear horizontal surface acoustic wave sensor

N. Fourati[1], C. Zerrouki[1], J.M. Fougnion[1], R. Lucas[2], J. Vergnaud[2], P. Boutin[3], R. Zerrouki[2] and C. Pernelle[3]

[1] Laboratoire de Physique, EA 4131, Cnam, 2 rue Conté 75003 Paris, FRANCE
fourati@cnam.fr
[2] Laboratoire de Chimie des Substances Naturelles, EA 1069, Faculté des sciences et techniques, 123 avenue Albert Thomas , F- 87060 Limoges, FRANCE
[3] Laboratoire de Génie Analytique, EA4131, Cnam, 292 rue Saint Martin 75003 Paris , FRANCE

Introduction: Shear horizontal surface acoustic wave (SH-SAW) devices, which are non-labelled sensors, offer significant advantages over current labelled techniques since they are fast, low cost and are ideal for detecting trace elements in liquid media. In this study we will present some chemical and biological detection investigations using lithium tantalate acoustic sensors.

Experimental section: Surface acoustic wave devices, realized in the 'Centrale Technologique Universitaire d'Orsay' consist of a dual delay line built on a 36°rot lithium tantalate piezoelectric substrate. Input and output interdigital transducers consisted of 30 pairs of split fingers with a periodicity of 40 µm, operating frequency was therefore 104 MHz. Between them is located the gold sensing area, over which a Kalrez® flow cell is placed to contain solutions for chemical or biological experiments (Fig. 1).

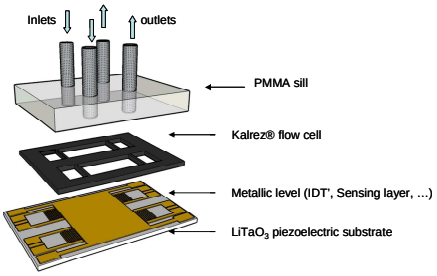

Fig. 1: Schematic representation of the surface acoustic wave device.

We have used several measurement systems to follow sensing applications: 1) A HP 8711C network analyzer to measure the amplitude and phase of the output electrical signal, 2) a dual-delay-line oscillator configuration and 3) a home made pulse mode system.
Development of specific bio or chemical recognition on a solid/liquid interface is closely related to the design of the recognition layer. Before any experimentation, SAW devices were immersed for 30 min into a piranha solution, and then rinsed with ultra pure water to obtain a clean and pre-activated surface, suitable for the next operations.

Results: several applications will be described in this communication. The first ones concern hybridization detection of:

- natural DNA strands by means of a probe-target DNA binding mechanism,
- short oligothymidine analogues (4-mer recognition length) with complementary adenine stretches of an oligodeoxynucleotide

In both cases, the probes are grafted beforehand on the gold sensing area of the sensor.

We will also show some results relating to the follow up of the chemical elements complexation (lead ions, methoxy poly(ethylene glycol), …) by a β Cyclodextrin self-assembled monolayer.

In situ monitoring of specific and nonspecific proteins bindings, by means of SH-SAW devices, will finally presented.
This work focuses on a simple approach that we developed, to detect and to characterize various chemical and biological species in liquid media, interacting with surface immobilized receptors.

References:

[1]David, C., Millot, M.C., Sébille, B., Lévy, Y., (2003) The reversible binding of hydrophobically end-capped poly(ethylene glycol)s to poly-β-cyclodextrin-coated gold surfaces: a surface plasmon resonance investigation, Sensors and Actuators B, 90, 286-295.
[2]Janshoff, A., Steinem, C., Michalke, A., Henke, C., Galla, H. J., (2000) Monofunctionalized β-cyclodextrins as sensor elements for the detection of small molecules, Sensors and Actuators B, 70, 243 - 253
[3]Saha, K., Bender, F., Gizeli, E., (2003) Comparative Study of IgG Binding to Proteins G and A: Nonequilibrium Kinetic and Binding Constant Determination with the Acoustic Waveguide Device, Anal. Chem. 75, 835-842
[4]Sakong, J., Roh, Y., Roh, H., (2006), Saw sensor system with micro fluidic channels to detect DNA molecules, IEEE, 1051-0117/06/$20.00

OC15- Functionalized gold nanoparticules for impedimetric immunosensors

I. Hafaiedh[1,2], F. Vocanson[3], A. Abdelghqni[4], Z. Sassi[2], F. Bessueille[1], D. Leonard[1], N. Jaffrezic-Renault[1]

1University of Lyon, Laboratory of Analytical Sciences, UMR-CNRS 5180, Claude Bernard University, Lyon I, 43 Boulevard du 11 Novembre 1918,69622 Villeurbanne Cedex, France
e-mail: imen_haf@yahoo.fr
[2] Ampere Laboratory, Bât L. De Vinci - INSA -20, avenue Albert Einstein, F-69621, Villeurbanne Cedex, France
[3] Laboratory Hubert Curien, UMR CNRS 5516 Bât. F18 Rue du professeur Benoit Lauras 42000Saint-Etienne, France
[4]Unité de Recherche de Physique des Semi-conducteurs et Capteurs, IPEST, La Marsa, 2070, Tunis, Tunisia

Abstract :
In the field of immunotests, recent approaches consist of labelfree detection as surface plasmon resonance (SPR), or electrochemical impedance spectroscopy, the antibody being firstly covalently immobilised on a gold surface. The use of antibody-functionalised gold nanoparticles [Mirkin and al., 1996] gives rise to an increasing interest because they not only allow increasing of the specific surface area, then of the quantity of grafted antibody but also of the sensitivity of detection [Andrew Lyon and al., 1998], leading to a lower detection limit.

Gold nanoparticles with a diameter around 20 nm were synthetised and successively functionalised with a thiol-disulfide and an activation agent such as EDC and PFP, allowing the linking of a biotinylated anti-E. coli antibody on their surface through grafted neutravidin, for the detection of the E. coli bacteria. The control of the different steps was performed using SPR, FTIR and AFM. The labelfree immunodetection using EIS was performed by monitoring the variation of the polarisation resistance when antibody-antigen complex is formed [Maalouf and al., 2007]. Quantitative results showed that the surface densities of biotinylated biomelecule on the gold nanoparticules modified gold electrode were approximately estimated to 5.1 10^{16} molecules mm^{-2}. Compared to the analyses carried out on a system base on the magnetic beads [4], the use of gold nanoparticles led to a detection limit of 1 CFU/ml (figure 1) compared to 10 CFU/ml obtained with paramagnetic nanoparticles [Maalouf and al., 2008].

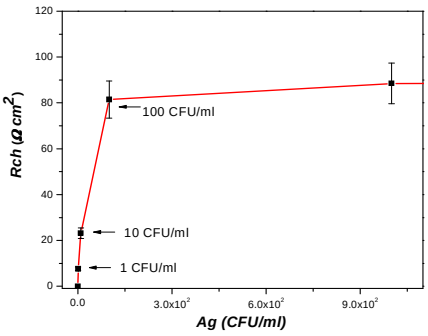

Figure 1: Calibration curves describing the variation of membrane resistance Rm against the pathogenic E. coli bacteria concentration

References

[1]Andrew Lyon, L. and Musik, M.D. (1998) Colloidal Au-Enhanced Surface Plasmon Resonance Immunosensing, *Analytical Chemistry*, 70 ,5177- 5183.

[2]Maalouf, R., Fournier-Wirth, Ch., Coste, J., Chebib, H., Saı1kali, Y., Vittori, O., Errachid, A., Cloarec, J.-P., Martelet, C. and Jaffrezic-Renault, N. (2007) Label-Free Detection of Bacteria by Electrochemical Impedance Spectroscopy: Comparison to Surface Plasmon Resonance, *Analytical Chemistry* ,79, 4879-4886.

[3]Maalouf, R., Mohamed Hassen, W., Ch. Fournier-Wirth, Ch., Coste, J. and Jaffrezic-Renault, N. (2008) Comparison of two innovatives approaches for bacterial detection: paramagnetic nanoparticles and self-assembled multilayer processes *Microchimica Acta*, 163, 157–161.

[4]Mirkin, C.A., Letsinger, R.L. , Mucic, R.C. and Storhoff, J. (1996) A DNA-based method for rationally assembling nanoparticles into macroscopic materials, *Nature*, 382, 607- 609.

OC16- Giant magnetoresistance: Fundamentals and applications

Abderrahmen Selmi
Faculté des Sciences de Monastir , Tunisia
E-mail: ab_selmi@yahoo.fr

Abstract:

Magnetoresistance is a change of the electrical resistance of a material when an external magnetic field is applied to it. The effect was first discovered by William Thomson in 1856. It was later observed in other kinds of materials such as perovskites and magnetic semiconductors. However, in bulk materials the effect was not large enough to allow potential applications. In 1988 Albert Fert and Peter Grünberg each independently obtained a Giant Magnetoresistance or GMR in ferromagnet/paramagnet multilayer structures. In these new devices, very weak magnetic variations produce major changes in electrical resistance. A system of this kind is a powerful tool for reading data from hard disks when information registered magnetically has to be converted to electric current.

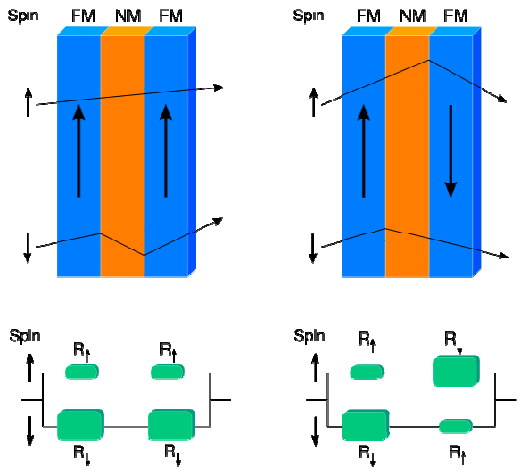

Fig: GMR multilayer structure and electrical equivalent circuit.

In 1997 the first read-out head based on the GMR effect was launched and this soon be came the standart technology. This technology permitted to miniaturize hard disks so radically in recent years. Applications GMR effect could be extended to the industrial, commercial, and military worlds like sensitive detectors for wheel-shaft speed; automotive antilock brakes, and auto-traction systems; motion and position sensors for electrical safety devices; current transformers or sensors for measuring direct and alternating current, power, and phase; metal detectors and other security devices.

References:

[1] P. Grünberg, R. Schreiber, Y. Pang, M. B. Brodsky, and H. Sowers (1986). ". Physical Review Letters 57 (19): 2442–2445.

[2] M. N. Baibich, J. M. Broto, A. Fert, F. Nguyen Van Dau, P. Étienne, G. Creuzet, A.Friederich,J.Chazelat
Phys. Rev. Lett. 61, 2472 (1988)

OC17- Dynamic wave scattering and rheological investigations on a temperature-sensitive hydrocolloidal system of silice-particles

H. Mahjoub[1], G. Ducouret[2] , T. Narita[2] and F. Lequeux[2]
[1]Laboratoire de Physique de la Matière Molle, Campus Universitaire
Institut National des Sciences Appliquées et de Technologie, TUNISIA
Faten16fr@yahoo.fr
[2] Laboratoire de Physico-chimie des Polymères et des Milieux Dispersés
ESPCI, 10 Rue Vauquelin, 75231 Paris cédex 05, FRANCE

Introduction: The colloidal suspensions which were the aim of several studies in concentred and diluted media present a highly diversified behaviors. This study tend to give a better comprehension of the macanisms concerned in the the flocculation phenomena. The interactions between particles, their radius and the volumic fraction have an important role, so it is necessary to work with a model system.

The structuration and the dynamics of colloidal suspensions of 100 nm as a redius of silicium particles in presence of a thermosensitive polymer (PNIPAM) were studied when they flocculate under the effect of temperature.

Content: To obtain monodispersed and controlled size spherical particles, we realized a STÖBER synthesis [Stober and al], the tetraethylorthosilicate was hydrolyzed and condensed in ethanol with water and ammoniaque solution. The obtained particles by nucleation are very small, they are submitted to many cycles of growth until they reach 105 nm as radius. Hence we obtain uniform monodispersed population.

The synthesis of the polymer, poly-N-isopropylacrylamide (PNIPAM) was done with the monomer NIPAM with a well defined protocole described in [Bokias and al]. The number molar weight determined by SEC (Steric Exclusion Chromatography) is 20000g.

In the process of mixing silicium particles and PNIPAM, the polymer is adsorbed on the spheres surfaces. The suspensions concentrated by osmotic stress were studied with a cone/plate geometry using a TA Instrument rheometer (ARES) equipped with Peltier effect. The system was protected against dryness with a very low viscosity silicon oil. Simultaneously, we carried out nano-rheological measures by Diffusing Wave Spectroscopy (DWS) . We present hereafter the results of a 35% volumic colloidal suspension.

The rheological properties of the colloidal suspension are tested first at 25°C, it is visco-elastic fluid. At ambient temperature, the polymer stabilize the particles by protecting them against coalescence: we have a repulsive- system. Above approximately 40°C, the PNIPAM flocculate and the particles aggregate to form a network, the systm gelifys at temperatures higher than 40°C and consolides slowly with a complex dynamic.

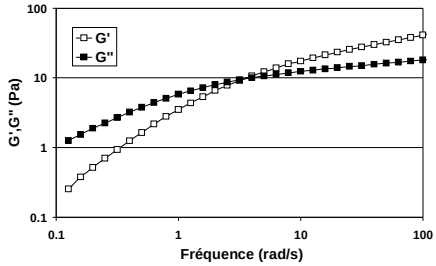

Figure 8: Elastic and viscous moduli at 25°C

Nanorheolgy or Dynamic Wave Spectroscopy [Gisler and al] allowed us to study our system dynamic at inaccessible frequencies by coventionnal rheology. The results show the existence of two relaxation times for the temperatures investigated. Above 45°C these times are higher than those found at 25°C. They correspond respectively at rapid fluctuations of the particles in the network and to slow arrangements of the aggregates at 25°C or to very slow fluctuation of the network at 45°C when the gel is formed.

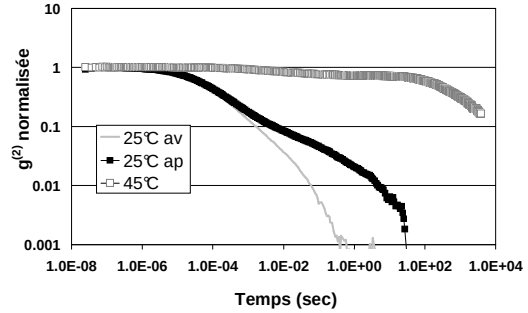

Figure 2: Normalized autocorrelation function at 25°C before and after heating and at 45°C.

References:

[1]Bokias, G. Durand, A. and Hourdet, D. (1998) Macromol. Chem. Phys.,199, 1387-1392.

[2] Gisler, T. Ball, R.C. and Weitz, D.A. (1998) Physical Review Letters, 82, 1064-1067.

Stober, W. Fink, A. and Bohn, E. (1968) J. of Colloid Interface Sci. , 26, 62.

OC18- Effect of a high-frequency actuation on the pull-in instability in MEMS

F. Lakrad, M. Belhaq

University Hassan II-Casablanca,
BP 5366 Maarif, Casablanca, Morocco
lakrad@hotmail.com

Introduction: Electrostatically actuated Microelectromechanical systems MEMS find many applications today in areas such as inertial sensors, relays, switches, etc. A serious limitation on the use of these devices lies in the pull-in phenomenon (Nayfeh et *al.*, 2007), which is a structural instability resulting from the interaction between elastic and electrostatic forces. This instability results from the unbalance between the electric actuation and the mechanical restoring force leading the suspended microbeam to hit the stationary electrode underneath it causing stiction and short circuit problems and hence the failure in the device's function (Walraven, 2003).
In the present work, we study the effect of a high-frequency AC tension on the pull-in instability induced by a DC tension in a microelectromechanical system.

Formulation of the problem: The microstructure is modelled as a single- degree-of-freedom system, see Figure 1. The equation of motion of the movable electrode is given by

$$m\ddot{x} + c\dot{x} + k\,x = \frac{\varepsilon A}{2(d-x)^2}V^2$$

Where x is the displacement of the movable electrode of mass m and of cross section area A. The dielectric constant of the gap medium is denoted ε and d is the initial capacitor gap width.
The voltage V is the sum of an DC voltage and a HF voltage

$$V = V_0 + U\cos(\Omega t)$$

The method of direct partition of motion (Thomsen, 2003) is used to split the fast and slow dynamics. Analysis of steady-states of the slow dynamic enables us to depict the effect of the AC voltage on the pull-in.
The main result of this paper indicates that it is possible to suppress the electrostatically induced pull-in instability for a range of values of the amplitude and the frequency of the high-frequency AC, see Figure 2.

Figures:

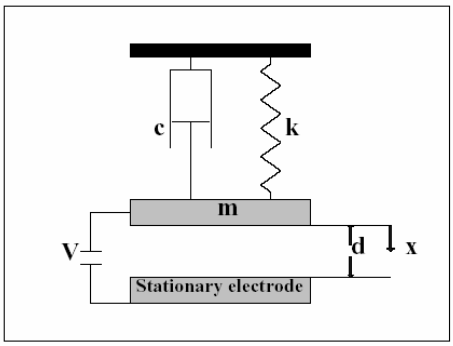

Figure 9: A single-degree-of-freedom model of a MEMS device.

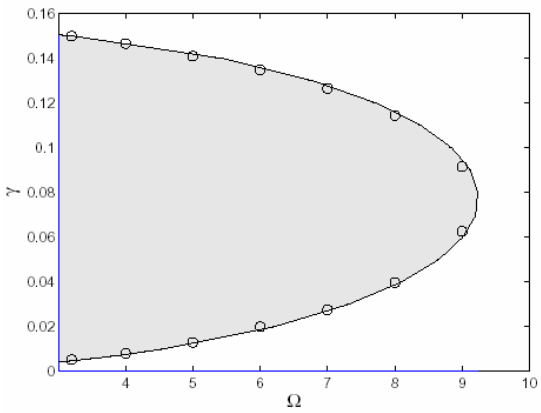

Figure 2: Zone of suppression of the static pull-in, in the plane of the HF voltage parameters.

References:

[1]Nayfeh, A.H., Younis, M.I. and Abdel-Rahman, E.M. (2007) Dynamic pull-in phenomenon in MEMS resonators, *Nonlinear Dynamics*, 48,153-163.
[2]Thomsen, J.J. (2003) *Vibrations and stability: advanced theory, analysis and tools*, Springer-Verlag, Berlin-Heidelberg.
[3]Walraven, J.A. (2003) *Future challenges for MEMS failure analysis*, Proceedings of ITC international test conference, paper 33.4, 850-855, 2003.

OC19- Conformational study of sulphated carrabiose molecule by DFT methods

M. Sekkal-Rahal, N. Yousfi

Laboratoire L2MSM, Faculté des Sciences. Université Djillali Liabes de Sidi-Bel-Abbes,
B.P. 89 . 22000 Sidi-Bel-Abbes. ALGERIA.
majsekkal@msn.com

The B3LYP density functional was employed with the 6-31G(d) basis set to perform relaxed energetic contour maps of the charged and the neutral forms of the 1,4 linked disaccharide from κ-carrageenan. Carrageenan is a linear polyoside abundantly used in food, chemical and pharmaceutical industries (Moir *et al*.) . The structure of one of the two repeating dimers constituting κ-carrageenan; 4-O-sulphated-β-D-galactopyranosyl 1,4 anhydro 3,6-α-D-galactopyranose. is studied in this work

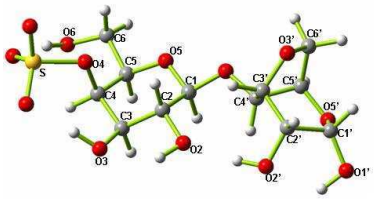

Figure 1: Structure of mono sulphated dimer from κ-carrageenan

These two last decades, many works dealing with conformational study of carbohydrates have appeared, most of them used classical methods, to explore the structure of the conformers, such as molecular mechanics (Tvaroska *et al*.). More recently, a number of papers, using *ab initio* or density functional theory (DFT) studies, have begun to appear (Navarro *et al*.).

We have used DFT, in particular the B3LYP hybrid procedure on the quoted dimer. The purpose consists mainly to explore the conformational space and to identify the conformers corresponding to the lower energies when varying the dihedral angles of the glycosidic linkage according to the procedure that is usually named Ramachandran plots.

DFT and in general *ab initio* methods are not so simple to use when dealing with compounds that have a variety of conformers such as carbohydrates, since, calculation of the conformational space or the energy hyper-surface of mono-, di-, or even trisaccharides by such methods requires enormous cpu time.

In this work, the purpose is to perform relaxed potential energy surfaces maps of the 1,4 linked dimer of κ-carrageenan. For this aim, we opted in a first stage for the use of a more explicit method by introducing only polarization functions into the basis set, thus we have realized three relaxed energy maps at the B3LYP/6-31G(d) level.

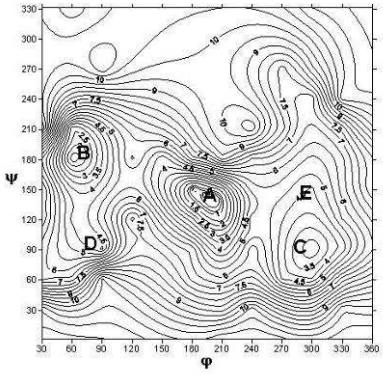

Figure 2: Relaxed isopotential map of the dimer I, at the B3LYP/6-31G(d) level in gas-phase.(E in kcal/mol).

The two dihedral angles Φ and Ψ of the Glycosidic linkage are the principal geometrical parameters to characterize the three-dimensional structure of disaccharides (Lii *et al*).

Following the recommendations proposed by the IUPAC we have used (Φ,Ψ) for the disaccharide, (such as Φ = O5-C1-O4'-C4' and Ψ = C1-O4'-C4'-C5'), The conformational maps have been built as suggested by French *et al*. by interpolating a set of data comprising 144 energy values, which was generated by varying each dihedral angle in increments of 30°. Once the set of the two specific values of Φ and Ψ angles fixed, they were kept frozen while optimizing all of the other geometrical parameters.

References:

[1]French A. D. (1989) Carbohydr. Res., 188, 206.
IUPAC-IUB (1971) Commission on Biochemical Nomenclature. Arch. Biochem. Biophys., 145, 405
[2]Lii, J.H., Ma, B.Y.and Allinger, N.L.(1999) J. Comput. Chem., 20, 1593.
[3]Moir, A.and Smith, D. A. (1990) Annu. Rev. Microbiol. , 44, 531.
[4]Navarro, D. A. and Stortz, C. A. (2008) Carbohydr. Res., 343, 2292.
[5]Tvaroska, I. (1984) Biopolymers, 23, 1951.

OC20- Structure and magnetic properties of fine particle $La_{0.7}Ca_{0.3}MnO_3$ prepared by mechanic synthesis method

W. Chérif [1], M. Ellouze[1] , F. Elhalouani[2]

[1] Faculté des Sciences de Sfax, B. P. 1171-3000 , TUNISIA .
wajdi_chrif@yahoo.fr
mohamed.ellouze@fss.rnu.tn
[2] Ecole Nationale d'Ingenieurs de Sfax, B. P. W 3038, TUNISIA .
foued.elhalouani@enis.rnu.tn

Introduction: Perovskite-type $LaMO_3$ (M = Mn, Co, Fe...) sample is of interest for the catalytic oxidative and reductive reactions associative with the regulation of waste gas emitted from vehicles[1]. In addition, much attention has been paid on their morphology and magnetic properties, leading to the possible use giant magneto-resistance [2, 3]. Perovskite-type manganites $Ln_{1-x}A_xMnO_3$ were Ln is a rare earth (Ln = La, Pr, Sm …) and A is a divalent element (A = Ca, Sr, Ba …) have attracted considerable attention because of their interesting magnetic and structure properties. $La_{0.7}Ca_{0.3}MnO_3$ compounds can be synthesized by several methods such as the ceramic method [4, 5, 6] or chemical method [7] and also by mechanical grinding . Recently, this method is much sought by researchers because of their advantages such as low-cost process, simple et it can develop very fine powders. In addition to bulk perovskite manganites, much attention has recently been paid to the investigation of their fine particle counterparts, which usually exhibit qualitatively new properties. From a morphology, this is the end grain and magnetic point of view it is changes in the magnetic transition temperatures.

Experimental: Different methods of preparing manganite oxide perovskite were used. Among these methods of preparation we have: the sol-gel method, the chemistry based on liquid-solid reactions such as crystallization, co-precipitation method and the mechanical synthesis. The choice of one of these methods is generally dependent on the type of desired microstructure and by the size of samples to be studied. For our work, we are interested in the method developed by mechanical milling. The principe of this method of preparation is to obtain from the following precursors: MnO_2 (99.9%), La_2O_3 (99.9%) and CaO (99.9%) the sample $La_{0.7}Ca_{0.3}MnO_3$. These materials were mixed in the appropriated stoichiometric ratio for the reaction:

$$0{,}35\ La_2O_3 + 0{,}3\ CaO + MnO_2 \rightarrow La_{0.7}Ca_{0.3}MnO_3$$

Results: Fine particle of $La_{0.7}Ca_{0.3}MnO_3$ was synthesized by the mechanical synthesis. The average crystallite size of 1 micrometre was obtained by both balayage electron microscopy and X-ray diffraction. Our x-ray diffraction confirm that the sample crystalise in the an orthorhombic structure with the Pnma space group. Magnetic measurements showed the sample hexibit a para-to-ferromagnetic transition temperature at T_C = 120 K. This Curie temperature was also obtained for the same sample elaborated with solid state method.

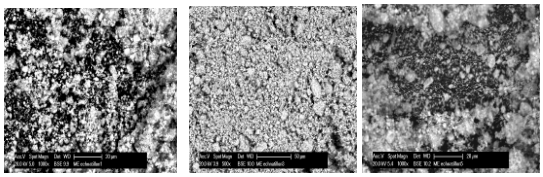

Fig. 1 : Photos of powder of $La_{0.7}Ca_{0.3}MnO_3$ milled at different times .

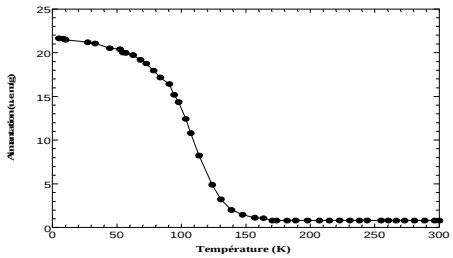

Fig. 2 : Magnetization as a function of temperature with applied magnetic field about 0.5T .

References:

[1] G.H.Joncker,J.H.Van Santen, *Physica, 16, 337 (1950).*

[2] J.B. Goodenough et A.L.Loeb, *J.Phys. Rev. ,98, 391 (1955).*

[3] C.Zener, *Phy. Rev, 82, 403 (1951).*

[4] *″Matériaux à propriétés spécifiques les matériaux magnétiques″. Rapport rédigé sous la responsabilité de* D. GIVORD, *Laboratoire Louis Néel, CNRS.*

[5] H.Gleiter, Prog.*Mater.Sci, 33, 233.(1989).*

[6] R.Berringer and H.Gleiter, *Encyclopedia of Mater.Sci and Eng, Oxford: pergamon, 1,339. (1988).*

[7] R.Z. Valier, A.V. Korznikov, R.R.Mulyukov, *Mater. Sci.Engin, A168 (1993), 141.*

OC21- Metal deposition on conductive and semi-conductive modified surfaces

S. Ameur[1,3], P. viel[1], C. bureau[2], S. Palacin[1]

[1] CEA/DSM/DRECAM/SPCSI, Chimie des Surfaces et Interfaces,
CEA Saclay, B,t 466, 91191 Gif-sur-Yvette Cedex (France)
sami.ameur@laposte.net
[2] Alchimer SA, 15 rue du buisson aux fraises, 91300 Massy (France)
[3] current adress : Unité de Recherche de Physique des
Semiconducteurs et Capteurs,IPEST, 2070 La Marsa, Tunisia

Introduction:

metal deposition onto electrically conductive and semiconductive surfaces is used in variety of applications, including microelectronics, biomedical and automotive. Two major routes are mainly distinguished for the deposition of metals onto electrically conductive and semiconductive surfaces. The electrochemical deposition route, or electrodeposition, according to which the reduction of a solution containing salts of the metal that it is desired to deposit onto the surface of interest, used as the working electrode, is schematically performed. Electrolysis of this solution allows the deposition of the metal of interest onto the surface, provided that the reduction potential required is compatible with the chosen solvent and the chosen support electrolyte. Spraying processes, such as chemical vapor deposition (CVD), physical vapor deposition (PVD) and related methods such as atomic layer CVD (ALCVD). These methods are generally used to produce a seed layer for the deposition of copper by electrodeposition in the Damascene process. Unfortunately, these methods require relatively complex and expensive pretreatments, such as the use of vacuum, irradiation, etc., Moreover, it is generally observed that various additives such as surfactants, gloss agents, etc. are required to obtain a uniform deposit of good quality. Adhesion problems are generally observed, especially at very low thicknesses do not necessarily preserve the chemical integrity of the precursors.

.

In this work, we report a method for producing thin metallic films, adhering, covering and conforming (for patterned surfaces) to conductive or semiconductive based on electrografting. Homogeneous and adhesive metal deposition on several electrically conductive and semiconductive surfaces was easily carried out by all-wet process.

Experimental work :

Several conductive or semi-conductive samples were used. Polymeric films were deposited by spin coating or electro-grafted onto these surfaces. For electrografted films synthesis was performed by cyclic vol

tammetry. The insertion of metallic precursors (cupric ions) has been made from ionic solutions. The saturation of polymeric film with the metallic precursor may be facilitated by the presence within polymeric film of functional groups capable of retaining the precursor by complexing it when it is in the ionic form. The complexation, or trapping of metal ions was followed by infra red measurements. The electrochemical reduction of metal precursors has allowed us to obtain adherent metal films, even when films are deposited by spin coating. The films obtained are mainly metal as it was shown by X-ray photon spectroscopy.

The complete formation of a copper seed-layer by electro-grafting from a mixing of vinylic monomers and copper precursors in a single bath and its use to obtain the electrofilling of trenches in a Damascene type interconnexion structure was illustrated. In the absence of the electro-grafting precursors, the seed-layer does not even form on the surface.

Posters Communications

P1- Plasma-assisted MBE growth of Ga (As, N) materials: growth conditions and optical properties

M. EZZDINI, S. REKAYA, R. HAMILA, F. SAIDI, L. SFAXI*, and H. MAAREF
Laboratoire de Physique des Semi-conducteurs et des Composantes Electronique
Faculté de Monastir, Avenue de L'environnement, 5000 Monastir (Tunisie)
E-mail corresponding author: larbi.sfaxi@fsm.rnu.tn

Introduction: GaAs-based materials containing a few percent of nitrogen (N) are attracting much attention due to their unique electronic and optical properties, and thus they are expected to be novel material for optoelectronic device grown on GaAs substrate [1, 2]. It is known that the very small N content can greatly reduce the band gap [3] due to the very large bowing factor of this material (as large as 10-20eV). Since, the quality of the diluted nitrides decreases rapidly with N composition . So, it is important to optimize the growth conditions for controlling the band gap and quality of the GaN_xAs_{1-x} material. In this work, we have studied the influence of growth conditions on the N incorporation in Ga(As,N) epilayers grown by radio-frequency (RF) plasma-assisted Molecular Beam Epitaxy (MBE).

Experimental:

In order to optimize N incorporation in the Ga(As, N) epilayers, four different samples, designated as (M1), (M2), (M3) and (M4), were grown at various growth rates (V_{growth}) and substrate temperatures (T_s) (table1), while the RF plasma power and the N flux from the direct nitrogen beam were kept at 300W and 2.1 10^{-6}torr, respectively. High resolution X-ray diffraction (HR-XRD) was used to measure the N compositions of the as-grown GaNAs samples. The optical properties of the samples were evaluated by low temperature (10K) photoluminescence (PL) measurements, using the 514.5 nm line of an Argon ion laser as the excitation source.

Results and Discussion:

Table (1) presents the nitrogen composition of the $GaAs_{1-x}N_x$ alloys determined from (HR-XRD) measurements in the investigated samples. These results show a decrease of the N concentration when the growth rate or substrate temperature increases. A higher N content of 2.77% is obtained for the epilayer grown at 500°C and 1.8 (Å/s). In addition, figure (1) shows the growth rate and substrate temperature dependence of the PL peak energy of $GaAs_{1-x}N_x$ alloys. As the growth rate and the substrate temperature increase, the PL peak energy increases, indicating less nitrogen is incorporated and confirming well the HR-XRD measurements. This tendency was in good agreement with the results reported by different growth methods and studies. There are two reasons for the decrease of N composition when the substrate temperature increases. One is that the N sticking coefficient decreases with the temperature, so the N atoms desorption from grown
surfaces increases as the temperature increases. Second, the re-association of N into N2 at the growing surface is suppressed at lower growth temperature, so more active N species will be available at the growing surface, leading to an increased N incorporation. Moreover, the nitrogen in principle behaves like a dopant in the GaAsN growth. This behaviour explains the decrease of the N composition in GaAsN epilayers as the growth rate increases. Our results are crucial to further control N incorporation in Ga(As, N) materials and improve crystal quality.

Figures and Tables:

Samples	T_s *(°C)*	V_{growth} *(Å/s)*	*N composition (%)*
M1	500	1.8	2.77
M2	500	3.5	1.32
M3	520	1.8	1.3
M4	520	4.4	~1.2

Table1: Summary of GaAsN growth rate, substrate temperature and N composition from HR-XRD measurements for the samples used in this study.

Figure 1: The growth rate dependence of 10K PL peak energy of $GaAs_{1-x}N_x$ epilayers grown at different growth temperature of 500 and 520°C.

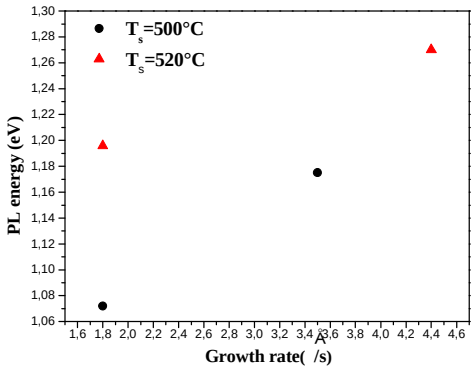

References:

[1] L. Bellaiche, S.-H. Wei, A. Zunger, Phys. Rev. B 54, (1996) 17568.
[2] W.G. Bi, C.W. Tu, Appl. Phys. Lett. 70, (1997) 1608.
[3] M. Reason, H. A. Mckay, W. Ye, S. Hanson, and R. S.Goldman and V. Rotberg , Appl; Phys . Lett. 85, (2004) 1692.

P2- Magnetic properties in $Cd_{1-x}Mn_xTe$ diluted magnetic semi-conductor quantum wells

S. Mnasri, S. Abdi-Ben Nasrallah, N. Sfina, and M. Said
Unité de Recherche de Physique des Solides, Département de Physique,
Faculté des Sciences de Monastir, 5019 Monastir, Tunisia
E-mail: samiaabdi@myway.com

Abstract:
Diluted magnetic semiconductors (DMS), where ferromagnetic interactions are mediated through free carriers, are particularly attractive since they offer the possibility of modulation of magnetic properties. In particular, DMSs of II–IV compounds as a typical material have attracted a considerable attention for the last few years owing to the carrier-mediated origin of the ferromagnetism and the localized spins and holes that can be introduced and controlled independently. A unique feature of these doped diluted-magnetic semiconductor quantum well is that the giant Zeeman splitting can be easily made larger than the Fermi energy. One thus obtains a fully polarized hole gas, i.e., one spin state in the valence band is free of holes while the other contains the whole hole gas. In our work, we have performed a theoretical study of the hole gas properties formed in $Cd_{1-x}Mn_xTe/CdTe/Cd_{1-x}Mn_xTe$ heterostructures by calculating the spin-dependent hole density. Our calculations are based on a self-consistent procedure to solve simultaneously the coupled Schrödinger and Poisson equations for spin up and spin down taking into account the p-d interaction between the hole and the Mn spins. In the mean field approximation, the local magnetic interaction of the spin carriers with the Mn spins is substituted by the interaction with an effective magnetic field of intensity V_c, while the electronegativity difference between the Mn and the CdTe atoms produces a potential discontinuity V_w between the Mn doped semiconductor and the undoped semiconductor. We have calculated the spin up and spin down densities. Results are illustrated in Figures 1 and 2 for ferromagnetic configuration for different values of band offset V_W. As shown in Figures, the carriers with spin up are mainly located in the magnetic CdMnTe layer whereas the spin down carriers are expelled from it and located in the non-magnetic layer. Then, the spins are separated from carriers in such structure. In the anti-ferromagnetic coupling (not shown), it is straight for word to point out the separation of spin up and spin down holes even if both spin orientations are located in the magnetic layers: the spin-up holes are mostly located on the right side of the structure while the spin-down holes are mainly concentrated in the left side.

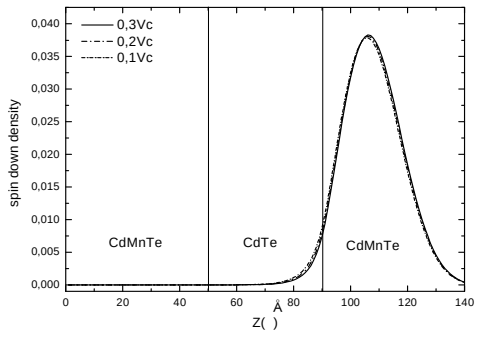

Figure.1

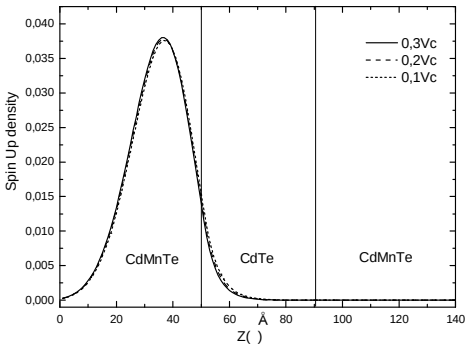

Figure.2

P3- Up-conversion fluorescence dynamics in Er^{3+}/Yb^{3+} co-doped tellurite glasses

A. Cherif, A. Kanoun

Laboratoire de Physique des Semi-conducteurs et Dispositifs Electroniques,
Faculté des sciences de Monastir, TUNISIA
cherif_af@yahoo.fr

Abstract: The infrared to visible conversion in zinc tellurite glasses (TZ), activated by Er^{3+} ions and sensitized by Yb^{3+} ions has been investigated under 980 nm pulsed laser excitation.

The up-conversion mechanism was studied by means of time-resolved luminescence spectroscopy, for the results, the up-conversion mechanisms are discussed in conjunction with their quadratic power dependence.

Introduction: The Using materials co-doped with Er^{3+}/Yb^{3+} or Tm^{3+}/Yb^{3+} with the aim of producing more efficient IR quantum counters. Yb^{3+} and Er^{3+} ions as suitable laser emitters for several interesting applications and with the advantages of diode-pumping and up-conversion mechanisms [1-4]. The different types of energy transfer up-conversion (ETU) processes were described very well in the literature. The up-conversion mechanism usually involves following process, ground state absorption (GSA), excited state absorption (ESA), energy transfer (ET), multiphonon relaxation (MR), cross relaxation (CR) and so on.
According to the energy matching conditions and the dependence on excitation power, the possible up-conversion mechanisms for the red and the green emissions are discussed based on the energy level of Er^{3+} and Yb^{3+}.

Figure. 1 shows the up-conversion spectra of the Er^{3+} (0.5 mol%) singly doped, and Er^{3+}/Yb^{3+} co-doped tellurite glasses ($70TeO_2$-30ZnO) as for 2.5 mol% Yb^{3+} content at room temperature, obtained under 980 nm pulsed laser excitation. We can see two emission bands peaked at 550 and 670 nm that correspond to transitions of Er^{3+} ions from excited states to the ground state. Intense green and red emission bands at around 550 and 670nm wavelength are attributed to the transitions from ($^4S_{3/2} \rightarrow {}^4I_{15/2}$) and ($^4F_{9/2} \rightarrow {}^4I_{15/2}$), respectively. All the up-conversion luminescences are enhanced strongly with Yb^{3+} contents increasing (2.5 mol %). It is because of the contribution of Yb^{3+} in energy transfer process.

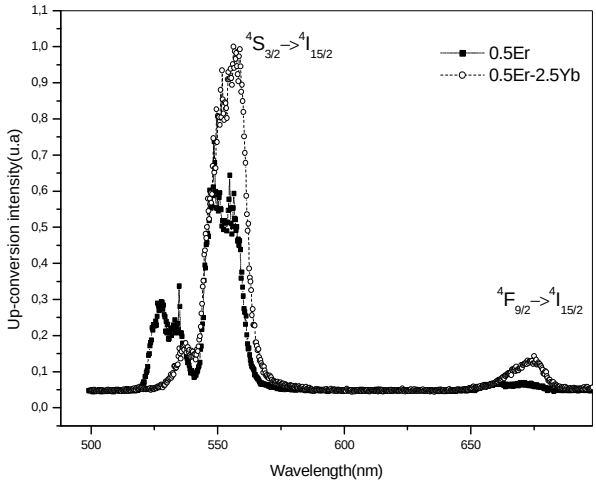

Figure 1. Up-conversion emission for Er^{3+}/Yb^{3+} (*0.5*/2.5 mol %) and Er^{3+} (0.5 mol %).

References:

[1] B. C. Hwang, S. Jiang, T. Luo, et al. *SPIE 3622 (1999) 10.*
[2] T. Ohtsuki, N. Peyghambarian, S. Honkanen, S. I. Najafi, *J. Appl. Phys.* 78 51995) 3617.
[3] D. R. MacFarlane, J. Javorniczky, P. J. Newman, et al. *J. Non cryst. Solids* 213-214 (1997) 158.
[4] H. Fujiwara, K. Sasaki, J. Appl. Phys. 86 (1999) 2385.

P4- Hyphenation of surface plasmon resonance imaging to matrix-assisted laser desorption ionization mass spectrometry by on-chip MALDI-MS analysis

Sophie Bellon[1,2], Marielle Anger-Leroy[1], Régis Daniel[2], William Buchmann[2], Florence Gonnet[2], Nathalie Jarroux[3], Chiraz Frydman[1,4]

1 GENOPTICS Bio Interactions, Orsay, France

2 CNRS, UMR8587, Université d'Evry-Val-d'Essonne, Laboratoire Analyse et Modélisation pour la Biologie et l'Environnement, F-91025 Evry, France

3 Laboratoire Matériaux Polymères aux Interfaces, Université d'Evry Val d'Essonne, France

4 HORIBA Scientific, Chilly Mazarin, France : Chiraz.frydman@horiba.com

Introduction: The combination of SPRi technology with MALDI mass spectrometry on the same surface is a powerful approach for the analysis of biomolecular interactions. Surface Plasmon Resonance is used to quantify interactions between capture ligands and surface-immobilized receptor combined with SPR, Mass Spectrometry (MS) enables the determination of the molecular weight of specifically bound ligands.
The SPR-MS system, implemented by GenOptics, allows the measurement of biomolecular interactions by SPRi, and then the detection of the retained ligands by MALDI mass spectrometry directly from the sensor surface. This system has been validated from an antibody-antigen biomolecular system as described below.

Given the design of the SPRi-sensor surface biochip developed by GenOptics, it has been conceived that the same surface could be used first to capture and quantify the bio-molecular interactions via SPRi technology, and second to work as a surface probe for MALDI MS analysis. Using the biochip developed in this study, we showed that its transfer in the MS apparatus consecutive to a SPRi experiment was simple. In addition, it required no intermediate treatment that could lead to sample lost and/or contaminations.

Experiment: The gold surface of the SPR sensor was functionalized with the amine coupling reagent N-hydroxysuccinimide (NHS). The proteins used as receptors were covalently linked to the surface through their primary amine functions by being simply dropped onto the SPR sensor. The model we used is two types of antibodies were arrayed: Anti-β-lactoglobulin and Anti-ovalbumin.

An MS compatible running buffer was choosen, such as 10 mM ammonium acetate (pH7.5), and a blocking lysine solution injected into the system to react with the remaining free active NHS groups. The biochip was then ready for SPR and analyte capture experiments. A mixture of proteins (β-lactoglobulin and ovalbumin) diluted in the running buffer was now injected in the flow cell and the analyte capture was followed in real time by SPR imaging (Fig.1 and Fig.2)

Figure 1: Following the analyte capture in real time on the SPRi-Plex™

Mass spectrometry was directly performed on the SPR chip following the affinity capture of the specific proteins, using a commercially available Applied Voyager MALDI-TOF instrument. Typical mass spectra obtained from the protein-bound antibody array show specific multiply charged protein ions (Fig.3)

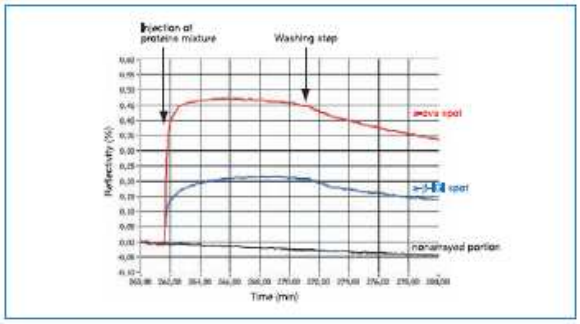

*Figure 2: **SPR analysis of interactions between a mixture of ovalbumin and β-lactoglobulin with their specific antibodies arrayed on the SPR sensor.** Reflectivity variations versus time of anti-ovalbumin (a-ova, 600 nM), anti-βlGl-lactoglobulin (a-βlGl, 600 nM) spots and of a nonarrayed portion of the chip (negative control) after injection of a 50 µg/mL mixture of β-lactoglobulin and ovalbumin*

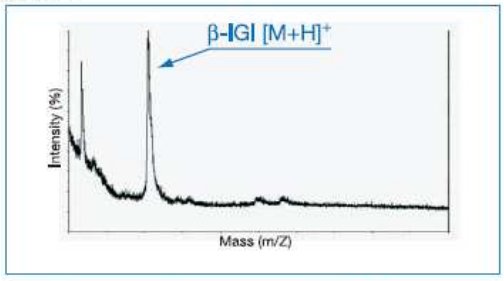

Figure 3: MALDI mass spectra obtained for β-lactoglobulin specifically captured on their antibodies spotted on the biochip, $[M+2H]^{2+}$ and $[M+H]^{+}$ of β-lactoglobulin.

Conclusion: The combination of SPRi with MALDI-MS on an array platform is an innovativetool for affinity separation and identification of specific ligands from complex solution.

P5- Carrier tunneling in quantum rings

W.Ouerghui [1], J. Martinez-Pastor [2], J. Gomis [2], M.A. Maaref[1], D. Granados [3] and J. M Garcia [3]

[1] Unité de Recherche des Physiques des Semiconducteurs et Capteurs, Institut Préparatoire aux Etudes Scientifiques et Techniques. La Marsa 2070, Tunis, Tunisia
ouerghuiwalid@yahoo.fr
[2] Instituto de Ciencia de los Materials, Universidad de Valencia, P. O. Box 22085, 46071 Valencia, Spain.
3 Instituto de Microelectrónica de Madrid, Isaac Newton 8, 28760 Tres Cantos, Madrid, Spain

Abstract:

We present results concerning the carrier transfer between In(Ga)As quantum rings in a stacked multi-layer structure, which is characterised by a bimodal size distribution. This transfer of carriers explains the observed temperature behaviour of diode lasers based on that kind of stacked layer structures. The inter-ring carrier transfer can be possible by phonon assisted tunnelling from the ground state of the small-ring family towards the big-ring family of the bimodal size distribution. This process is thermally activated in the range 40-80 K.

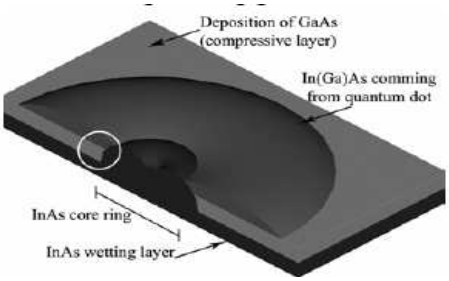

From the application point of view, the presence of such a high lateral ring-ring coupling in the QR ensemble can be the origin of the important increase of the threshold current characteristic temperature T_o, which have been recently reported in laser diodes for this kind of QR ensembles [1].

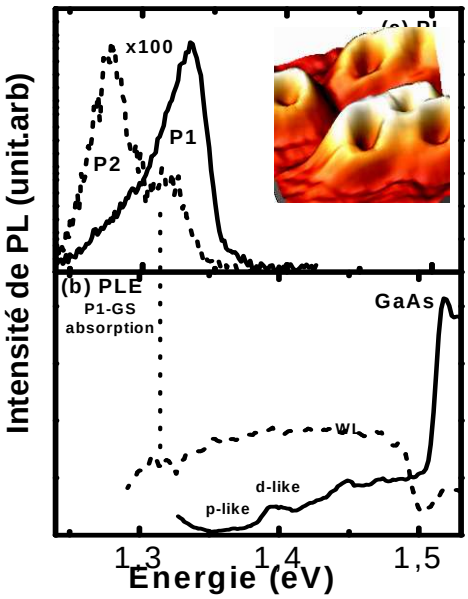

Figure. (a) Spectre de PL sous une excitation résonante (trait discontinu) et non-résonante (ligne continue) de l'échantillon ; (b) Spectre de PLE.

[1] F. Suarez, D. Granados, M.L. Dotor and J.M. Garcia, Nanothechnology **15**, S126 (2004).

P6- Dielectric studies of natural fibre reinforced composites for automotive applications

A. Triki[a], M. Guicha[b], Med. Ben hassen[b] and Z. Fakhfakh[a]
[a] LAMACOP; Faculté des Sciences de Sfax 3018 (TUNISIA)
[b] Unité de recherche textile, Institut supérieure des études Technologiques de Ksar Hallel (TUNISIA)

Abstract:

Composites materials are used for various engineering applications. Today automotive industries show large interest in natural fibre composites [1], so called eco-composites which are the subjects of many scientific and research projects, as well as many commercial program [2]. These natural fibre composites compete with and substitute glass mat thermoplastics in wide spread use [1]. In this work, we focussed on the dielectric characterization of polymer composites of unsaturated polyester resin matrix filled with non-woven Alfa and wool fibres. Dielectric spectroscopy was performed in the frequency range 10^{-1} Hz to 10^{6} Hz and temperature interval from 40°C to 150°C. This study reveals two relaxations processes. The first was associated to conductivity resulting of the carriers charges diffusion noted for high temperature and low frequencies. The second one attributed to interfacial MWS relaxation is due to the accumulation of charges at the natural fibre/unsaturated polyester interfaces. This study confirms the absence of any water in all fibres since no relaxations due to the water dipoles was observed.

References:
[1] R. Joffe, L. Wallström, L. A. Berglund, International Scientific Colloquium Modelling for saving resources, Riga 17-18 May 54-59 (2001).
[2] B. G. Gaceva, M. Avella, M. Malineonico, M. Buzaroska, A. Grozdanov, G. Gentiles, E. M. Errico, Poymer Composites, 28, 98-107 (2007)

P7- Band offset calculations of diluted magnetic heterostructure ZnMnSe/ZnSSe

S. Ben Afia[1], M. Triki[2], S. Jaziri[3], H. Belmabrouk[1]

[1]Unité de Recherche de Physique des Solides Faculté des Sciences de Monastir 5000, TUNISIA
e-mail: sonia_benafia@yahoo.fr
[2]Laboratoire de Physique de la Matière Condensée Faculté des Sciences de Tunis, TUNISIA
[3]Laboratoire de Physique des Matériaux Faculté des Sciences de Bizerte 7021, TUNISIA

Abstract

During the last few years, there has been a regained interest in the study of dilute magnetic semiconductors (DMS). In particular, II-VI semimagnetic semiconductor alloys with Mn2+ ions are interesting materials with regard to their remarkable magneto-optical properties. Especially with the advent of modern epitaxial growth techniques, it has become possible to grow semiconductor structures to achieve the desired properties and devices applications. Among II-VI wide gap structures, ZnMnSe / ZnSSe semimagnetic heterostructures are of particular interest due to their promising magneto-optical properties that offer a possible application on the blue-green lasers. These properties are mainly driven by the potential across the interface between the two compounds. This potential is known as the band offset. However, the computation of the band offsets requires the knowledge of some electronic band parameters such as band gap energy. Therefore, taking into account the recent behaviour of the ZnS_xSe_{1-x} band gap ranging from 2.60 to 3.67 eV [1] theoretical study is made to calculate the band offset of pseudo morphically strained $Zn_{0.96}Mn_{0.04}Se$ / ZnS_xSe_{1-x} interface. Hence, on the basis of model 'solid theory', the strain effects electrons, heavy holes (hh) and light holes (lh) are investigated as a function of sulphur composition *x* ranging from 0 to 1 with and without taken into account the effect of an applied magnetic field. In the frame of a mean field approximation, main peculiar feature is revealed indicates that $Zn_{0.96}Mn_{0.04}Se$ / ZnS_xSe_{1-x} heterostructure allows a direct interband transition for the carriers for molar fraction *x* ranging between 0 and 4%. Over this range of sulphur content, the $Zn_{0.96}Mn_{0.04}Se$ / ZnS_xSe_{1-x} heterostructure is of type II band alignment. Our result provides useful information for experimentalists and opens the way to realise devices based on $Zn_{0.96}Mn_{0.04}Se$ /ZnS_xSe_{1-x} structures for $0 \leq x \leq 1$.

References:

[1]S. Ben Afia, H. Belmabrouk, M. Said, S. Abdi-Ben Nasrallah and N. Bouarissa, (2005) Materials Science and Engineering C, 25, 691, 2005.

P8- Photothermal measurements of non-radiative lifetime of doped GaSb

F. Saadallah, S. Abroug, N. Yacoubi

Unite de Photothermie de Nabeul, Institut Préparatoire aux Etudes d'Ingénieurs de Nabeul, TUNISIA
Faycel1@yahoo.fr

Introduction:

Photothermal deflection [1-3] is used in order to reveal the influence of doping on non radiative carrier lifetime in GaSb when illuminated by a modulated and monochromatic light beam.

Theoretical simulations are obtained from an adapted theoretical model, based on the resolution of both heat and carrier diffusion equations, taking into account the distinction between non-radiative and radiative carrier lifetimes.

Photothermal amplitude and phase versus square root frequency are measured for different doping levels. From the fitting of these curves with theoretical ones we have determined thermal diffusivity as well as non radiative lifetime.

Figure 1 shows that when increasing of doping concentration, the obtained non radiative lifetime is reduced, however surface recombination velocity and thermal diffusivity are enhanced.

In the other hand, figure 2 shows that thermal diffusivity decreases linearly as a function of $1/N^2$. this is probably due to the effect of recombination process on thermal wave diffusion.

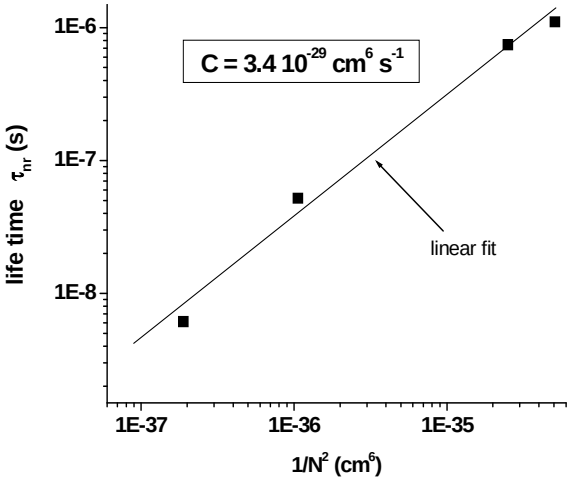

Figure 1: non radiative lifetime versus the ineverse squared doping concentration ($1/N^2$)

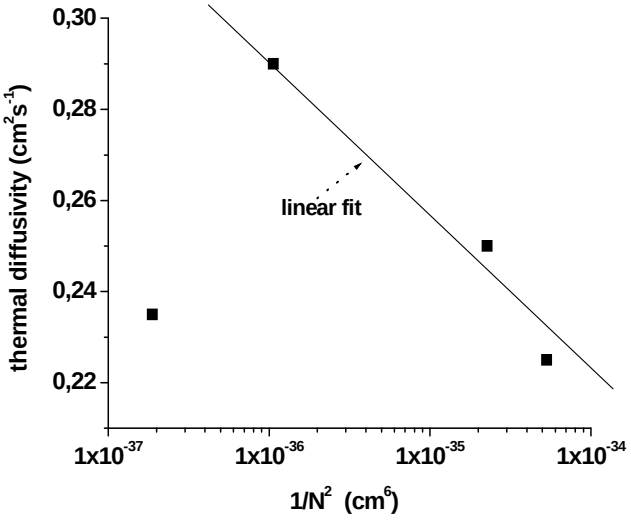

Figure 1: thermal diffusivity versus the ineverse squared doping concentration ($1/N^2$)

References:

[1]F. Saadallah, N. Yacoubi, F. Genty and C. Alibert, Appl. Opt. **41** (2002) 7561.

[2] F. Saadallah, N. Yacoubi, F. Genty and C. Alibert, J. Appl. Phys. **94** (8), 1 (2003).

[3] C. Khélia, K. Boubaker, T. Ben Nasrallah, M. Amlouk, S. Belgacem, F. Saadallah, N. Yacoubi, J. Crystal Growth, **311** (4) 1032 (2009)

P9- Effect of carriers transfer behaviour on the optical properties of InAs quantum dots embedded in AlGaAs/GaAs heterojunction

H. Khmissi, L. Sfaxi, L. Bouzaïene, F. Saidi and H. Maaref

Laboratoire de Physique des Semiconducteurs et des Composants Electroniques, Faculté des Sciences de Monastir, Avenue de l'environnement 5019 Monastir, TUNISIA
Corresponding author : hammadi_khmissi@yahoo.fr

Abstract

In this paper, we have investigated the optical properties of InAs quantum dots embedded near the channel of a AlGaAs/GaAs High Electron Mobility Transistor. In order to study the influence of the two-dimensional electron gas on the luminescence of quantum dots, we have prepared different structures in which we varied the thickness (d) separating the interface of AlGaAs/GaAs heterojunction from the InAs quantum dots layer. Various photoluminescence behaviours have been observed when d decreases. PL spectra showed the existence of two peaks which can be attributed to the transition energy from the ground state (E1-HH1) and the first excited state (E2-HH2). A blue shift, a decrease of the PL intensity and an increase of the full width at half maximum of the PL peaks were observed, when the InAs quantum dots layer close to the two dimensional electron gas.

***Keyword**: InAs quantum dots, AlGaAs/GaAs heterojunction, Photoluminescence, 2DEG*

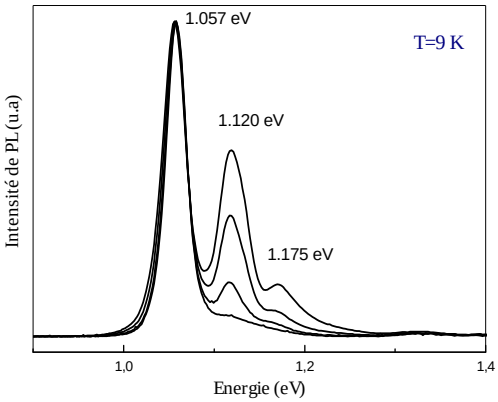

Fig 1: Evolution of PL spectra of the reference sample S0 with power density excitation.

Table I: FWHM of ground state and first excited state of S1, S2 and S3

Structures	S1	S2	S3
FWHM of the ground state peak (meV)	31	32	36
FWHM of the first excited state peak (meV)	79	87	92

References

[1] B. Etienne, E. Paris, J. Phys. **48** 2049 (1987).
[2] L. Bouzaïene, L. Sfaxi, H. Sghaeïr, and H. Maaref J. Appl. Phys. **85** 8223 (1999).
[3] L. Sfaxi, L. Bouzaine, H. Maaref, Microelectron. J. **30** 769 (1999).
[4] B. M. Ashkinadze, E. Linder, E. Cohen, and L. N. Pfeiffer, Phys. Rev. B. **74** 245310 (2006).
[5] Y. Arakawa, H. Sakaki, App. Phys. Lett. **40** 939 (1982).
[6] M. Grundmann, O. Stier and D. Bimberg, Phys. Rev. B. **52** 11969 (1995).
[7] L. Bouzaïene, L. Sfaxi, H. Maaref, Microelectronics Journal. **35** 897 (2004).
[8] M. Baira, L. Sfaxi, L. Bouzaiene, H. Maaref, N. Chauvin, and C. Bru-Chevallier, J. Appl. Phys. **104** 064314 (2008).
[9] K. H. Schmidt, M. Versen, U. Kunze, D. Reuter and A. D. Wieck, Phys. Rev. B. **62** 23 (2000).
[10] G. Medeiros-Ribeiro, J. M. Garcia, and P. M. Petroff, Phys. Rev.B **56**. 3609 (1997).

P10- Conductor polymers for biosensor applications

H.ben Fredj[1*], S. Helali[1], Z .Sassi[2], N. Jaffrezic-Renault[3], L. Vonna[4], A. Abdelghani[1]

[1] Unité de Recherche de Physique des Semiconducteurs et Capteurs, IPEST La Marsa,Tunisia.
*Corresponding author : haykel20032003@yahoo.fr
[2] INSA de Lyon, UMR 5005, Laboratoire Ampère, 69622 Villeurbanne, Lyon, France
[3] Laboratoire de Sciences Analytiques, Université de Claude Bernard, Lyon, France
[4]Institut de Science des Matériaux de Mulhouse, 15 rue Jean Starcky BP2488, 68057 Mulhouse Cedex, France

Introduction: Electrochemical, structural and morphological studies were performed on polyaniline film prepared in different solvents and electrolytes. For this purpose, cyclic voltammetry, fourier transformed infra-red spectroscopy, scanning electron microscopy and atomic force microscopy were successively applied. Based on neutravidin entrapment inside the electrogenerated polyaniline followed by specific Fab fragment-antibody grafting, atrazine immunosensor was developed. The impedance measurements with polyaniline polymer reveal that immunosensor could detect significantly 0.01 ng/ml atrazine. This lower limit detection is due to the delocalized electron structure present in the polyaniline film. For unspecific detection, no response was recorded after injection of different concentrations of rabbit Ig G.

Introduction: Since the discovery of an increase by nearly 10 orders of magnitude of the electrical conductivity of polyacetylene when it was doped with iodine in 1977 [1] conjugated polymers have been studied intensively. Polypyrrole (PPy) has mostly been applied, mainly due to its high conductivity, good thermal and environmental stability, high redox and capacitive current and biocompatibility [2,3]. PPy has been used in batteries [4], supercapacitors, sensors , actuators and corrosion protections . Polypyrrole can be synthesized by chemical polymerization or electrochemical activation . However, it is well known from a number of experimental studies that various parameters such as the solvent, electrolyte, electrode, deposition time, temperature, current density, and applied voltage all affect both its structures and electroactivities . Particularly, the type of the counter ion and doping level have great effect on redox character and the electrical state of the generated film.Polyaniline was another extensively studied polymer which has high storage ability, good conductivity and versatile properties. Therefore, PANI was the first conducting polymer to be commercialized and now has applications ranging from batteries to biosensors . Polyaniline are mostly carried out using aniline hydrochloride solution or a mixture of an aniline monomer and a dilute hydrochloride acid . In this paper, we present a comparative approach based on characterizing the chemical structure, morphology and redox behavior of polypyrrole and polyaniline prepared in different solvents and electrolytes.

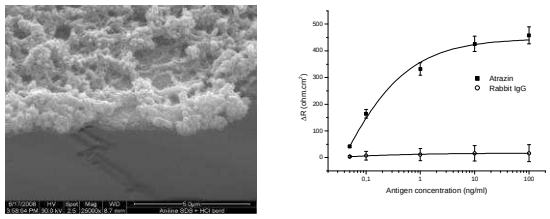

(a) (b)

Figure 1: (a)SEM micrographs of Polyaniline film prepared in HCL. (b) Calibration plot of the variation of ΔR with antigen concentration. The change of the charge transfer resistance ΔR is obtained by subtracting the resistance of the immune complex from the resistance of the immobilized probe.

For biosensor application, the incorporation of neutravidin inside the polymer film prepared in SDS lead to an increase in the diameter of Nyquist plot. This result proves the insulating character of protein molecules inducing the positive change in charge transfer resistance. Neutravidin was therefore successfully embedded within the polymer film. However, when we grafted the biotinylated anti-triazine Fab fragment, a significant decrease in charge transfer resistance was depicted ..

References:

[1] C.K. Chiang, A.J. Heeger, A.G. MacDiarmid, Phy. Lett. A, 60, 375 **(**1977).
[2] Q.-Wu Zhang, X. Zhou and H.-S. Yang, J. Power Sources, 125, 141 (2004).
[3] M.S. Kim, H.K. Kim, S.W. Byun, S.H. Jeong, Y.K. Hong, J.S. Joo, K.T. Song, J.K. Kim, C.J. Lee and J.Y. Lee, Synth. Met. 126, 233 (2002).
[4] J.G. Killian, B.M. Coffey, F. Gao, T.O. Poehler, P.C. Searson, J. Electrochem Soc. 142, 936 (1996).
[5] H. Ben Fredj, S. Helali, L. Vonna, L. Vidal, A. Abdelghani, Talanta, 75, 740 (2008)

P11- Formation of silver nanoparticles in ion-exchanged silicate glass by thermal annealing

A. H. Hamzaoui[1], K. Farah[2], F. Hosni[2], A. Mejri[2], H. Ben Ouada[3]
[1]Laboratoire de valorisation des ressources naturelles et matériaux de récupération, Centre National de Recherche en Sciences des Matériaux, Borj Cedria, B.P. 95, Hammam-Lif 2050, Tunisia
[2]Laboratoire de Radiotraitement, Centre National des Sciences et Technologie Nucléaires, 2020 Sidi-Thabet, Tunisia
ka_farah@yahoo.fr
[3]Laboratoire de Physique et Chimie des Interfaces, Faculté des Sciences de Monastir, 5000. Tunisia

Abstract: The introduction of nanosize metal particle such as silver into glass surfaces, in replacement of alkali ions by ion exchange, has been used for a long time to colour the surface of decorative glass (Seward, 1980; Rao, 2002; Ageev et al., 2007; Bandyopadhyay, 2008), for ionizing radiation dosimetry (Schulman et al., 1951) and recently for fabricating optical devices (Bach and Neuroth, 1998). A microscope slide glasses have been subjected to ion exchange at 320°C in a molten mixture of $AgNO_3$ and $NaNO_3$ with molar ratio of 5:95, and 10:90 for 60 min. The ion exchange process was followed by annealing at the temperature of 550°C for different time periods ranging from 30 to 120 min. Optical properties of the ion exchanged glass are measured using UV–Vis absorption spectroscopy. The absorption spectra represent an envelope of two separate bands at 350 and 430 nm. The first band appears only in the samples heat treated for 30 minutes. For annealing time more than 30 min, the absorption spectra became sharp and well defined, indicating that it has no contribution from the band at 350 nm. The position of this band shifted slightly towards shorter wavelengths, and its intensity increased with increasing time of heat treatment. The band at 350 nm, which was observed at the initial stage of thermal annealing, was attributed to the formation of neutral silver atoms. Thus, reduction of silver ions occurs at the in initial stages of thermal annealing, leading to the formation of neutral silver atoms, incapable of absorbing light in the visible range, thereby not affecting the colour of the glass. Increasing the time of thermal annealing to 120 min leads the aggregation of silver atoms to form nanosize silver particles $(Ag^0)_n$ inducing the characteristic band at 430 nm and glass turns brown. This absorption peak corresponds to the surface-plasmon resonance (SPR) of the silver clusters and confirms the formation of silver clusters in the glass. The average cluster radius R of the clusters is calculated from the full width half maximum, $\Delta\lambda$ (FWHM) of the optical absorption peak using the formula: $R = \frac{V_f \lambda^2{}_m}{2\pi C \Delta\lambda}$

Where V_f is the Fermi velocity of the electron in the bulk metal (silver=1.39×108 cm/s), $\Delta\lambda$ is the full width at half maximum of the absorption band and λ_m is the characteristic wavelength at which SPR occurs. The FWHM is determined by assuming the absorption peak as a Lorentzian distribution (Doremus, 1965). Both λ_m and $\Delta\lambda$ depend on the substrate and size of the metal nanoclusters forming the composites. The radiuses of the cluster found from this calculation are between 1-1.5 nm. Depend on the time of thermal annealing and of the quantity of silver introduced into the glass surface.

References

[1] Ageev, L. A., Miloslavskiĭ V. K. and Makovetskiĭ, E. D. (2007) Coloring of silica glass with silver nanoparticles, Optics and Spectroscopy 102, 442–448.
[2]Bach, H., Neuroth, N. (1998) The Properties of Optical Glass, Springer, Berlin.
Bandyopadhyay, A. K. (2008) Nano Materiels, New Age International (P) Ltd., Publishers, Kolkata, India.
[3]Doremus, R. H. (1965) Optical properties of small silver particles, *J. Chem. Phys. 42, 414-417.*
Rao, K. J. (2002) Structural Chemistry of Glasses, Elsevier Science & Technology Books.
[4]Schulman J. H., Ginther, R. J., C. C. Klick, R. S. Alger and Levy R. A. (1951) Dosimetry of X-rays and gamma rays by photoluminescence, J. Appl. Phys. 22, 1479-14871.
[5]Seward, T. P. (1980) Coloration and optical anisotropy in silver-containing glasses, J. Non-Cryst. Solids 40, 499-513.

P12- Excimer-laser assisted metal-organic deposition of manganite thin films for bolometric applications

K. Daoudi[1, 2], M.Oueslati[1], A. Selmi[2], and T. Tsuchiya[3]

[1] Unité de Spectroscopie Raman – Faculté des Sciences de Tunis, Tunisie

[2] Département de Physique - Faculté des Sciences de Monastir, Tunisie

Kais.Daoudi@fsm.rnu.tn

[3] National Institute of Advanced Industrial Science and Technology (AIST), Tsukuba, Japon.

Perovskite-like $La_{1-x}A_xMnO_3$ (A: Ca, Ba, or Sr) have been widely investigated in recent years in view of potential technological applications in read head memory, spin sensitive devices, and IR bolometric applications [1]. The epitaxial growth of such manganite material in thin film form at low temperature is a vital challenge for further integration in large scale integrated circuit (LSIC) silicon devices. The reductions of the substrate temperature (≲500°C), or of the processing time, are also desirable in order to minimize impurity diffusion and to avoid junction destruction. In this context, we investigated recently the excimer-laser assisted metal-organic deposition (ELAMOD) process for the epitaxial growth of manganite thin films for IR bolometric application [1].

$La_{0.7}Ca_{0.3}MnO_3$ (LCMO) thin films have been epitaxially grown on on (001) single-crystal $SrTiO_3$ (STO) substrates. The starting solutions are made from metal-naphthenate of La, Ca, and Mn, diluted with toluene until obtaining the appropriate concentration and viscosity. Then spin-coated onto single-crystal substrates of $SrTiO_3$ (STO), dried at 100°C and preheated at 500°C to decompose the organic part. Finally for the crystallization and the epitaxial growth, the metal-organic films are irradiated using a KrF (λ=248 nm) excimer laser at 80 mJ/cm^2.

To understand the formation mechanism of the LCMO thin films, we systematically studied the obtained films at different numbers of pulses using X-ray diffraction and cross-section transmission electron microscopy (XTEM).

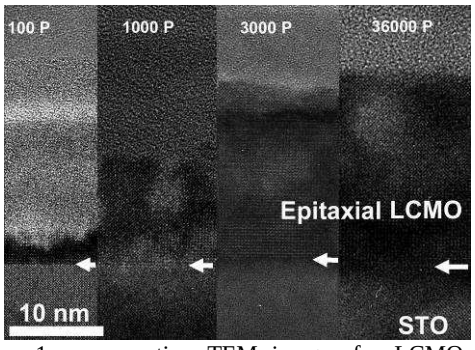

Figure 1: cross-section TEM images for LCMO film grown on STO substrate at a fluence of 80 mJ/cm2 for 100 – 36000 pulses counts at 500°C.

After 100 laser pulses irradiation, the films were found to be partially crystallized at the interface whereas the film was irradiated by the laser from the surface of the film (Fig. 1) . The crystallized part of the film increases with increasing the irradiation time. The completely crystallized film was obtained after 3000 pulses (5 min at a laser frequency of 10 Hz). The interface between film and substrate was very clear. On the other hand, in the case of thermal MOD at 1000°C, the interface between LCMO film and STO substrate was not clear [3]. Thus, the excimer laser irradiation is found to be more effective for preventing the mixing the film and substrate materials.

By increasing the irradiation time, the *R*(*T*) characteristics of the LCMO films changes from that one of a semiconducting material to a typical characteristics of manganite material indicating an important improvement of the oxygen content of the films. For bolometric application we investigated the temperature coefficient of resistance (TCR which determines the device responsivity) of the LCMO films. Promising values of TCR have been obtained.

Finally using the ELAMOD process we can easely epitaxially grow manganite thin films at 500°C for further integration in silicon based based microbolometric devices.

References

[1]Goyal A., Rajeswari M., Shreekala R., Lofland S.E., Bhagat S.M., Boettcher T., Kwon C., Ramesh R. and Venkatesan T., (1997), Material characteristics of perovskite manganese oxide thin films for bolometric applications, *Applied Physics Letters* 71, 2535-2537.

[2]Daoudi K., Tsuchiya T. and Kumagai T., (2005) Pulsed-laser crystallization and epitaxial growth of metal–organicfilms of Ca-doped LaMnO3 on STO and LSAT substrates, *Applied Surface Science*, 253, 6527–6530.

[3]Daoudi K., Tsuchiya T., Yamaguchi I., Manabe T., Mizuta S. and Kumagai T., (2005) Microstructural and electrical properties of La0.7Ca0.3MnO3 thin films grown on SrTiO3 and LaAlO3 substrates using metal-organic deposition, *Journal of Applied Physics* 98, 013507-013512.

P13- Study of electrical properties of $La_{0.67}Ba0_{.33}Mn_{1-x}Fe_xO_3$ pervoskites

A. Abdellatif [1] , H. Rahmouni [1] , M. Baazaoui [2] , S. Zemni [2] , K. Khirouni [1]

[1] Laboratoire de Physique des Matériaux et Nanomatériaux appliqué à l'Environnement, Faculté des Sciences de Gabès, Département de Physique, 6079 Gabès, Tunisie
[2] Laboratoire de Physico-Chimie des Matériaux, Faculté des Sciences de Monastir, Département de Physique, 5019, Monastir, Tunisie

The atomic radii of Mn and Fe are closed to each other. So when we substitute Mn by Fe in $La_{0.67}Ba_{0.33}MnO_3$, the crystalline structure is not modified and a weak concentration of defects is introduced. Then the electrical conductivity of the material depends on free electron concentration and can be adjusted by the amount of the introduced element. To investigate the effect of Fe on electrical conductivity, we study by admittance spectroscopy samples of $La_{0.67}Ba_{0.33}Mn_{1-x}Fe_xO_3$ ($0 \leq x \leq 0.20$) at different temperature and under different voltage bias.

For $x \leq 0$, the material has a metallic behavior and a metal-semiconductor transition is observed around a temperature T_g. The value of T_g decreases when x increases. For $x > 0.1$, the material has an insulator behavior and the metal-semiconductor transition disappears.

At low temperature (T< 200) the conductivity is governed by hoping mechanism. For greater temperature both hopping mechanism and free carrier transport contribute to the conductivity.

The presence of free electron is confirmed by the variation of the polarization of the sample. We find that there is no effect of voltage sign an admittance spectrum. However, when the value of the applied voltage increases, the behavior changes from insulator one to metallic one at high temperature. The activation energy of the defects involved in electrical conductivity is deduced from the measurement. As shown in figure 1, it increases with x.

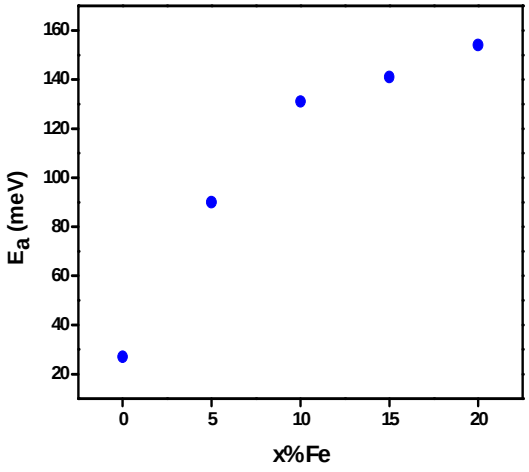

Figure 1: The variation of activation energy deduced from admittance spectra with Fe composition

P14- Effect of gamma irradiation and thermal annealing on the nanocluster formation in silver ion-exchanged silicate glass

K. Farah[1], A. H. Hamzaoui[2], F. Hosni[1], A. Mejri[1], H. Ben Ouada[3]
[1]Laboratoire de Radiotraitement, Centre National des Sciences et Technologie Nucléaires, 2020 Sidi-Thabet, Tunisia , e-mail : ka_farah@yahoo.fr
[2]Laboratoire de valorisation des ressources naturelles et matériaux de récupération, Centre National de Recherche en Sciences des Matériaux, Borj Cedria, B.P. 95, Hammam-Lif 2050, Tunisia
[3]Laboratoire de Physique et Chimie des Interfaces, Faculté des Sciences de Monastir, 5000. Tunisia.

Abstract

Small silver particles embedded in glass matrix are widely studied because of their potential applications for glass colouration (Seward, 1980; Rao, 2002; Ageev et al., 2007; Bandyopadhyay, 2008), for ionizing radiation dosimetry (Schulman et al., 1951) and recently for fabricating optical devices (Bach and Neuroth, 1998). Ion exchange process with irradiation and thermal treatment is an important method for obtaining silver nanoclusters in glasses and provided an alternative way of forming metallic nanoclusters in glass to ion implantation. A microscope slide glasses have been subjected to ion exchange at 320°C in a molten mixture of $AgNO_3$ and $NaNO_3$ with molar ratio of 5:95 for 60 min. The ion exchange process was followed by annealing at the temperature of 550°C for different time periods ranging from 10 to 582 min. Optical properties of the ion exchanged glass are measured using UV–Vis absorption spectroscopy (figure 1). The gamma irradiation induced holes and electrons in the glass structure leading to the creation of a brown colour, and silver ions trapped electrons to form silver atoms. The silver atoms diffused and then aggregated to form nanoclusters after heating at 550°C. The surface plasmon absorption of silver nanoclusters in the glass indicated that the nanoclusters radius grew between 0.9 and 1.43 nm with increasing of annealing time from 10 to 242 min and then saturated. Usually, the growth of metallic clusters in glass is considered as a diffusion-limited process (Bartels et al., 1991; Rao and Doremus, 1996). We found that our data can be fitted by a first order formation kinetic function, which confirmed the diffusion-control process. The average cluster radius R of the clusters is calculated from the full width half maximum, Δλ (FWHM) of the optical absorption peak using the formula: $R = \frac{V_f \lambda^2{}_m}{2\pi C \Delta\lambda}$

Where V_f is the Fermi velocity of the electron in the bulk metal (silver=1.39×108 cm/s), Δλ is the full width at half maximum of the absorption band and λ_m is the characteristic wavelength at which SPR occurs. The FWHM is determined by assuming the absorption peak as a Lorentzian distribution (Doremus, 1965). Both λ_m and Δλ depend on the substrate and size of the metal nanoclusters forming the composites.

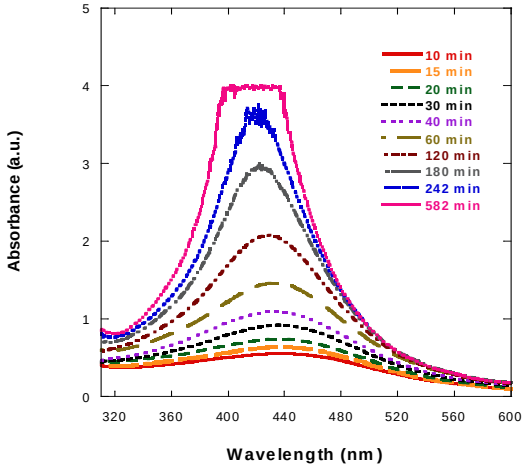

Figure 1: Absorption spectra of ion-exchanged silicate glass, irradiated with γ rays at 250 kGy and annealed at 550°C for the indicated times

References

[1]Ageev, L. A., Miloslavskiĭ V. K. and Makovetskiĭ, E. D. (2007) Coloring of silica glass with silver nanoparticles, Optics and Spectroscopy 102, 442–448.Ii
[2]Bach, H., Neuroth, N. (1998) The Properties of Optical Glass, Springer, Berlin.
[3]Bandyopadhyay,, A. K. (2008) Nano Materiels, New Age International (P) Ltd., Publishers, Kolkata, India.P
[4]Bartels, J., Lembke, U., Pascova, R., Schmelzer, J., Gutzow, I. (1991) Evolution of cluster size distribution in nucleation and growth process. J. Non-Cryst. Solids 136, 181-197.
[5]Doremus, R. (1965) Optical properties of small silver particles, *J. Chem. Phys. 42, 414-417.*
Rao, P., Doremus, R., (1996) Kinetics of growth of nanosized gold clusters in glass, J. Non-Cryst. Solids 203, 202-205.
[6]Rao, K. J. (2002) Structural Chemistry of Glasses, Elsevier Science & Technology Books.
[7]Schulman J. H., Ginther, R. J., C. C. Klick, R. S. Alger and Levy R. A. (1951) Dosimetry of X-rays and gamma rays by photoluminescence, J. Appl. Phys. 22, 1479-1487

P15- Electrical investigation of WO_3 thin layers for ethanol and acetone vapors detection

A. Labidi[a], A. Bejaoui[a], C. Lambert-Mauriat[b] , K. Aguir[b] , M. Maaref[a]

[a] URPSC (UR 99/13-18) Unité de Recherche de Physique des Semiconducteurs et Capteurs, IPEST, BP 51, La Marsa 2070, Tunis, Tunisia.
[b] IM2NP (UMR 6242 CNRS), Université Paul CEZANNE Aix-Marseille III, FST, Campus de St. Jérôme, Service 152 - 13397 Marseille Cedex 20, France.

1. Abstract

The aim of this work is the development of tungsten trioxide sensors for the detection of organics vapors of Ethanol and Acetone. Two WO_3 sensors were realized by reactive RF magnetron sputtering under two different Ar/O_2 rates, during the deposition process. DC and AC impedance spectra of the sensors, allowed us to understand the detection processes of the WO_3 layers.

2. Conductance and response of the sensors under acetone and ethanol vapors

The sensor response versus ethanol and acetone concentrations with an exponent about 1 [1]as illustrated in the fig.1.

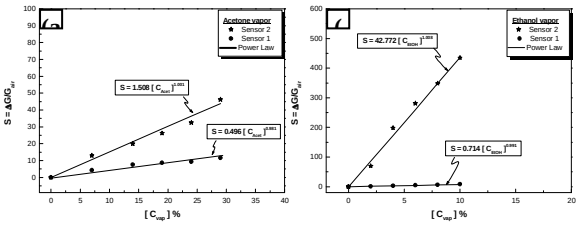

Fig. 1: Sensors responses: (a) under acetone and (b) under ethanol.

The main reactions in our case are the oxidizing of ethanol [2] and acetone[3] vapors

The morphological study of the WO_3 sensitive layers, investigated by atomic force microscopy (AFM) allowed us to explain the observed differences in the response of the sensors. The WO_3 layer of the sensor n°2 presents a homogenous granular structure with small grain size, whereas the active layer of the sensor n°1 is smooth, see Fig.3. So the equivalent specific surface is more important for the sensor n°2. The observed higher response of this sensor could be explained by the ethanol and the acetone molecules size difference, too. Indeed the surface cover rate is higher for the smaller molecules of ethanol.

3. AC measurements and modeling

In Fig. 2 we note that the impedance decreases as the vapor concentration increases. The electrical modeling of the Nyquist spectra by *R-C* circuits, including a resistance R_b in parallel with a capacity C_b shows the existence of an alone semi-circle for different vapors concentrations. So we can deduce that the molecules are adsorbed on the surface of the material without diffusion in the bulk. Therefore only the global resistance of the sensor is changed, since an alone semi-circle is obtained by the impedance modeling, so neither the grain boundaries nor the grain-electrode interfaces take part in the detection process.

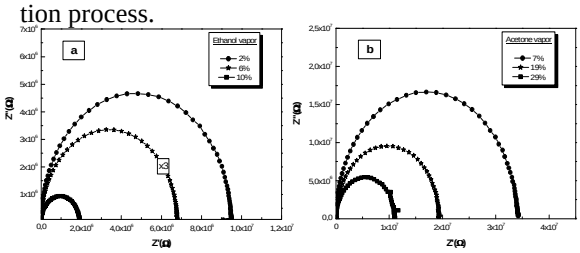

Fig. 2**: AC impedance variation of sensor n°2, under ethanol** (a) **and acetone** (b) **vapors.**

4. References

[1] N. Barsan and U. Weimar, J. Electroceram. 7 (2001) 143-167.

[2] F. Hellegouarc'h, F. Arefi-Khonsari, R. Planade and J. Amouroux, Sens. Actuators B 73 (2001) 27-34.

[3] M. Peschard, Chimie Descriptive, imprimerie Bussière à Saint-Amand, France, p 236 (1965).

P16- Organic nanocomposites for photovoltaic applications

A. Ltaief*, N. Chehata and A. Bouazizi

Laboratoire de Physique et Chimie des Interfaces, Boulevard de l'Environnemenrt, 5019 Monastir - Tunisia
* Corresponding Author : Dr. Adnen Ltaief (adnen_ltaief@yahoo.fr)

Organic photovoltaics (OPVs) are promising low cost alternative to silicon solar cells, thus a great deal of effort is being devoted, both academic and industrial loboratories, to increase the power conversion efficiency and scale-up of the production processes. Organic solar cells are devices, which operate inversely to OLEDs, they convert radiation from the optical range into electricity. Photon absorption in the organic-based composites produces primarily bound-state excitons. Dissociation of these charge pairs is facilitated by the potential difference across a polymer-metal junction, provided by agglomeration of excitons near the interface. The dissociation can be accomplished via electron acceptor impurities, too [1]. Under illumination, a transfer of electrons to the acceptors will take place and the holes will be preferentially transported through the conjugated organic polymer. This process is known as photoinduced charge transfer [2]. An alternative feature of the OPVs based on conjugated polymers is that they can be elaborated by coating process (e.g., spin-coating or inkjet printing) to cover large areas, and may be formed on flexible plastic substrates. This was made possibly by the discovery of photoinduced electron transfer from the excited state of the conjugated polymer (as the donor) onto fullerene C_{60} (as the acceptor) [3]. Much effort has gone into finding the best combination of donor-acceptor pairs, and the optimum fabrication process [4]. Since the discovery of photoinduced charge transfer, a variety of acceptor materials have been introduced into conjugated organic polymers to elaborate photovoltaic devices. 1-(3-methoxycarbonyl)propyl-1-phenyl[6,6]C_{61} known as PCBM is effective in bulk heterojunction solar cells because of its high solubility in common organic solvents, such as toluene and better electron mobility as compared to fullerene C_{60}.

We herein report for the first time on the use of another type of carbon derivatives, known as carbon nanopearls (CNP) (see figure 1), incorporated into MEH-PPV polymer to elaborate nanocomposites for organic photovoltaic devices. We demonstrate that a charge transfer processes occurs inside the nanocomposites, as represented in figure 2. Optical and electrical studied have been investigated to characterize this new nanocomposite: MEH-PPV:CNP, with different CNP concentrations into the polymer matrix, in order to optimize an effective component in the OPVs for enhanced performance.

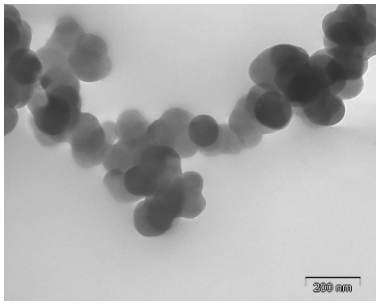

Figure 1: SEM image of carbon nanoperles (CNPs)

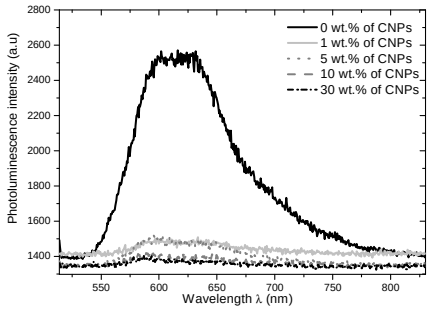

Figure 2: Photoluminescence spectra of organic nanocomposites

References:

[1]: M. Granstrom, K. Petritsch, A.C. Arias, A. Lux, M.R. Anderson and R.H. Friend, Nature 395 (1998), 257.

[2]: A. Ltaief, J. Davenas, A. Bouazizi, R. Ben Chaâbane, P. Alcouffe and H. Ben Ouada , Materials Science and Engineering: C 25 (1) (2005) 67-75.

[3]: N.S. Sariciftci, L. Smilowitz, A J. Heeger and F. Wudl, Science, 258 (1992), 1471.

[4]: A. Ltaief, A. Bouazizi, J. Davenas , P. Alcouffe, Thin Solid Films 516 (2008) 1578− 1583.

P17- Electrochemical impedance spectroscopy for specific detection of *Enterovirus*

M.B. Mejri[1,2], M. Marrakchi[3], H. Baccar[1], S. Helali[1], M. Aouni[2], N. Jaffrezic-Renault[4], A. Abdelghani[1]

[1] Unité de Recherche de Physique des Semi-conducteurs et Capteurs, IPEST, La Marsa, 2070 Tunis, Tunisia
[2] Laboratoire des maladies transmissibles et substances biologiquement actives (LR99ES27), Faculté de Pharmacie, 5000 Monastir, Tunisie
[3] Laboratoire d'Ecologie et Technologie Microbienne, INSAT, Centre Urbain Nord, BP676, 1080 Tunis Cedex, Tunisia . mounamarrakchi@yahoo.fr
[4] Université de Lyon, Laboratoire de Sciences Analytiques, Université Claude Bernard Lyon 1, 69622 Villeurbanne Cédex, France.

Abstract:

The genus enterovirus is constituted by a wide number of viral species having in common many of morphological and genetic characters. These viruses present a high epidemiological power and are in question of various human diseases (Hot 2003). Many techniques were used to detect enterovirus. The nucleic acid detection by PCR remains the most successful tool for their detection although this technique is faced at many problems such as the sensitivity to the inhibitors as well as the big genomic variability of these viruses (Koopmans 2004). Until now, there is no reliable standard and easy to use test. Biosensors appear as a powerful tool for viral detection. Indeed, they give the advantage of the ease of manipulation as well as of the real time analysis. Thus, in this work, we describe the development of an immunosensor based on functionalized gold electrode allowing enteroviruses detection. The biosensor is based on the grafting of specific monoclonal enterovirus antibodies onto functionalized gold electrode. For sensor fonctionnalisation, the thiol is chemisorbed on the gold electrode and it is used as the base interface for the deposition of different layers. The different steps of immunosensor conception were characterized by electrochemical impedance spectroscopy (EIS) (figure 1). For enterovirus detection, different volumes corresponding to different concentrations of viral particles were added. As shown in figure 2, linear relationship between the impedance values and the quantitity of virus was established in the range from 10 to 500 vp for 7 mL. The minimum detectable concentration was around 10 vp for 7 mL or 1.4 vp/mL.

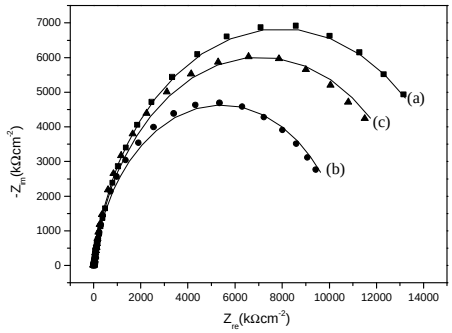

Figure 10: Nyquist diagram (Zr vs. Zi) for the impedance measurements corresponding to: (a) SAM/Au-electrode; (b) antibody/SAM/Au-electrode; (c) blocked with BSA/SAM/Au-electrode.

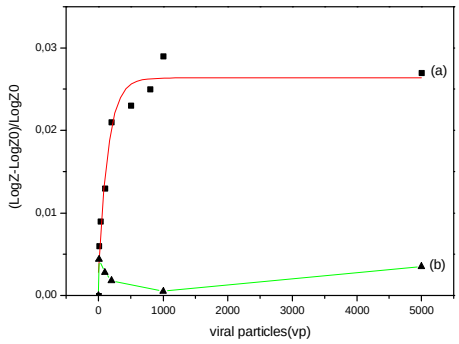

Figure 2: Calibration plots of the variation of impedance with the concentration of viral particles: (a) specific detection; (b) non specific detection

References:

[1] Hot D., Legeay O., Jacques J., Gantzer C.,. Caudrelier Y, Guyard K., Lange M. and Andréoletti L. (2003) Detection of somatic phages, infectious enteroviruses and enterovirus genomes as indicators of human enteric viral pollution in surface water, *Water Res.* 37, 4703.
[2] Koopmans M. and Duizer E. (2004) Foodborne viruses: an emerging problem, *Int. J. Food Microbiol.* 90, 23.

P18- Study of aluminum alloys in nanocrystalline grain synthesis by mechanical milling high energy and consolidated the room temperature and high pressure

M. Ghrib[1], T. Ghrib[1], N. Yacoubi[1,*], A. W. Kolsi[2] and H. Ezzawia[1]
[1]Institut Préparatoire Aux Etudes d'Ingénieur de Nabeul IPEIN Merazka 8000 Nabeul-Tunisie
[2]Laboratoire de Photovoltaïque et des Semi-conducteurs et des nano-structure ,(CRTEn), Technopôle de Borj-Cédria *B.P. 95, 2050 Hammam-Lif,Tunisia.*
[3]Facuté des sciences de Sfax.

INTRODUCTION

It has been well established that high-energy mechanical milling is one of the major techniques for producing powders with nanocrus talline structures [1,2]. The consolidation of high energy mechanically milled powder is an essential process for achieving the final objectives [3]. Consolidation of milled powders into bulk, full-density compacts preserving nanometric grain size, which is crucial for possible application of nanophase materials, is not easy to achieve. In fact, full consolidation of nanocrystalline or amorphous aluminium alloy powder during conventional extrusion was achieved only at temperatures of 450°C [4].On the other hand, obtaining bulk nanocrystalline Al alloys by consolidation technique is of the interest not only due to the improved hardness and strength but also because of expectations of better ductility and thermal properties comparing with their coarse-grained counterparts. The aim of this work is to study the microstructure produced by severe plastic deformation (SPD) technique under room temperature pressure consolidation using nanocrystalline Al-based alloy powders prepared by high-energy mechanical milling and to investigate their mechanical and thermal behaviours. The thermal properties are determined by applying the Photothermal Deflection (PTD) technique which is a non destructive technique was applied for determining the optical and thermal properties of several materials [5,6].

EXPERIMENTAL RESULTS

X-Ray diffraction analysis

Fig. 1 shows the typical X-ray diffraction patterns of Al alloy after room temperature consolidation and as a function of annealing temperature. It contains the (111), (200), (311) and (222) fundamental reflections. From the XRD data and X-ray emission spectrometry in the SEM, these peaks were found to be relative to Al_9Fe- phase.

Microscopic observations

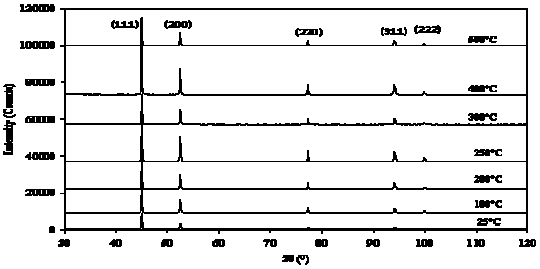

Figure 1: XRD patterns of Al alloy obtained

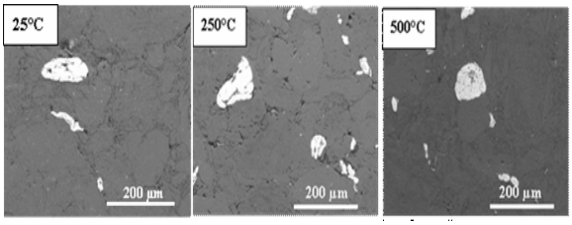

Figure 2: SEM-images for

Determination of the thermal properties

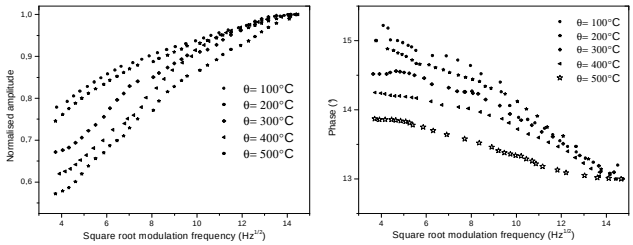

Figure 3: Experimental variation of the amplitude and phase

[1] Gaffet E, Le Caër G. Encyclopedia of nanoscience and nanotechnology Edited by Nalwa HS. 2004; X: 1-39.
[2] Koch CC. Nanostructured Materials 1997; 9: 13-22.
[3] Yavari, Botta Filho WJ, Rodrigues CAD, Cardoso KR, Valiev R, Scripta Mater. 2002; 46: 711–716.
[4] Senkov ON, Senkova SV, Scott JM, Miracle DB. Materials Science and Engineering 2005; A 393: 12-21.
[5] A. Mandelis, Photo acoustic and Thermal Wave Phenomenon in Semiconductors, Elsevier, New York, 1987.
[6] Taher Ghrib, Fatah Bejaoui, Abdelwahheb Hamdi, Noureddine Yacoubi, Thermochimica Acta 473 (2008) 86–91.

P19- The effect of the excitation density and of the temperature on the photoluminescence circular polarization of AlInAs/AlGaAs quantum dots

N. Sellami[1], A. Melliti[1], A. Sahli[1], M. A. Maaref[1], C. Testelin[2],R.Kuszelewiez[3]
[1]Unité de Recherche de Physique des Semiconducteurs et Capteurs, IPEST, La Marsa 2070, TUNISIA
trikinajette@yahoo.fr
[2] Institut des NanoSciences de Paris, Campus Boucicaut, Universités Paris 6 et 7, CNRS, UMR7588, 140 rue de Lourmel, 75015 Paris, FRANCE[3]*Laboratoire de Photonique et* Nanostructures, CNRS, UPR 20, FRANCE

Abstract: In this paper, we present a study of photoluminescence (PL) from AlInAs/AlGaAs quantum dot (QD) structures grown by molecular beam epitaxy. Specifically, we describe the effects of the temperature and of the excitation density on the photoluminescence circular polarization. We have found that the circular polarization degree depends on temperature. This behavior can be explained by the acoustic phonon process [Tackeuchi] who becomes more important in our self assembled QD's. This importance originates from the low energy tail of the continuum states associated with wetting layers who is very close to the QD's.
On the other hand, the study of the excitation density dependent circular polarization degree shows an increase for the sample of weak dot density, containing 10^{10} cm^{-2} of QD's (sample A). However in the case of large dot density, containing 2.10^{11} cm^{-2} of QD's (sample B) the circular polarization degree is practically constant when the excitation density is varied from 0.116 W. cm^{-2} to 9 W. cm^{-2} . This behavior can be explained by the the effect of spin redistribution over the energy spectrum due to the differential Pauli blocking [Kalevich]. However, in isolated QD's, the circular polarization degree increases due to an increase of the excited states population. In the coupled QD's, the circular polarization remains constant while the excitation density is not high enough to fill a considerable part of the QD ground states.

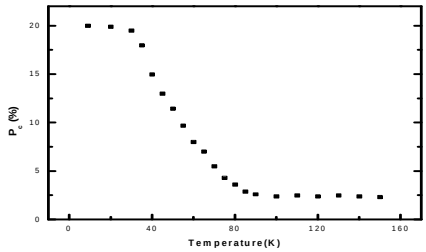

Figure 1: Temperature dependence of circularly polarization degree

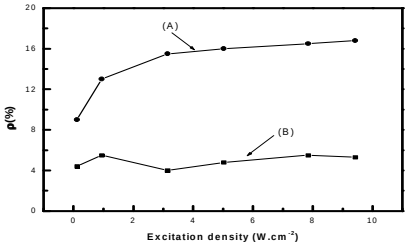

Figure 2: Excitation density dependence of circularly polarization degree

References:

[1] A. Tackeuchi, R. Ohtsubo, K. Yamaguchi, M. Murayama, T. K. Itamura, T. Kuroda, T. Takagahara (2004), Appl. Phys., Lett. 84 3576
[2] V. K. Kalevich, M. Paillard, K. V. Kavokin, X. Marie, A. R. Kovsh, T. Amand, A. E. Zhukov, Yu. G. Musikhin, V. M. Ustinov, E. Vanelle, and B. P. Zakharchenya, (2001) Spin redistribution due to Pauli blocking in quantum dots, Physique Review. B 64 , 045309

P20- Electrical characterization of InN/InP heterojunction with quantum effect

N. Mecirdi[1], Z. Benamara[1], B. Akkal[1],
B. Gruzza[2], S. Benkhalifa[2], C. Robert-Goumet[2], L. Bideux[2]
[1] Laboratoire de Microélectronique Appliquée, Université de Sidi bel Abbès, 22000 Sidi Bel Abbès, Algérie.
[2] Laboratoire des Sciences des Matériaux pour l'Electronique et d'Automatique, Université Blaise Pascal de Clermont II, Les Cézeaux, 63400 Aubière Cedex, France.

Introduction: An extremely thin (4- monolayers) InN film was realised by the nitridation of InP substrates using a Glow Discharge Source (GDS). The electrical properties of the elaborate hetero-junction are investigated by current-voltage (I-V) and capacitance-voltage (C-V) measurements. From I-V curves, we notice a strong tension of threshold 4.47 V and great serial resistance 1.1 KΩ. The ideality factor η determined by applying positive potential in InN and negative potential along InP is found to be 1.38. From the C-V curve, we observed a variation around zero volts (between -0.5Volt and 0.5Volt) see figure 1. and a constant capacitance for positive voltage. This indicates that our structures present special behaviour. The diagram band of InN/InP hetero-structures was modelled to understand the phenomena transport in these diodes (see figure 2). However, a quantum effect that appears in miniaturized hetero-structure and new nonelectric devices has been proposed to explain the experimental observations [7].

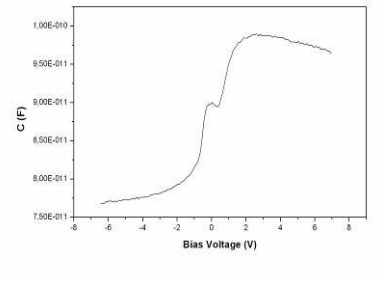

Figure 1 : The C-V characteristics plotted at high frequency (1MHz).

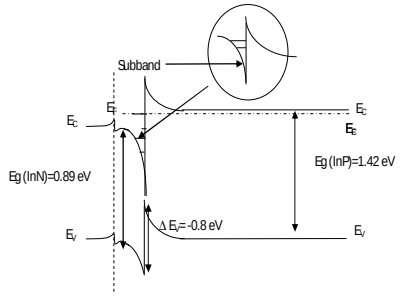

Figure 2: The diagram band (Conduction Band level) of InN/InP for zero bias voltage.

References:

[1]Anderson R.L., Solid State Electron. 5 (1962) 341.
[2]Achard B., Gruzza B., Pariset C. Surf. Sci., 160, L519 (1985)
[3]Brennan K. F., Brown A. S.: theory of modern electronic semiconductor devices
(John Wiley & Sons, New York, 2002).
[4]Akkal B., Benamara Z., Abid H., Talbi A., Gruzza B., Materials Chemistry and Physics 85, 27-31(2004)
[5]Akkal B., Benamara Z., Gruzza B., Bideux L., Vacuum 57, 219(2000).
[6]Akkal B., Benamara Z., Abid H., Talbi A., Gruzza B. Materials Chimistry and physics 85 , 27-33(2004).
[7]Benamara Z., Akkal B., Talbi A., Gruzza B., Bideux L., Mater. Sci. Eng. C 21, 287(2002).
[8]Bhuiyan A. G., Hashimoto A., Yamamoto A. J. Appl. Phys., 94, 2779 (2003).
[9]Beuchet G., Bennet M., Thebault P., Duchemin J. P. J. Cryst. Growth, 57, 379 (1982).
Bideux L., Gruzza B., Porte A., Robert H. Surf. Interface. Anal., 20, 803(1993)
[10]Chellali M., Akkal B., Tizi S., Benamara Z., Gruzza B., Robert C., Bideux L., Mater. Sci. Eng. B,77, 19(2000).
[11]Davydov V. Y., Klochikhin A. A., Emstev V. V., Ivanov S. V., V. V. Vekshin, F. Bechstedt, J. Furthmuller, H. Harima, A. V. Mudryi, A. Hashimoto, A. Yamamoto, J. Adrhold, J. Graul, and E. E. Haller. Phys. Stat. Sol.(b) 230, R4 (2002).
[12]Farag A.A.M., Terra F.S., Mahmoud G.M., Sensors and Actuators: A Physical, 150, 231-236 (2009)
Gautard D, Laporte J.L., Cadoret M., Pariset C. J.Cryst.Growth. 71, 125(1985)
[13]Gruzza B., Achard B., Pariset C. Surf. Sci., 162, 202(1985)
[14]Mangat P.S., Soukiassian P., Huttel Y., Hurych Z., Gruzza B., PorteA. Appl. Phys. Lett., 63, 1957 (1993)

P21- Phase determination with direct methods

A. Direm, H. Boussekine et N. Benali-Cherif

Laboratoire des Structures, Propriétés et Interactions Inter Atomiques (LASPI^{2}A).
Institut des Sciences Exactes, Technologie et Informatique.
Centre Universitaire de Khenchela 40000, Algérie.
Amani_Direm@yahoo.fr

Abstract : The crystal structure determination with X-Ray diffraction provides very important information about the arrangement of the atoms in the crystalline coumpounds which can be used to understand their different physical and chemical properties. In an X-ray diffraction experiment, we measure the intensities of reflections and perform a Fourier synthesis. The calculation of an electron density map, which provides an interpretable picture of a molecule, requires both intensities and phases. Unfortunately, the most important parameter we need for locating the atoms in the unit cell : ''the phase value" is lost. This severe lack of information is the so-called ''phase problem'' of crystallography. The standard techniques and approaches (Multan [3, 5], ShelXD [6], Sir99 [2], etc.), developed in order to solve this problem, are based on the application of direct methods which estimate the phases of the Fourier transform of the scattering density from the observed intensities. We will describe in detail the different steps and procedures followed for the structural resolution of our compounds [1].

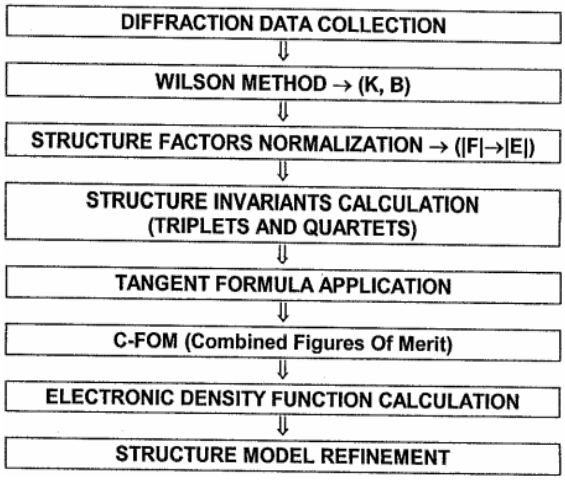

Figure.1: Main Steps in a typical direct methods procedure [4]

References:

[1]Benali-Cherif, N., Direm, A., Allouche, F. & Soudani, S. (2007) Hydrogen bonding in 4-Carboxyanilinium dihydrogenphosphate. *Acta Cryst*, E63, 2272–2274.
[2]Burla, M. C., Camalli, M., Carrozzini, B., Cascarano, G. L., Giacovazzo, C., Polidori, G. & Spagna, R. (1999) SIR99, a program for the automatic solution of small and large crystal structures. *Acta Cryst*, A55, 991-999.
[3]Germain, G. & Woolfson, M. M. (1968) On the application of phase relationships to complex structures. *Acta Cryst*, B24, 91-96.
[4]Giacovazzo, C., Capitelli, F., Cuocci, C. & Ianigro, M. (2002) Direct methods and Applications to Electron Crystallography, *Elsevier Science* (USA).
[5] Main, P., Fiske, S. J., Hull, S. E. Lessinger, L., Germain, G., Declercq, J. P. & Woolfson, M. M. (1980) *MULTAN80: A System of Computer Programs for the Automatic Solution of Crystal Structures from X-ray Diffraction Data*, University of York and Louvain.
[6]Sheldrick, G. M. (1998) (ed. S. Fortier) SHELX: Applications to macromolecules. In: *Direct Methods for Solving Macromolecular Structure,*. Dordrecht: Kluwer Academic Publishers

P22- 2-methylanilinium nitrate

H. Boussekine, A. Direm et N. Benali-Cherif

Laboratoire des Structures, Propriétés et Interactions Inter Atomiques (LASPI^{2}A).
Institut des Sciences Exactes, Technologie et Informatique.
Centre Universitaire de Khenchela 40000, Algérie.
houda.bouss@hotmail.fr

Key words : 2-Methylaniline, The asymmetric unit, hydrogen-bonding, hybrid materials, anilinium derivatives.

Abstract : O-toluidine is used in the manufacture of rubber vulcanization accelerator, hypnotic and anesthetic pharmaceuticals, and pesticides. 2-Methylaniline is highly toxic to humans when absorbed through the skin, inhaled as vapor or swallowed; hemoglobine is changed to methemoglobinand and caused damage to the cells of the central nervous system.
The crystal structure of o-methylanilinium nitrate, was determined as part of our investigations on the structural characteristics of organic-inorganic layered compounds and an ongoing study on D-H…A hydrogen-bonding in systems of hybrid materials including anilinium derivatives such as 4-Carboxyanilinium hydrogensulfate (Benali-Cherif, Direm et al., 2007), 2-carboxyanilinium dihydrogenphosphite (Benali-Cherif, Allouche et al., 2007) and Guaninium phosphate and guaninium phosphate salts (Bendeif et al. 2007).
The asymmetric unit of o-methylanilinium contains a monoprotonated o-methylanilinium cation and nitrated anion (Figure 1). Intra atomic bond distances and angles in the title compound shows the monoprotonation of the organic entity and confirms the presence of the nitrate (NO_3^-) anion, all atoms in the asymmetric unit except three are positioned on a mirror plane (x, ¼, z).The crystal structure determination with X-Ray diffraction provides very important information about the arrangement of the atoms in the crystalline coumpounds which can be used to understand their different physical and chemical properties.

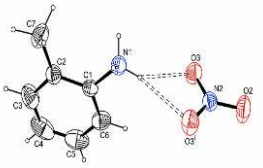

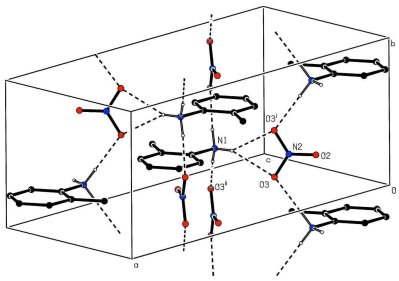

Figure 1: The asymmetric unit of o-methylanilinium

The structure of ($C_7H_{10}N^+$. NO_3^-) is composed of cationic ($C_7H_{10}N^+$), and anionic (NO_3^-) entities which are linked by N_H…O hydrogen bonds to build up layers developing parallel to the (100) pane (Figure. 2).

Figure 2: Partial packing view showing the hydrogen- bonding network.

References:

[1] Benali-Cherif, N, Allouche, F, Direm, A, Boukli-H-Benmenni, L, et Soudani, K, Acta Cryst. E63, o2643-o2645, (2007).
[2]Benali-Cherif, N, Direm, A, Allouche, F, Boukli-H-Benmenni, L, et Soudani, K, Acta Cryst. E63, o2054-o2056, (2007).
[3]Benali-Cherif, N, Allouche, F, Direm, A & Soudani, K. Acta Cryst. E65, o664–o665 (2009)

P23- Study of the behavior of mortars based of cements composed toward the attacks of acids waters

M. Driss[1], A. Kerbouche[2] et N. Oumrani[3].

[1]Laboratoire des Sciences et Techniques de l'Eau (L.S.T.E), Université de Mascara, BP 637, Mascara, Algérie.
driss_miloud@yahoo.fr / driss_miloud@univ-mascara.dz
[2]Laboratoire L.A.B.M.A.T. Département of Civil Engineering -ENSET- B.P.1523, El Mnaouer ,Oran, Algérie.
[3]Post graduant en Hydraulique et Directeur du Barrage Chourfa, Mascara, Algérie.

Abstract:
The lifespan of a concrete structure is often related to the capacity of concrete to prevent aggressive agents, which can be soluble in water, penetrated by its porosity. This may be an environmental protection and to better understand the problems associated with acid water and the environment. Some environments are aggressive for concrete, they can cause significant chemical attack, swelling causing the collapse of concrete,... This is in particular the case of zones subjected to the frost, marine environments and chemical environments (including industry and agricultural).

The purpose of our study is to follow the evolution of different attacks acidic solutions include: hydrochloric acid, nitric acid, sulfuric acid and phosphoric acid on mortars elaborated in different terms according to the standard ASTMC 267-96 to make cubic samples are made according to standard NFP15-403 with different cements from three cement plant in north-west Algeria for a period of immersion of 1 to 42 days by quantifying the loss of resistance (bending and compression) and mass losses related.

The acid sulphate solutions lead to a formation of surface gypsum and ettringite in contact with the cement matrix. For nitric acid solution, the formation of soluble calcium nitrate and phosphatic acid formation of calcium hydrogen phosphate hydrate is very superficial. Finally, hydrochloric acid, the surface of the mortar is covered with calcium chloride dihydrate and iron hydroxide. The mechanical resistance and mass losses are related more or less affected by the nature of acids in the order with the most aggressive HCI and HNO_3, H_2SO_4 and then finally some modification for H_3PO_4.

Figure: the state of prismatic specimens after acids attacks.

References:

[1]Achoura, D. Lanos, C. Jauberthie, R et Redjel, B. (2004) *Inflience d'une substitution partielle du ciment par laitier de hauts foureaux sur la résistance des mortiers en milieu acide*, Journal physique IV France 118, pp 159 -164,2004.

[2]Boukerrouche, N. Amouri, C et Houari H (2008) *Influence des paramétres de composition et d'environnement*, Université Mentouri Constantine, Colloque national, Pathologie des constructions : Du diagnostic et la réparation, 25 et 26 Novembre 2008, Constantine Algérie.

[3]Khelifa, R. Rahim, N et Al-Mukhtar, M (2004) *Influence des ciments à base d'ajouts minéraux locaux sur les propriétés mécaniques des mortiers et des bétons*, XXIIEMES RENCONTRES AUGC – VILLE & GENIE CIVIL 3 & 4 juin Université de Marne-la-Vallée, France.

[4]Roy, D.M. Arjunan, P &. Silsbee, M. R (2001) Effect of silica fume and lom-calcium fly ash on chemical resistance of concrete, *Journal of Cement and Concrete Research*, Vol. 2, pp 1809-1813, 2001.

[5]Janotka, I. (1999) *the influence of zeolitic cement and sand on resistance of mortar subjected to hydrochloric acid solution attack*, CERAMICS, Silikaty, Vol 43, N°2, pp 61-66. 1999.

[6]Yamani, N. Elasdi, K et Zaim, M. *(1992) l'utilisation du sable de mer et le concassage dans le morties de ciment*, Revue Marocaine du génie civil, N°42, Dec 1992.

P24- Physical design kit pre-layout and post-layout validation

M. Haddoug [1], G.Gaaliche [2], W.Boujarra [3]

STMicroelectronics, TR&D -CCDS -Program Management & Services
CMOS & Derivative Physical Design Kit
[1] moumtez.haddoug@st.com, [2] ghassen.gaaliche@st.com, [3] wahbi.boujarra@st.com

Introduction: The complexity of Physical Design Kits (PDK) is in exponential increase. As a result, framework manual validation is beginning to be a laborious step and can no more follow this evolution. In this paper, we introduce the pre-layout and post-layout automatic validation frame-work based on emulating designer interactions with PDK, net-listing and comparison, layout parasitic extraction, regression test, results compilation and de-bug capabilities.

Validation of schematic and model simulation: Increased level of automation is crucial because the time consuming, complex and essential validation costs are to be controlled. In this section we evaluate the dependencies between tools, data and environment in Front End process design kits (Pre-layout simulation). Vsim tool allows creating different schematics to validate a specific models functionality and effect, coverage of all selected simulation sets and a regression engine which executes sets of comparing simulation result and netlist. [1],[2],[4],[6],[8],[9]

Table 1: Percentage gain time by technology:

techno	*Possibly Case*	*Manuel simulation time (h)*	*Vsim simulation time (h,min)*	*Gain (%)*
65nm	480	40	6,0	85
250nm	360	30	5,0	83.3
55nm	165	13	4,5	68.5
32nm	98	8	3,13	59.7
90nm	70	5	1,30	70
65nm: Img	50	4	1,15	68.7

Validation of post layout simulation (PLS) modules: The TestCaseBuilder tool generates the basic test-cases used for PLS modules validation. We introduce an automated Quality Assurance (QA) procedure, using the same tool Vsim that helps validating: netlist parameters, pins order, device model names, PLS/LVS (Layout Vs. Schematic) extraction as well as the intra-device parasitic extraction accuracy and non-regression test. [3],[5],[7],[10]

Table 2: Manual vs. Automated QA times.

Technology node	*Manual QA*	*Automated QA*
0.13um	8 hours	11min 43sec
65nm	24 hours	28 min
45nm	8 hours	6min 56sec
32nm	16 hours	14min 36sec

Conclusion:
Technology independent automation tools (Vsim, TestCaseBuilder…) allows accelerating the FW PDK verification process (especially pre-layout and post-layout simulation), increasing the productivity and improving a global high level quality of PDK thanks to bigger test-vectors generated.

References

[1] Agilent. Ads (rfde) Users Guide.
http://www. agilent.com
[2] Cadence. IC and mmsim Users Guide. Skill language programming.
http://www. cadence.com
[3] Davis, J.A.; Meindl, J.D. (2003) Interconnect technology and Design for Gigascale integration, Kluwer Academic Publishers, p67-105.
[4] Jacques Gautier (2004). Modèles électriques pour la conception des circuits intégrés silicium.
[5] Moez, K.K.; Elmasry, M.I. (2005) Post Layout Simulation of RF CMOS Integrated Circuits with Passive Components, IEEE Circuits and Systems. 48th Midwest Symposium, 762 - 765 Vol. 1
[6] Mentor. Eldo Users Guide.
http://www. mentor.com
[7] Scott, M.C.; Peralta, M.O.; Carothers, J.D. (2003) System and framework for QA of process design kits, Quality Electronic Design, 2003. Proceedings. Fourth International Symposium, 138 – 143 Vol. 2
[8] ST-Microelectronics. Design Kit and ArtistKit Users Guide. http://www.st.com
[9] Synopsys. Hspice Users Guide.
http://www. synopsys.com
[10] Zemke, C.; Lagu, J.; Brelsford, K. (2005) Numerical Analysis of Parasitic Effects in Deep Submicron Technologies, SNUG San Jose.

P25- A low power ASIC design of a FSS motion estimator for H.264AVC

Salah Dhahri[1], Leila Kabbai[1], Abdelkrim Zitouni[1], Kholdoun Torki[2], Rached Tourki[1]
[1]Laboratory of Electronic and Micro-Electronic (LAB-IT06)
Faculty of Sciences of Monastir, 5019, Tunisia
[2]TIMA-CMP Laboratory, INPG, 46, Félix Viallet 38031, Grenoble Cédex, France

Abstract:

In the past few decades, we have been running towards the Digital Age. Telephony networks, fiber optic networks, Internet, satellites, third-generation (3G) wireless networks, these advanced transmission technologies and network infrastructure ensure digital information can flood into every corner around us. So, many application of digital image processing are enhanced by motion estimation algorithms. In a video Codec such as H264AVC, motion estimation comprises one of the most important compression methods for video communications. Since this task is computationally intensive to result in large power consumption, a low-power design is essential for portable or mobile systems. This paper presents a new Four Steep Search (FSS) motion estimation architecture design. Our basic idea is based on pipelining the treatment on using nine processing-elements (PE) and shutting down each PE when it is not under running by gating its clock with a specific signal. Two versions (Synchronous and gated clock) of a FSS motion estimator have been designed and implemented with a 45 nm CMOS ASIC technology. Experimental results show that the gated clock version allows a power consumption witch is 36.32% time lower than the power dissipated by the synchronous version. A comparison with other FSS architectures presented in the literature which are designed with different technology has been also presented. This comparison shows that our gated clock architecture is characterized by the higher speed and the lower dissipated power.

Results: In order to verify the functionality correctness and to estimate the power dissipation of the proposed ME, we have modeled its architecture by VHDL as an edge-triggered synchronous system. The design has been synthesized by using Xilinx ISE9.2 FPGA and ASIC design tool.

A power measurement has been performed by the X-Power Xilinx tool and has been performed by the environment Synopsys (Design Vision tool) and the Cadence environment (Encounter Tool) by using the technology CMOS 45 nm. The maximal frequency (330 MHz) as generated by the synthesis tool has been used for the switching power estimation of the synchronous architecture and the stoppable clock based architectureExperimental result of the proposed architecture and the synchronous architecture are shown in Table 1 and Table2.

Table 1: Results of conception of synchronous and GALS estimator by the FPGA environment

	synchronous version	**GALS version**
Number of cycle	92945	12825
Number of LUT	3396	2264
Power (mW)	25.49	16.23
Power Gain	36.32%	

Table2: Results of conception of synchronous and GALS estimator by the Synopsys environment

Estimator	**Total Surface (mm^2)**	**Total Power (mW)**
Synchronous	0,026	3,88
GALS	0,024	2,9

P26- Microscopic observations and dielectric behavior showing a demixing phenomenon in chiral tilted smectics liquid crystals

T. Soltani[1], A. Gharbi[1], J.P. Marcerou[2], H.T. Nguyen[2]

[1]Laboratoire de Physique de la Matière Molle; Faculté des Sciences de Tunis, TUNISIA

tawfik_sol@yahoo.fr

[2]Centre de Recherche Paul Pascal, Pessac, FRANCE

Abstract :

The structures of the subphases present in a liquid crystal are almost completely known yet but many complex phenomena are still not understood. So the experimental and theoretical studies are still interesting. We have synthesized and studied three types of liquid crystal. The experimental results show an unexpected behavior in planar cell capacitors:

i) The ferroelectric SmC* phase coexists with anticlinic and/or ferrielectric phase in a temperature range where the ground phase is purely ferrielectric.

ii) This demixing phenomenon is not due of the thickness effect; rather it is probably induced by an electric effect: coexistence of polar phase with a non polar phase.

Our results confirm the existence of the demixing phenomenon in the liquid crystal exhibiting ferroelectric phase but we show that it does not disappear when increasing the sample thickness.

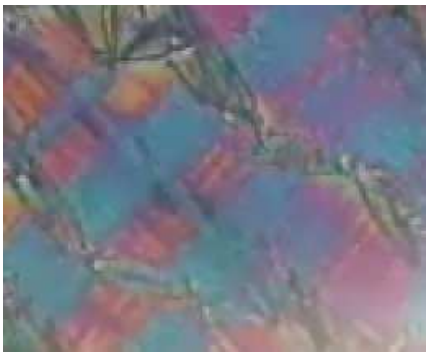

Figure 1: The texture of a coexistence of two phases

This unexpected phenomenon is explained: the ferroelectric phase is responsible for its occurrence and it is due to a polarization effect and not to a thickness effect.

This result allowed us to explain the dielectric behavior in the ferrielectric and anticlinic phases in thin planar cells.

P27- A new 3D abacus as a tool for phothovoltaic-thermal (PV-T) binary and ternary semiconductors scaling

S. Dabbous, T. Ben Nasrallah, A. Amlouk, K. Boubaker, M. Amlouk and S. Belgacem

Unité de physique des dispositifs à semi-conducteurs, Faculté des sciences de Tunis,
Université de Tunis El Manar, 2092 Tunis - Tunisie.
mmbb11112000@yahoo.fr

Introduction: This study presents a new 3D abacus for scaling binary an ternary semiconductors layered materials. This abacus gathers originally three relevant and determinant parameters in the choice of oxides, sulfured compounds and similar PVC semiconductors constituants:

- The electronic bangap E_g.
- The Vickers Microhardness Hv.
- The Amlouk-Boubaker Optothermal Expansivity ψ_{AB}.

The latter parameter ψ_{AB}, has beeen defined in precedent published studies (Fridjine et al., 2009; Ben Mahmoud et al., 2009) as the ratio of the thermal diffusivity to the optical effective absorptivity (Amlouk, 2009). In the last three decades, choice of semiconductor materials for PVC buffer or windows layers was generally and sometimes soley based on the bandgap range requirements. This feature was legitimous and appropriate until appearance of new generation PV-T cells and light-heat converter devices. Actually, and due to environment and economical constraints, the thermal performance as well as the mechanic resistance are more and more taken into account.

Prelude: In our laboratory, we tried since 1985, to produce binary and ternary compounds for light conversion purpose. In the earliest attempts, zinc-doped In_2S_3 (namely $ZnIn_2S_4$), selenized ZnS (namely $ZnS_{1-x}Se_x \mid_{0\le x<0.5}$) and binary oxides (ZnO, TiO_2, WO_3...) have been synthesized using several processes. It was noticed that parallel to the expected enhancement in terms of bandgap shift, many other structural and morphological changes occurred.

In the same context, the recent experiment on lightly Ytterbium-doped ZnO thin films, and pure ZnO layer prepared at different substrate temperatures (Amlouk, 2009), exhibited drastical changes in physical parameters more than in optical characteristic.

Additional investigations yielded spectacular results about thermal and mechanical changes during elaboration process.

The 3D abacus: Consequently, it was appropriate to evaluate these changes using common tools (Roughness measurements, mechanical tests…). The gathered results evoked the need of a scaling tool as a guide to material global performance evaluation and comparison.

Starting from the recorded data, two parameters have been defined:

- The optical effective absorptivity $\hat{\alpha}$.
- The Optothermal Expansivity ψ_{AB}.

A new 3D abacus (Fig. 1) has been established with respect to bandgap E_g, Vickers Microhardness Hv and the Optothermal Expansivity ψ_{AB}.

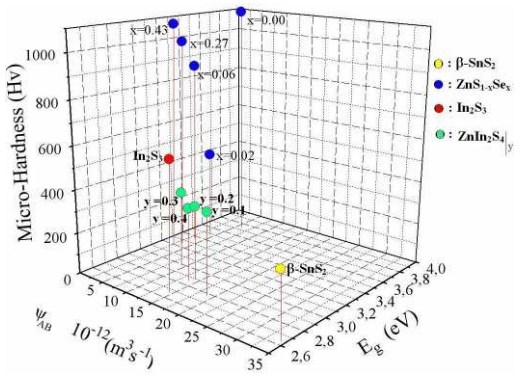

Figure 11: 3D E_g - ψ_{AB} - Hv abacus.

References:

[1]Amlouk A., Boubaker K. and Amlouk M. (2009) Effects of substrate temperature on sprayed ZnO thin films optical and morphological properties in terms of Amlouk–Boubaker opto-thermal expansivity ψ_{AB}. Journal of Alloys and Compounds 482, 164-167.

(2]Ben Mahmoud K.B. and Amlouk M. (2009) The 3D Amlouk–Boubaker expansivity–energy gap–hardness abacus: A new tool for optimizing semiconductor thin film materials, *Materials Letters*, 63, 991–994.

[3] Fridjine S., Boubaker K. and Amlouk M. (2009) The Optothermal expansivity: A Boubaker polynomials expansion-related parameter for optimizing PV-T hybrid solar cells functional materials. *Functional Materials Letters*, 2, 127-135.

P28- Study of the ferromagnetic transition of a nanoscale samples by the PTD technique

T. Ghrib[1] , M.S. Ben Kraîem[2], N.Yacoubi[1], , A. Cheikhrouhou[2] and C. Bordel[3]

[1] Photothermal Laboratory, IPEIN, 8000 Nabeul, TUNISIA.
taher.ghrib@yahoo.fr.
[2]Laboratoire de Physique des Matériaux, Faculté des Sciences de Sfax,
B.P. 802 – 3018 Sfax, TUNISIE.
[3]Groupe de Physique des Matériaux UNR CNRS 6634,BP12,
saint etienne du Rouvay Cedex, FRANCE.

Abstract: The study of the material characterised by its specific physical proerties giving an important changes after certains operations as the material used for its high electrical resistances.
these samples appear to those invented by Albert Fert and Peter Grünberg in 1988, which are thin layers characterized by giant magnetoresistance.

Introduction : In this work we have investigate samples consisting of stacking 20 nanoscale layers alternating of Fe and Mn.
Our study was, first, to develop a simple model to simulate and study the influence of indirect exchange coupling on the magnetic and thermal properties of multilayer (Fe / Mn). By studies that made it has been shown the dependence of the coupling constant versus the thickness of the layer of manganese.
To show the effect of the manganese layer thickness on the coupling constant, we have maintained the iron layer thickness constant and we have varied the thickness of the manganese layer from 0.3 to 1.7nm. Experience shows that depending on the manganese layer thickness there are two magnetic coupling types ferromagnetic and antiferromagnetic . A study with the PTD technique [1] shows the ferromagnetic-antiferromagnetic transition is realised a thickness of Mn in the range 1.5nm (fig.1).
This study is to follow the evolution of the photothermal signal versus the modulation frequency of the pump beam that heats the samples and find the values of thermal conductivity and thermal diffusivity that give the coincidence between the experimental (fig.2) and theoretical curves using an adequate theoretical model.
We remarck after this study that for a Mn thickness superior to 1.5 nm the thermal resistivity sudden an important increase like the electrical one.

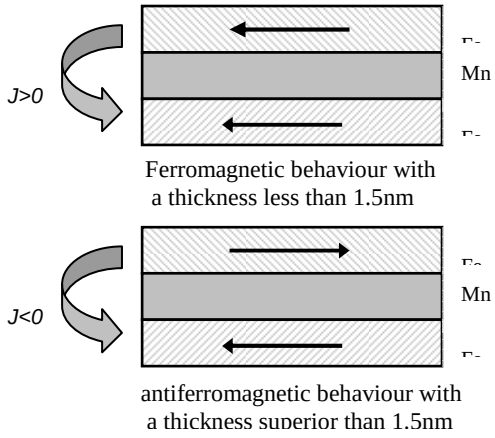

Figure 1

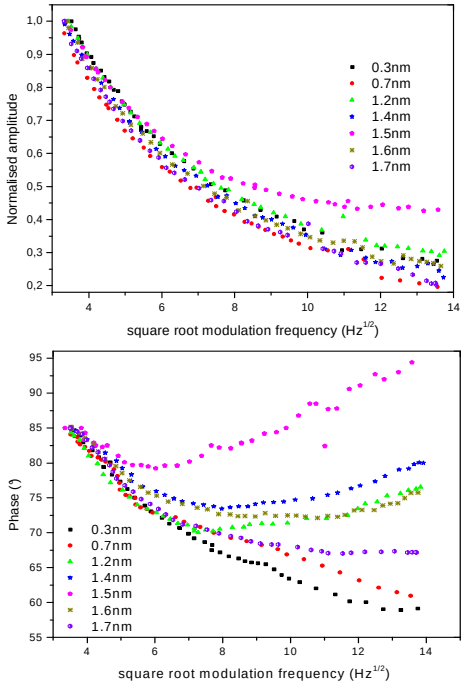

Figure 2

Reference:

[1] T. Ghrib, Y. Noureddine, F. Saadallah, J. Sensors and Actuators A 135, pp 346–354, 2007.

P29- Study and realization of an electric process to fight against harmful insects « KAHRATRAP »

Y.Benmimoun[1], S.Flazi[2], A.Tilmatine[3] & O.Rabah[3]
[1] Directeur du laboratoire « L.S.T.E » université de Mascara
ybenmimoun2000@yahoo.com
[2] Université des sciences et de la technologie d'Oran
[3] Université de Sidi Belabbes

Abstract:A device for catching insects, using a high voltage electrical discharge, called KAHRATRAP, is designed and builds up by the first author of this paper. The aim of this paper is to describe the electrical operation mode of this apparatus such as the high voltage supply and the electrical discharge which this supply produces for the elimination of insects. Moreover, we analyze the influence of climatic parameters such as temperature, humidity and speed of wind on the efficiency of the apparatus. This experimental device was used during 4 months in a vegetable field, operating during the night from 18h to 6h to capture harmful insects. The reading of insect numbers is done according to a procedure using a binocular magnifying glass, an entomologist tool and boxes for the collection of insects.

Keywords: C*atching Insects Device, High Voltage Electrical Discharge, KAHRATRAP*

Description of the apparatus: KAHRATRAP is an electrical solution used to fight harmful insects (figure 1), it was designed with variable parameters (lamps, color of lamp's lights, power of lamps, height of suspension, field of attraction…).

Figure 1: Photography of the realized apparatus KAHRATRAP

Figures:

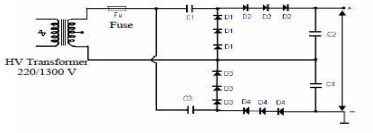

Figure 3: Electrical circuit of the high voltage supply

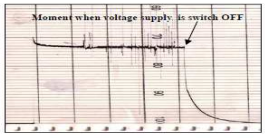

Figure 4.a: Voltage fluctuation during the operation of the apparatus

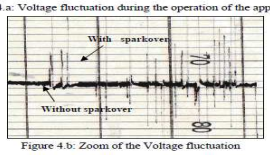

Figure 4.b: Zoom of the Voltage fluctuation

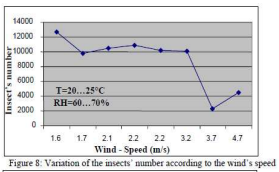

Figure 8: Variation of the insects' number according to the wind's speed

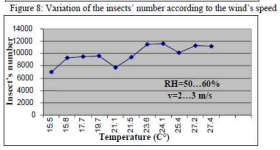

Figure 9: Variation of the insects' number according to the temperature

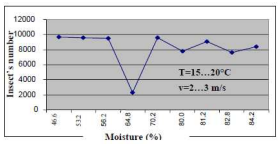

Figure 10: Variation of the insects' number according to humidity

voltage supply: The principal element of this apparatus is the direct-current high voltage generator which must support the thousands of sparks which occur during the operation of the device. Figure 4.b shows an increasing zoom of voltage fluctuation around the average value of 7.5 kV. The greatest part of the consumed energy is due to the power of four "reflectors" lamps of 60W each, and two fluorescent tubes of 36 Watts each.

Results: The results presented in this paper are related to a certain class of insects whose size varies from a millimeter to approximately five centimeters. The trappings were carried out in a firm located at DOUAR EL' MCHAREF in the area of MASCARA (ALGERIA) at 478 m of altitude, for a 04 months-period (July 01st, 2004 to October 30th, 2004).

Discussion: The experiments were carried out during the night from18h to 6h to trap harmful insects. The eyes of the insects made up of a great number of light sensors laid out in mosaic, have a very wide field of vision and are adapted to detect fast moving objects. Figure 11.a shows the aspect of the light emitted by the lamps at a distance of 150 m and figure 11.b at a distance of 350 m. The increase of wind's speed reduces the number of caught insects and decreases the efficiency of this process (figure8). The influence of temperature on the trapping efficiency, illustrated by figure 9, shows that the quantity of caught insects increases slightly with the rise of temperature. The obtained results, illustrated by figure 10 shows and confirm, indeed, this tendency. Let us note that the result corresponding to humidity of 64.8% was obtained in a night with strong winds and rain precipitations.

References: Dascalescu, N.J.(1994) Felici, N.J (1966) Hislop, E.C. (1993) Kuffel, E. Zaengl, W.S. Kuffel, J(2000).

P30- Shear horizontal surface acoustic wave sensors for specific and non specific streptavidin-anti streptavidin recognition

Y. Bergaoui[1], J.M. Fougnion[2], C. Zerrouki[2], N. Fourati[2] and A. Abdelghani[1]

[1]Unité de Recherche de Physique des Semiconducteurs et Capteurs, IPEST, 2070 La Marsa, Tunisie
[2]Laboratoire de Physique, EA 4131, Cnam, 2 rue Conté 75003 Paris, FRANCE
fourati@cnam.fr

Introduction: Surface acoustic wave sensors are extremely versatile devices able to detect molecular recognition unit combined with antigen or antibody [1-3]. When molecular recognition occurs, a mass change is generated and wave's velocity is modified. Phase and amplitude variations can then be recorded, at a fixed frequency, to estimate mass loading.
In this study, we have realized a biosensor based on biotine-streptavidine bonding. Specific and non specific recognitions tests were then made using anti-streptavidin and sheep antibody immunoglobulin G (sheep IgG) respectively.

SH-SAW architecture: Delay line shear horizontal surface acoustic wave (SH-SAW) sensor, consists of a delay line built on a 36°rot Lithium Tantalate piezoelectric substrate. Chromium/gold (20/80 nm) interdigital transducers (IDTs) were photolithographically patterned with a periodicity λ of 40 µm which corresponds to an operating frequency of about 104 MHz. A Kalrez® flow cell is placed over the region between the IDTs to contain solutions. A HP 8711C network analyzer was used to measure the amplitude and phase of the output electrical signal.

Results: An immunosensor has been developed using SH-SAW device. The biorecognition surface, formed on gold layer, is a mixed layer of 1,2-dipalmitoyl-sn-glycero-3-phosphoethanolamine-N-(biotinyl) (biotinyl-PE) and 16-mercaptohexadecanoic acid (MHDA). Biotinylated lipid layer specifically bound streptavidin [4] and, subsequently, antistreptavidin molecules.
Fig. 1 shows that antistreptavidin injections lead to phase shifts: for low concentrations, phase changes linearly while at high ones SH-SAW phase response saturates. By plotting phase variations versus antistreptavidin concentrations, we have determined the sensitivity *S* of our SAW sensor from the linear region: $S = 0.04°$ / nMol.

The specificity of our immunosensor was tested in parallel by adding IgG sheep molecules: no phase change was recorded (Fig. 1).

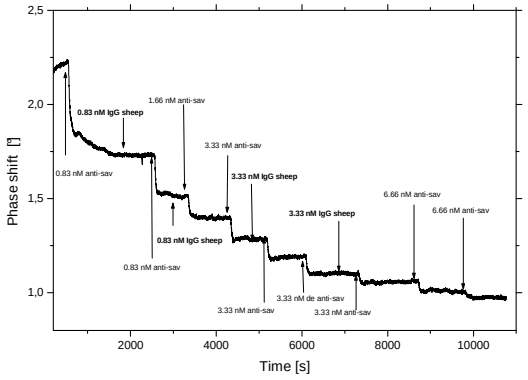

Fig. 1: Real time phase variations during antistreptavidin and IgG sheep additions.

The present work has shown the real potential of SH-SAW sensors to detect specific biorecognition layers. In a forthcoming study, we will investigate antistreptavidin binding to Horseradish peroxidase conjugated streptavidin (HRP-streptavidin).

References:

[1] Gizeli, E., Liley, M., Lowe,C, R., Vogel, R. (1997) Antibody Binding to a Functionalized Supported Lipid Layer: A Direct Acoustic Immunosensor, Anal. Chem, 69, 4808-4813.
[2] Ha, Z., Zhou, K., Chen, X., Yang, Z., He, L. (2007) Study of a Piezoelectric SAW Immunosensor for the detection of Alpha-fetoprotein, IEEE, 1-4244-1120-3/07/$25.00
[3] Lslnge, K., Voigt, A., Ram, M., (2003) Surface acoustic wave biosensors for biomolecular interaction analysis, IEEE, 0-7803-813 3-5/03/$17.0M0 O03
[4] Bergaoui, Y., Zerrouki, C., Fougnion, J. M,. Fourati, N., Abdelghani, A., (2009) Sensitivity estimation and biosensing potential of lithium tantalate shear horizontal surface acoustic wave sensor, Sensors Letters, In press.

P31- Two-dimensional imaging of nanoscale particles sizes

Redjem Hadef
Faculté des Sciences et de la Technologie, Université Larbi Ben M'Hidi, Oum El Bouaghi, Algérie
rhadef@rocketmail.com

Abtsract: Soot is formed from combustion processes in locally fuel-rich zones at elevated temperature and consists mainly of carbon, and contains up to 10% hydrogen on a molar basis, and even more in young soot. Briefly, its evolution proceeds in three chemical and physical steps [1,2]: the formation and growth of large aromatic hydrocarbons and their transition to particles (soot particle inception), the growth of solid particles by addition of components from the gas phase (surface growth), and the coagulation of primary particles to large aggregates (particle agglomeration). The emission of soot from combustors, or flames, results from the competition between soot formation and oxidation. Soot particles smaller than about 300 nm are known to penetrate deep into the lungs and alveoli and, due to this location and their physico-chemical properties, have a negative impact on health [3]. They are also contributing to adverse changes to the earth's climate through their role in high-altitude cloud formation [4]. As a result of the increased awareness of soot as a pollutant, as well as tighter emission legislation worldwide, the topic of soot formation and oxidation and their interaction with transport processes continues to be the focus of extensive fundamental investigations and practical applications in research for designing technical combustion devices. Thus, in order to validate new theories, experimental data describing soot characteristics must be available. As a matter of fact, since most of the relevant information must be obtained by non-invasive, spatially resolved and instantaneous measurements, these needs can be satisfied by using optical techniques. Over the past 20 years, laser-induced incandescence (LII) has proven in numerous studies to be a useful diagnostic tool for spatially and temporally resolved measurement of soot volume fraction in a wide range of applications, such as laminar and turbulent flames, in-cylinder combustion, and engine exhaust gas characterization. Although instrumentation and interpretation are still under debate [5,6], addressing particularly the effects of laser fluence, spectral and temporal gating, optical depth, particle size distribution and shape, as well as laser-induced photochemistry [7] and change of particle morphology, LII seems remarkably robust compared to the more conventional techniques for soot characterization including soot volume fraction by gravimetric or light extinction techniques [8] and the multiwavelength emission technique [9] and soot morphology (primary particle diameter and aggregate size distribution) by laser scattering [10] as well as thermophoretic sampling/transmission electron microscopy particle diagnostic . A time-resolved variant of LII (TiRe-LII) has been introduced by Will et al. to allow for particle sizing, profiting from the size-dependent cooling behaviour of the laser-heated particles. The method has been applied successfully to soot distributions in diverse combustion systems
In this investigation, a two-dimensional field of soot particle size has been determined from the temporal profile of the LII signal. The experiments were performed in a laminar diffusion ethylene-air flame. The data analyzed with the help of a validated LII model will be useful for the further development of soot formation models

References :

[1]. Bockhorn H., and Schäfer T. [1994] *Soot Fo mation in Combustion*, H. Bockhorn (Ed.)Springer-Verlag, Heidelberg Germany
[2]. Haynes B.S., and Wagner H.Gg. [1981]*Prog. Energy Combust. Sci*. 7, pp. 229-173
[3]. Wilson R, and Spengler J.D. [1996] *Paticles in our Air: Concentrations and Health Effects*, Harvard University Press, Cabridge, USA
[4]. Jacobson M.Z. [2001] *Nature* 409,pp.695–697
[5]. Schulz C., Koch B.F., Hofmann M., Michelsen H.A., Will S., Bougie B., Suntz.R., and Smallwood G. [2006] , *Appl. Phys.B* 83, pp. 333-354
[6]. Michelsen H.A., Liu F., Kock F., Bladh H., Boiarciuc A., Charwath M., Dreier T.,Hadef R., Hofmann M. , Reimann J., Will. S., Bengtsson P.-E., Bockhorn H., Foucher, F., Geigle K.P., Mounaïm-Rousselle C.,Schulz C., Stirn R., and Tribalet B. [2007], *Appl. Phys. B*. 87, pp. 712-745
[7].Goulay F., Schrader P.E., Nemes, L. and Dansson M.A. [2009] *Proc. Combust. Inst.* 32, pp. 963-970
[8]. Choi M.Y., Mulholland G.W., Hamins A., and Kashiwagi T. [1995], *Combust. Flame* 102, pp. 161-169
[9]. De Iuliis S., Barbini M., Benecchi S., Cignoli F., and Zizak G. [1998], *Combust. Flame* 115, pp. 253-261
[10]. Lamprecht A., Eimer W., and Kohse Höinghaus K.[1999], *Combust. Flame* 118**,** pp. 140-150.

P32- Electrochemical study of horseradish peroxidase biosensor based on functionalised magnetic beads and polypyrrole film

Saloua.Helali[1*], Hamdi Baccar[1], Adnane Abdelghani[1]

Unité de Recherche de Physique des Semiconducteurs et Capteurs, IPEST La Marsa,Tunisia.
*Corresponding author : e-mail: salwahleli@yahoo.fr

Abstract

Metal and semiconductor nanoparticles have received considerable attention during recent years. They have unique chemical, electrical and optical properties due to their size-dependent characteristics and quantum-sized effect. They prove to be promising for practical applications in many fields such as; electronic nanodevices, molecular catalysts, multi-functional reagents and biosensors. Nanoparticles are very different from their bulk materials in their electronic, optical and catalytic properties originating from their quantum-scale dimensions. Nanoparticles can bring four advantages when they are immobilised on macro-electrodes used for electroanalysis: enhancement of mass transport, electrocatalysis, high effective surface area and control over electrode microenvironment. Therefore, much work has been carried out for their immobilisation, characterization and use for the detection of many electro-active species.

Devices based on nanomaterials are emerging as a powerful and general class of ultrasensitive sensors for the direct detection of biological and chemical species. In this work, we present a two innovative way to immobilize a horseradish peroxidase (HRP) for the detection of hydrogen peroxide (H_2O_2). The strong avidin–biotin affinity is used to stack up successive monomolecular layers of horseradish peroxidase on gold electrodes. The first sensor was based on a monolayer of magnetic particles coated with streptavidin enabling after reaction with biotin the deposition of horseradish peroxidase conjugated streptavidin, formed on a gold electrode after application of a magnetic field. The second sensor was based on same magnetic particles with HRP entrapment during electrochemical deposition of polypyrrole. The cyclic voltammetry and amperometry techniques were used to monitor biosensor building-up process. The current response of the biosensors is dependent on the nature of the layer and the concentration of H_2O_2. The results show that the sensor

based on polypyrrole with magnetic particles/ horseradish peroxidase has a higher sensitivity (2.3µA/mM) than the sensor based on magnetic particles/ horseradish peroxidase (1.7µA/mM) due to conductive properties of polypyrrole.

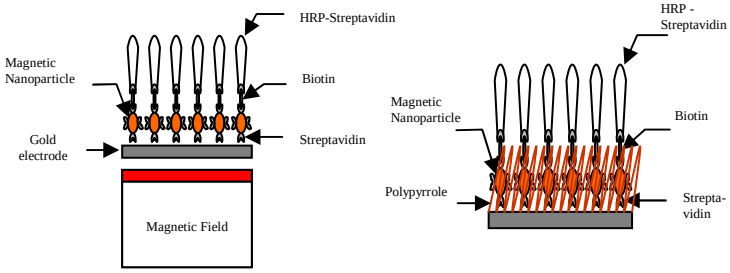

Figure1. Schematic representation of the two biosensor architecture a) without polypyrrole and b) with polypyrrole.

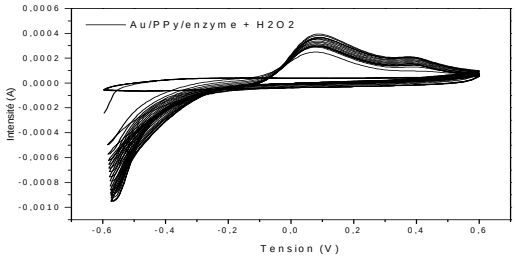

Figure 2. Cyclic voltammograms for polypyrrole/ magnetic nanoparticles/ streptavidin – HRP layer on gold in PBS at pH 7.0 (scan rate: 50mVs^{-1}) with injenction of 0.23 mM H_2O_2

References:

[1]C.Esseghaier, Y.Bergaoui, S.Helali, A.Tlili, S.Ameur, A.Abdelghani, ensors and Actuators B, Chemical, Volume 134, Issue 1, 28 August 2008, Pages112-116.

P33- Tuning InAs/GaAs quantum dot's emission wavelength by ion implantation and subsequent annealing

Z. Zaâboub[1] , B. Ilahi[1], L. Sfaxi[1], H. Maaref [1], B. Salem[2,3], V. Aimez[2], D. Morris[2].
[1]Laboratoire de Physique des Semiconducteurs et des Composants Electroniques, Faculté des Sciences, Avenue de l'environnement 5019 Monastir, Tunisia.
zouhour_zaaboub@yahoo.fr
[2]Centre de Recherche en Nanofabrication et Nanocaractérisation, (Québec) Canada J1K 2R1.
[3] Present address: Département de Recherche Fondamentale sur la Matière Condensée, CEA Grenoble, 17 rue des Martyrs, F-38054 Grenoble Cedex 9, France

Introduction: With the development of microelectronic and optoelectronic devices and consequent increasing need for miniaturization, the integration of optical devices with different functions and properties on the same chip becomes highly desirable. Using intermixing techniques, which allows post-growth tuning of the emission wavelength, active devices with different wavelengths can be fabricated on the same chip for monolithic integration. Ion-implantation combined with a rapid thermal annealing treatment offers many advantages such as compatibility with planar processing and accurate control of the concentration and depth distribution of the point defects by varying the ion dose, energy and mask profile. Controlled intermixing of the QD structure in selected regions with high uniformity can be obtained using appropriate ion implantation masks.

Layout: In this work, we investigated the effect of proton and phosphorous ion implantation at various doses, followed by rapid thermal annealing (RTA) on the optical properties of InAs/GaAs QDs using low temperature photoluminescence (PL) measurement. The chosen RTA conditions correspond to the highest annealing temperature where the PL band is still non-shifted. This allows one to investigate In/Ga intermixing controllable mainly by the phosphorous-ion-implantation conditions [1].

Content: Proton implantation at room temperature at different doses (5×10^{10}–10^{14}ions cm^{-2}) with acceleration energy of 18 keV allows a blueshift of 121 nm while keeping the QDs tridimentional carriers confinement (*inset of fig 1*) and around 46% of the initial integrated PL intensity [2]. However, the phosphorous ions implantation with acceleration energy of 50 keV induces wavelengths shift around 35 nm while keeping the QDs character. So, for phosphorous implantation doses higher than 10^{12} ions/cm^2, the high damage concentration and the subsequent formation of complexes defects are expected to be responsible for the drastic decrease of the integrated PL intensity and the significant broadening of the QD emission band [3]. These dissimilarities in results are attributed to the amount and the nature of defects created in the structure which depends on the ion spices and the implantation energy.

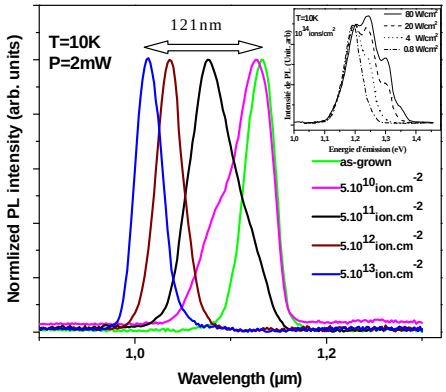

Figure 12: Normalized PL spectra at 10 K of InAs/GaAs QDs samples as a function of the proton implantation dose.

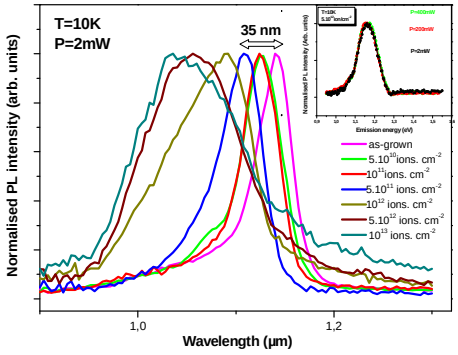

Figure 2: Normalized PL spectra at 10 K of InAs/GaAs QDs samples as a function of the phosphorous ion implantation dose.

References:

[1] B. Ilahi, Z. Zaâboub, B. Salem, D. Morris, V. Aimez, L. Sfaxi, and H.Maaref, *Materials Science in Semiconductor Processing* (2009) *in Press*

[2] B. Ilahi, B. Salem, V. Aimez, L. Sfaxi, H. Maaref and D. Morris, *Nanotechnology* **17** 3707 (2006)

[3] Z. Zaaboub, B. Ilahi, L. Sfaxi, H. Maaref B. Salem, V. Aimez, and D. Morris, Physics Letters A **372** 4714–4717 (2008)

P34- Calculation of exciton energy levels in III-V self assembled quantum dots

I.Saïdi, K. Sellami*, and K. Boujdaria

Laboratoire de Physique des Matériaux, Faculté des Sciences de Bizerte 7021 Jarzouna, Tunisia
e-mail: karimsellami@yahoo.fr

Introduction: As a consequence of their fully quantized electronic states and high radiative efficiencies, largely due to their unique properties arising from δ function like profile of the density of states, self assembled quantum dots have enabled major advances in fundamental physics studies of zero dimensionality semiconductor systems [1]. The understanding of the behavior of an electron-hole pair (exciton) confined in a quantum dot is of utmost importance in the interpretation of exciton spectra, and in the fabrication of optoelectrinc devices with new functions or to improve the performance of the existing devices.

Theretical model: In the frame work of the effective mass approximation the electron (hole) hamiltonien is written as:

$$H_{e(h)} = \frac{P^2_{e(h)//}}{2m^*_{e(h)//}} + \frac{P^2_{e(h)\perp}}{2m^*_{e(h)\perp}} + V_{conf}(r)$$

Where $m^*_{e(h)//}$ and $m^*_{e(h)\perp}$ are respectively the electron (hole) masses for the implane and motions, V_{conf} denotes the quntum dot confinement potential that takes into account the shape of the nanostructure.

Hence it can be exprend as $V(r) = V_0(1 - D(z,\rho))$, where V_0 is the band offsed potential and D is the quantum domain Wich is written as:

$D(z,\rho) = D^{QD}(z,\rho) + D^{WL}(z,\rho)$ where and D^{WL} stands for respectively the quantum and wetting layer domains that can be written as: $D^{WL}(z,\rho) = \theta(z)\theta(d - z)$

and

$D^{QD}(Z,\rho) = \theta(z-d)\theta(h_2 + d - z)\theta(h_1 + d\,z - \rho\tan(\alpha))$

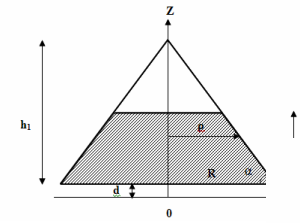

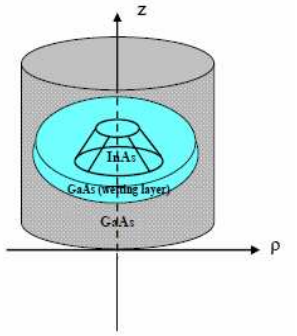

θ is the heavside function. The parameters d, h_1, h_2 are schematically represented below.

Results: In this present work we studied theoretically, within the effective approximation, the electron and hole states in self assembled InAs/GaAs quantum dot. Using an accurate numerical diagonalization method on the following Fourrier-Bessel function basis over a large cylinder domain:

$$\psi_n(r_{e(h)}) = \sum_{i\rangle 0, j\rangle 0} c^n_{i,j}\alpha^n_i e^{in\theta_e} J_n\left(\frac{\lambda^n_i}{R}\rho_e\right)\sin\left(\frac{\pi j}{Z}z\right)$$ Where

Z and R are the high and the radius of large cylinder. λ^n_i is the ith root of the n-order Bessel function J_n. $c^n_{i,j}$ is the normalization constance.

We calculated numerically the electron and hole eigen energies and associated wave functions. Our result revealed that this calculation method provide more accurate results compared to the commonly used variationnal method. We considered therafter the Coulomb interaction between the charge carriers in the quantum dot, and calculated the exciton energy levels. We investigated also the effect of the nanostructure size variation on the exciton energy spectrum. It is clearly found that the latter changes

significantly when the quantum size parameters are modified. Given this striking quantum dot size dependent property, these systems provide the opportunity to control and tune their optical and electronic properties through theses parameters [2]. These theoretical results could be crucial as they could be able to explain well the different photoluminescence spectra of quantum dot excitons, and simulate the behaviour of these excitonic properties versus the size variation.

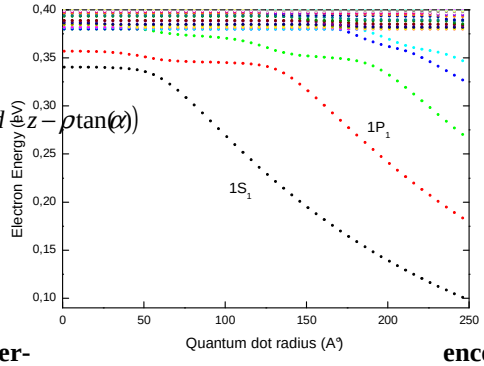

References:

[1] T Grange, R Ferreira, and G Bastard, Phys. Rev. B 76, (2007) 241304(R).

[2] K. Sellami andS. Jaziri, Materials Science and Engineering C 26 (2006) 555 .

P35- Electrical study of Ti doped $La_{0.7}Sr_{0.3}MnO_3$

H. Rahmouni[(a)], R. Jemai[(a)], N. Kallel[(b)], A. Selmi[(c)] and K. Khirouni[(a)].

[(a)] Laboratoire de Physique des Matériaux et des Nanomatériaux appliquée à l'Environnement, Faculté des Sciences de Gabès cité Erriadh 6079 Gabès, Tunisia.

rahmounihedi@yahoo.fr

[(b)] Laboratoire de Physico-Chimie des Matériaux, Département de Physique, Faculté des Sciences de Monastir B. P. 22. 5019 Monastir, Tunisia.

[(c)] Laboratoire de Physique des Semiconducteurs et des Composants Electroniques, Faculté des Sciences de Monastir, Avenue de l'Environnement 5018 Monastir, Tunisia.

Abstract: Transport measurements have been performed on Ti doped $La_{0.7}Sr_{0.3}MnO_3$ using impedance spectroscopy technique, in order to study its electrical properties. In contrary to free compound, when titanium is introduced, the conductance becomes frequency and temperature dependent. From DC conductance study, electronic conduction is found to be dominated by thermally activated hopping and depending strongly on Ti content. Activation energy is deduced from the variation of conductance with temperature. This energy decreases from 168 meV to 143 meV when x increases from 0.05 to 0.20. The AC conductance spectrum is found to obey Jonscher universal power law. Finally, at ambient temperature, DC conductance decreases with the value of x and proves a clear effect of titanium in transport properties of the material. This decrease of conductance is explained by a reduction of Mn^{3+}-O-Mn^{4+} network responsible of electrical conduction in perovskite.

Figures

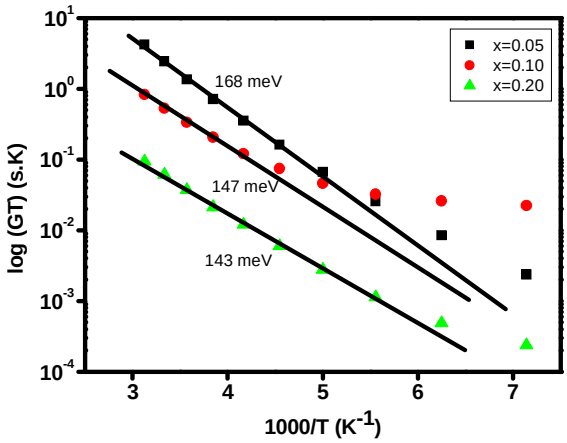

Figure 1: Variation of the $\log(G_{DC}T)$ as a function of (1000/T) for $La_{0.7}Sr_{0.3}Mn_{1-x}Ti_xO_3$ samples

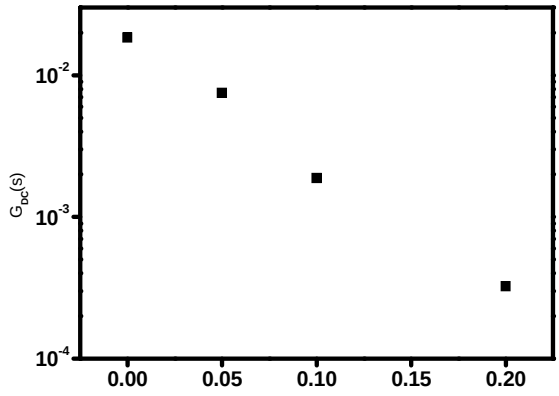

Figure 2: Variation of DC conductance G_{DC} at room temperature as a function of Ti concentration x.

References

[1]A. M. Ahmed. Physica B 352 (2004) 330.
[2]J.A.M. Van Roosmalan, J.P.P. Huijsmans and L. Plomp. Solid State Ionics 66 (1993) 279-284.
[3]M. Nadeem, M. J. Akhtar, A. Y. Khan. Solid. State. Com. 134 (2005) 431.
[4]M. Nadeem, M. J. Akhtar, A. Y. Khan, R. Shaheen M. N. Haque. Chem. Phys. Let. 366 (2002) 433.
[5]M. Viret, L. Ranoo, J. M. D. Coey. Phys. Rev.B. 55 (1997) 8067

P36- Infrared lineshapes of hydrogen bonds within the linear response theory

Noureddine Issaoui[1], Najeh Rekik[1] ,Brahim Oujia[1] , Marek J. Wójcik[2] .

[1]ILaboratoire de Physique Quantique, Faculté des Sciences de Monastir,
Route de Kairouan, 5000 Monastir, TUNISIA
Issaoui_noureddine@yahoo.fr
[2] Laboratory of Molecular Spectroscopy, Faculty of Chemistry, Jagiellonian University,
Ingardena 3, 30-060 Kraków, Poland

Introduction: Hydrogen bonding has long been recognized as a specific interaction between an -X-H bond of one molecule, described as the proton donor, and an atom Y of another molecule, described as the proton acceptor. Hydrogen bonds have been studied by four methods: Chemical, crystallographic, spectroscopic, and theoretical. This review is mainly concerned with the last two, although both here and in the literature, they are all closely linked together. Infrared specters seem to contain precise information on the nature of hydrogen bonds, as at the level of the molecular dynamics and as at the level of the electronic structure. The great preciseness of infrared spectroscopic techniques authorizes the theoretical reconstruction and the interpretation of these complex specters, but requires for it a fine modeling, and consequently complete, of the hydrogen bonds and of its environment. The explanation of the strong expansion spectral of the band aroused several propositions, which are founders of the theoretical study of hydrogen bonds.The purpose of this work is to reproduce theoretical infrared specters of the vibration of X-H of the hydrogen bonds. This model is working within the linear response theory (LRT) according to which the spectral density is the Fourier transform of the autocorrelation function (ACF) of the dipole moment operator involved in the υ_{S}(X-H) IR transition.

We have presented a quantum non-adiabatic treatment of H-bonds in which effects of anharmonicities of the high frequency X-H...Y and the low frequency X-H...Y modes on the υ_{S}(X-H) infrared lineshapes of H-bonds systems and Fermi resonances are considered. The anharmonic coupling between the high frequency and the low frequency modes is treated within strong anharmonic coupling theory and the relaxation is included following quantum treatment of Rosch and Ratner <cite>Rosch1974</cite>. The intrinsic anharmonicity of the fast mode by accounting for quadratic dependence of both the angular frequency and the equilibrium position of theX-H...Y stretching mode on the X-H...Ymotion and their frequency is described by a double well potential whereas frequency of the slow mode by Morse potential.

The numerical results are in fairly good agreement with the experimental behavior of the first and the second moment of the X-H bands, observed when varying the temperature <cite>N2ch2</cite>. The calculation shows that the modulation of the angular frequency of the fast mode and its equilibrium position by the slow mode coordinate generate an improvement of the fine structure of the spectrum and provide a direct evidence of the increase of the level density and the spectral broadening <cite>rekik22007ch5, N7</cite>. The calculations show also that the indirect damping plays an important role in the features of the line shapes of hydrogen-bonded systems by favouring more sensitive smoothing of the full spectra if Fermi resonances is considered <cite>N1</cite> and by favouring a fine structure of the low frequency tail than that of the high-frequency one in cases without Fermi resonances whereas the direct one entrains a broadening of the spectrum <cite>N5</cite>. Results show that mixing of all these effects results in a broad and complicated structure and expects to provide efficient energy relaxation pathways by using large dampings parameters for the condensed phase and weaker dampings for the gas one <cite>N6ch5</cite>.

P37- Electrical study of 30% Cr doped $La_{0.7}Sr_{0.3}MnO_3$ material by impedance spectroscopy

H. Rahmouni[(a)], R. Jemai[(a)], N. Kallel[(b)], A. Selmi[(c)] and K. Khirouni[(a)].
[(a)] Laboratoire de Physique des Matériaux et des Nanomatériaux appliquée à l'Environnement, Faculté des Sciences de Gabès cité Erriadh 6079 Gabès, Tunisia.
rahmounihedi@yahoo.fr
[(b)] Laboratoire de Physico-Chimie des Matériaux, Département de Physique, Faculté des Sciences de Monastir B. P. 22. 5019 Monastir, Tunisia.
[(c)] Laboratoire de Physique des Semiconducteurs et des Composants Electroniques, Faculté des Sciences de Monastir, Avenue de l'Environnement 5018 Monastir, Tunisia.

Abstract: Transport measurements have been performed on $La_{0.7}Sr_{0.3}Mn_{0.7}Cr_{0.3}O_3$ using impedance spectroscopy technique, in order to study its electrical properties. Impedance spectrum results indicate that the electrical properties of the material are strongly dependent on temperature and frequency. Evidences of temperature dependent electrical relaxation phenomena in the material have also been observed. Impedance spectrum analysis shows that the material can be described as a grain and grain boundary medium and permits to estimate the grain boundary contribution. Electronic conduction is found to be dominated by thermally activated hopping of small polarons at high temperature and variable range hopping at low temperature. Activation energy inferred from conductance spectrum matches very well with the value estimated from relaxation time indicating that relaxation process and conductivity have the same origin.

Figures

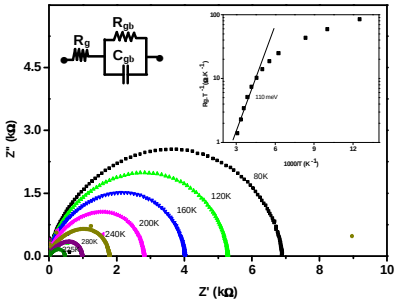

Figure 1: Ac impedance diagram of $La_{0.7}Sr_{0.3}Mn_{0.7}Cr_{0.3}O_3$ sample at different temperatures.

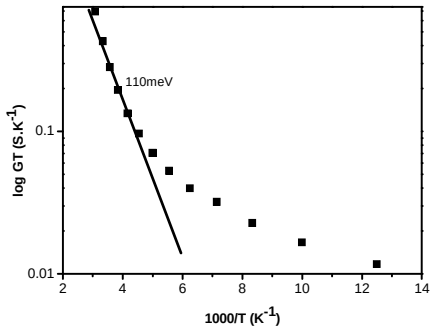

Figure2: Variation of log(GT) as a function of (1000/T) for $La_{0.7}Sr_{0.3}Mn_{0.7}Cr_{0.3}O_3$ sample

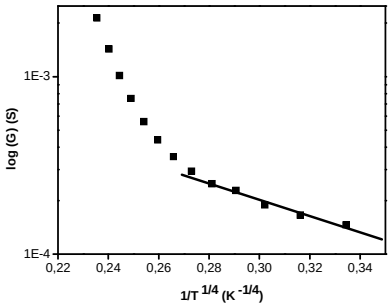

Figure 3: Variation of $\log G_{DC}$ versus $(1/T)^{1/4}$ of sample $La_{0.7}Sr_{0.3}Mn_{0.7}Cr_{0.3}O_3$.

References

[1] A. M. Ahmed. Physica B 352 (2004) 330.
[2]In-Bo Shim, Key-Taeck Park, Chul-Sung Kim, Young-Jei Oh; J. Magn. Magn. Materials 226-230 (2001) 733
[3]J.Hu, H.Qin, J.Magn.Magn.Mater 231(2001)L1
[4]J.Hu, H.Qin, J.Magn.Magn.Mater 234(2001)419
[5]Shrabanee Sen, R.N.P.Chaudhary. Mater. Chem. Phys. 87 (2004) 256.
[6]S. Mollah, H. L. Hazang, H. D. Yang, Sadipta Pal, S. Taran, B. K. Chavdhuri
[7] J. Magn. Magn. Mater. 284 (2004) 383.

P38- Growth of GaAlAs multilayers on porous Si by molecular beam epitaxy for the photovoltaic applications

B.Azeza , L.Sfaxi ; R.Mghaieth*, H.Maaref

Laboratoire de Physique des Semi-conducteurs et des Composants Electroniques
Faculté des Sciences de Monastir, Avenue de l'environnement 5019 Monastir, Tunisie
*Corresponding author.
Tel: +216 73 500 274; Fax: +216 73 500 278
E-mail: ridha.mghaieth@fsm.rnu.tn

[1]presenting author

Abstract

The combination of thin GaAs and GaAlAs layers were successfully grown on porous silicon (PSi) substrate using molecular beam epitaxy (MBE) for photovoltaic applications.

The porous silicon substrates are considered to be a flexible material because of the presence of a large number of pores witch was formed by electro-chemical etching of silicon wafer in hydrofluoric acid (HF). The substrate used was (100) oriented, born-doped P-type silicon with (1-10 Ωcm) resistivity. We have reviewed the initial stage and the re-combination of GaAs epitaxial layers grown on silicon substrates by reflection high-energy electron diffraction (RHEED). In addition, to clarify the effect of each layer on the substrate layer, the crystanility was observed by RHEED. Also, the photoluminescences peaks indicated on spectrum are observed and attributed to the diverse layers deposited on porous silicon. The growth conditions and the characterizations of the structures were studied and indicate promising structures for photo-voltaic applications.

Figure 1 shows (2×4) reconstruction indicates the good quality of the GaAs layer deposited on porous silicon (PSi). Figure 2 shows the photoluminescence spectrum of the GaAlAs/GaAs on PSi at 11K.

Fig.1 RHEED of the GaAs layers deposited on PSi

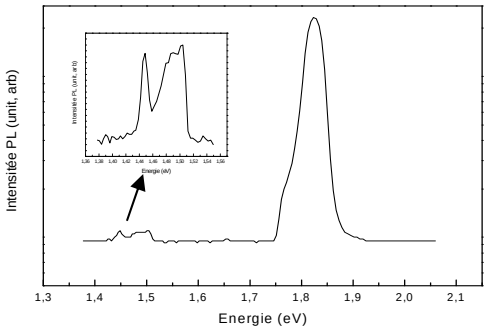

Fig.2 11K photoluminescence spectrum of a GaAlAs/GaAs/PSi

Reference

[1]T.W.Kang and J.Y.Leem (1996) Microelectrnics journal.
[2]S. Saravanan and Y. Hayashi (2002) Crystal Growth
[3]Mohamed Lajnef and Afrah Badaoui (2008) American Journal of Applied Sciences.

P39- Effect of phosphorus ion implantation-induced intermixing on the optical properties of self-assembled InAs/InP quantum sticks

M. H. Hadj Alouane[1,*], B. Ilahi[1], H. Maaref [1], B. Salem[2,4], V. Aimez[2], D. Morris[2], A. Turala[3], P. Regreny[3], and M. Gendry[3]

[1]Laboratoire de Physique des Semiconducteurs et des Composants Electroniques, Faculté des Sciences, Avenue de l'environnement 5019 Monastir, Tunisia.
bouraoui.ilahi@fsm.rnu.tn
[2]Centre de Recherche en Nanofabrication et Nanocaractérisation (CRN2), Université de Sherbrooke, (Québec) Canada J1K 2R1.
[3]Institut des Nanotechnologies de Lyon, UMR 5270, Bat. F7, 36 avenues Guy de Collongue, 69134 Ecully Cedex, France.
[4] Present address: Département de Recherche Fondamentale sur la Matière Condensée, CEA Grenoble, 17 rue des Martyrs, F-38054 Grenoble Cedex 9,France

Introduction: Ion-implantation-induced intermixing turns out to be particularly interesting, owing to its compatibility with planar processing. Indeed, one can accurately control the concentration and depth distribution of the point defects by varying the ion dose and energy and/or mask profile. Using suitable ion implantation masks, this approach, allows the feasibility of selective and controlled intermixing in QDs' structures, so one can selectively tune the optical transition energies in the same sample surface.

Layout: In this work, the temperature dependent photoluminescence (PL) measurements have been employed to study the interdiffusion process in InAs/InP quantum sticks (QSs) induced by phosphorus ion implantation in a 50 nm thick InGaAs sacrificial layer and subsequent rapid thermal annealing (RTA). The implantation process was carried out at 200°C at various doses (10^{11} - 5.10^{14} ions cm^{-2}), where the ions were accelerated at 18 KeV [1].

Content: Our measurements show that the intermixing degree alters both the QSs optical emission energy and PL linewidth. A pronounced blue-shift of the PL peaks can be observed for samples subjected to phosphorus implantation and RTA without degradation of the sample's quality (Fig 1). The PL linewidth variation with temperature is found to experience an atypical behavior do to the enhanced QS size distribution do to a non uniform intermixing at the lower ion implantation doses [2] (Fig 2). We also note that no major modification were observed in the temperature dependence PL properties for the only annealed sample indicating that the observed behavior is purely induced by ion implantation generated point defects in the InGaAs sacrificial layer.

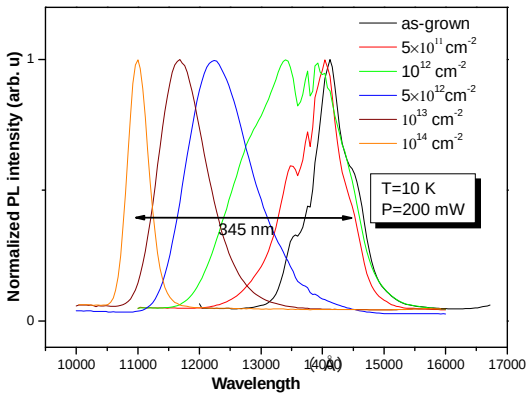

Figure 13: Normalized PL spectra at 10 K of intermixed InAs/InP QS samples as a function of the phosphorus ion implantation dose.

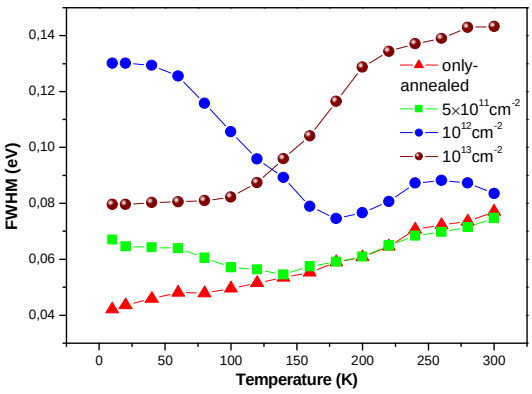

Figure 2: Temperature dependent PL FWHM as a function of the phosphorus ion implantation dose.

References:

[1] B. Salem et al *Applied Physics Letters* 87, 241115 (2005)
[2] Z. Zaaboub et al *Nanotechnology* 19 (28), 285715 (2008)

P40- Numerical modelling of micro-sensors electrical behavior for biomedical and environmental applications

J.Chermiti[1], F. Aouni,[2], M. Ben Ali[1,3], N. Jaffrezic-Renault[4]

[1] Institut Supérieur des Sciences Appliquées et de Technologie de Sousse, TUNISIA
[2] Laboratoire de Physique et Chimie des Interfaces, Faculté des Sciences de Monastir, 5019 Monastir, TUNISIA
[3] Unité de Recherche de Physique des Semi-conducteurs et Capteur, IPSET la Marsa, TUNISIA
[4] Laboratoire de Sciences Analytiques, UMR 5180, Université Claude Bernard Lyon 1, FRANCE

Current trends in health science and biomedical research indicate a continuous need for technologies that allow for the achievement of accurate measurements and consistent results. The purpose of this work was to develop a numerical platform for the modelling and the analysis of biochemical sensors based on semiconductor (EIS, ISFET) and metal transducer (Fig.1). The principal asset of platform is the extraction of macroscopic and microscopic parameters of the sensors. In addition to its compatibility with different purchase environment of measurement. In order to validate the numerical platform, it was applied to two types of applications: biomedical and ion-detection.

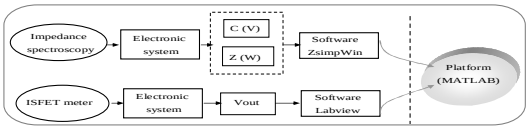

Figure 1: General aspect of numerical platform

A variety of organic molecules have been used as sensitive membrane for ions detection in particular the thiacalix[4]arene (TCA). Previous researches demonstrated that the chemical sensing properties of TCA film, deposited onto semiconductor substrates, are strongly dependent upon the film thickness (Ben Ali, M. 2001). The modelling of measurements shows that the membrane sensibility is better (32, 8 mV/decade) with 20 nm of thickness. According to the site binding model (Eq.1) developed in reference (Aouni, F. 2004), microscopic properties of EIS/TCA structure for copper detection, such as sites number (Ns) and complexation coefficient (pk), are determined (Tab.1).

$$P\left[X^{Z+}\right] = -\log\left[X^{Z+}\right] = \frac{Z\,q\,\psi_o}{2.3\,K\,T} + \log\left(\frac{q\,Ns}{C_{eq}\,\psi_o} - 1\right) - pk \qquad (1)$$

Where Ψ_0 is the potential of the insulator/electrolyte interface, Z is the valence number and C_{eq} is the capacitance of the Stern layer.

Table1: effect of film thickness on sensor properties

Film thickness(nm)	*Sensitivity (mV/decade)*	*Linear range (µM)*	*Ns (/cm²)*	*pK*
20	(32,8±0,8)	2,5-19	$4x10^{21}$	4 ,3
100	(18,84±0,60)	2,5-19	$6x10^{19}$	2,6

After that, the microsensor ISFET was functionalized with the optimal TCA film for Cu^{2+} ion detection. The modelling sensitivity was 28 mV/decade, this value is close to the Nernestian one. The accessibility sites concentration is about $7x10^{20}$ cm^{-2}. This result is in good agreement with the response observed on EIS structures. For biosensors application, recently, a novel formaldehyde (F.A) sensitive biosensor based on bacterial formaldehyde dehydrogenase (FDH) as a bio-recognition element has been developed. In order to investigate the effect of borate buffer concentration, the response of $Si/SiO_2/Si_3N_4$/rFDH structure toward (F.A) was controlled for different concentration. The proposed biosensor output signal decreases substantially with the increase of buffer concentration and the best sensitivity is observed in 2.5 mM borate buffer (Fig.2) (Ben Ali, M. 2007).The site binding model (Eq.1) does not take into account the effect buffer concentration. Consequently, we tried to improve the model by adding the function below (Eq.2):

$$S\left(c\right) = \delta + \alpha\, c^{-\beta} \qquad (2)$$

Where S is the sensibility, c the buffer concentration and (δ, β and α) are dependent onto the membrane type and structure. The ISFET/FDH and $Si/SiO_2/Si_3N_4$/rFDH structures have the same behaviour towards the buffer concentration effect for detection of Cu^{2+} ions.

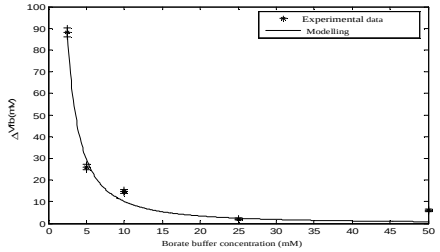

Figure 2: Shift of the flat-band voltage with increasing the concentration of borate buffer

References:

[1]Aouni, F., Rouis, A., Ben Ouada, H., Mlika, R., Dridi, C. and Lamartine,R. (2004) Electrical characterisation of calixarene-sensitive spin-coated layers, *Materials Science and Engineering,* C 24, 491–495

[2]Ben Ali, M., Jaffrezic, N., Martelet, C., Ben Ouada, H. Davenas,J. and Charbonnier, M. (2001) Characterization of copper ion sensing thiacalixw4xarene films evaporated on semiconductor substrates, *Materials Science and Engineering,* C14, 17–23

[3]Ben Ali, M., Gonchar,M., Gaydac,G., Paryzhak, S.,Maaref, M.A., Jaffrezic-Renault, N. And Korpan,Y., (2007) Formaldehyde-sensitive sensor based on recombinant formaldehyde dehydrogenase using capacitance versus voltage measurements, Biosensors and Bioelectronics, 22, 2790–2795

P41- The electronic properties of Ga(As,N) ternary and superlattice (SL) systems

Noureddine Mehnane[1], Fouzia Badi[1], Mohammed Reda Aced[2], Hamza Abid[1], Nadir Sekkal[3,4,5]

[1]Applied Materials Laboratory, Université de Sidi Bel Abbès, 22000 Sidi Bel Abbès, Algeria.
[2] Laboratoire de Transmission et Traitement Numérique du Signal (LTTNS) Centre de Recherches (ex-CFTE), Université de Sidi Bel Abbès, 22000 Sidi Bel Abbès, Algeria.
[3] Département de Physique-Chimie, Ecole Normale Supérieure de l'Enseignement Technique, BP 1523, El M'Naouer, 31000 Oran, Algeria
[4] Condensed Matter Section, The Abdus Salam International Centre for Theoretical Physics (ICTP), Strada Costiera 11, 34014 Trieste, Italy.
[5] Physia-Laboratory, BP 47 (RP), 22000 Sidi Bel Abbès, Algeria

Introduction: With means of the PLW-FPLMTO first principles method which treats accurately both open and compact structures, the electronic properties of both $GaAs_{1-x}N_x$ ternary alloy and $(GaAs)_m/(GaN)_n$ in Superlattice have been calculated (seen in table 1). The investigations about the anomalous gap variation found for a proportion of 25% (m = 3, n = 1) of N in both ternaries and SLs and also for the proportion of 50% (m = n = 2) for the SL has enabled us to conclude that the coupling between 4d-As and 2p-N orbitals is probably one other microscopic cause of this behavior and of the large bowing observed in GaAsN dilute nitride

Table 1: The structural parameters for binaries, ternaries and SLs (calculated with FPLMTO+LDA)

	V_0(Å^3)	a_0(Å)	$a_{0,SL}$ (Å)	c_0/a_0	B(GPa)	B'
GaN	22.4757375	4.4797889	-	1	192.56388191	4.96264
GaAs	44.98899044	5.6457556	-	1	68.69926115	4.76511
$GaAs_{0.25}N_{0.75}$	28.65194321	4.85741	-	1	126.8067732672	4.81765
$GaAs_{0.50}N_{0.50}$	34.642662975	5.17476	-	1	106.65302856	3.4297
$GaAs_{0.75}N_{0.25}$	40.221519802	5.438838	-	1	81.644732208	3.87108
SL(1,3)	28.01784969	4.821309	3.4091800	$2\sqrt{2}$	118.5687462336	5.51879
SL(2,2)	35.70867977	5.227306	3.6962636	$2\sqrt{2}$	88.1174677344	6.18076
SL(3,1)	39.62977594	5.412034	3.8268861	$2\sqrt{2}$	83.115808464	4.43744

.

References:

[1]Bellaiche L., S.-H. Wei, A. Zunger, Phys. Rev. B 54 (1996) 17568.
[2]Bernard J.E., A. Zunger, Phys. Rev. B 36 (1987) 3199 Jalmarson H.P.H, P. Vogl, D.J.Wolford, J.D. Dow, Phys. Rev. Lett. 44 (1980) 810.
[3]Kent P.R.C., A. Zunger, Phys. Rev. Lett. 86 (2001) 2613.
[4]Kim T.S., T.V. Cuong, C.S. Park, J.Y. Park, H.J. Lee, E.K. Suh, C.H. Hong, J. Kor, Phys. Soc. 43 (2003) 273. Lindsay A., E.P. O'Reilly, Sol. State. Comm. 112 (1999) 443.
[5]Onabe K., D. Aoki, J. Wu, H. Yaguchi, Y. Shiraki, Phys. Stat. Sol. A 176 (1999) 231.
[6]Shan W., W. Walukiewicz, K.M. Yu, J. Wu, J.W. Ager III, E.E. Haller, H.P. Xin, C.W. Tu, Appl. Phys. Lett. 76 (2000) 3251.
[7]Shan W., W. Walukiewicz, J.W. Ager III, E.E. Haller, J.F. Geisz, D.J. Friedman J.M. Olson, S.R. Kurtz, Phys. Rev. Lett. 82 (1999) 1221
[8]Phillipsin J.C., A.M. Alper, L. Margrave, A.S. Nowick, In Bonds and Bands in Semiconductors, Academic Press, New York, 1973.
[9]Thomas D.G., J.J. Hopfeld, C.J. Frosch, Phys. Rev. Lett. 15 (1965) 857
[10]Wolford D.J., J.A. Bradley, K. Fry, J. Thompson, in: J.D. Chadi, W.A. Harrison (Eds.), Physics of Semiconductors, Springer, New York, 1984, p. 627.
[11]Wei S.-H., A. Zunger, Phys. Rev. Lett. 76 (1996) 664.
[12]Wei S.-H., A. Zunger, J. Appl. Phys. 78 (1995) 3846

P42- Design and optimization of a 1.55 µm waveguide based on silicon planar photonic crystals

R. BCHIR[1], A. BARDAOUI[1], M. MACHHOUT[2], R. CHTOUROU[1] and H. EZZAOUIA[1]
[1]Laboratoire dePhotovoltaique, Semiconducteurs et Nanostructures, CRTEn, Route touristique Soliman BP 95 Hammam-Lif 2050 TUNISIA
[2]Laboratoire d'Electronique et Microelectronique, Faculté des Sciences de Monastir TUNISIA

riadh.bchir@crten.rnrt.tn
afrah.bardaoui@crten.rnrt.tn

Abstract-In this work, we focus on silicon based photonic crystals slabs (planar photonic crystals, PPC). Band structure calculations were performed using a block- iterative frequency-domain code to find the design parameters of both triangular and square photonic crystal slab lattices of air holes. We have varied the thickness of the Silicon slab and the pore radius in order to obtain optimum design parameters leading to a large and complete bandgap. The structure was optimized for the confinement of 1.55µm wavelength. Removing rows of holes forms a line defect in the triangular or in square PPC structure leading to the formation of a planar photonic crystal waveguide (PPCW). The frequency domain method for Maxwell's equations in a planewave basis was used to calculate the dispersion relations for the guided modes for several widths of the PPCWs.

Keywords: Planar Photonic Crystal (PPC), Band structure, Planar photonic crystal waveguide (PPCW), Guided modes.

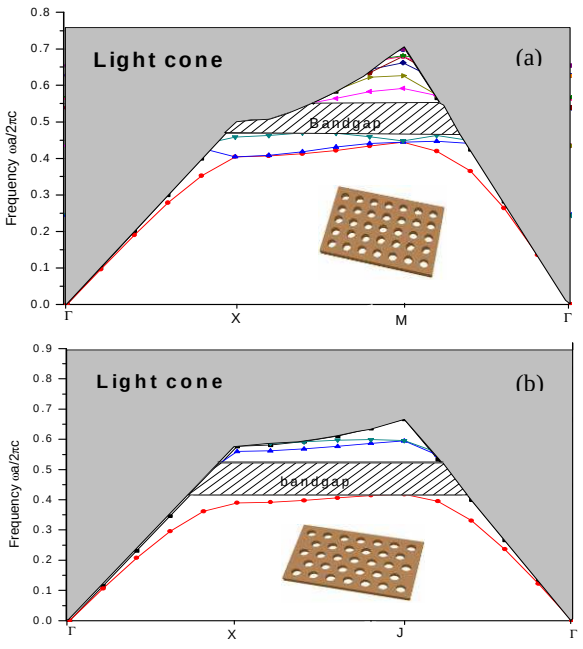

Figure1: Band diagrams for photonic crystal slabs (a) TM-like (odd) modes for a square lattice (b) TE-like (even) modes for a triangular lattice.

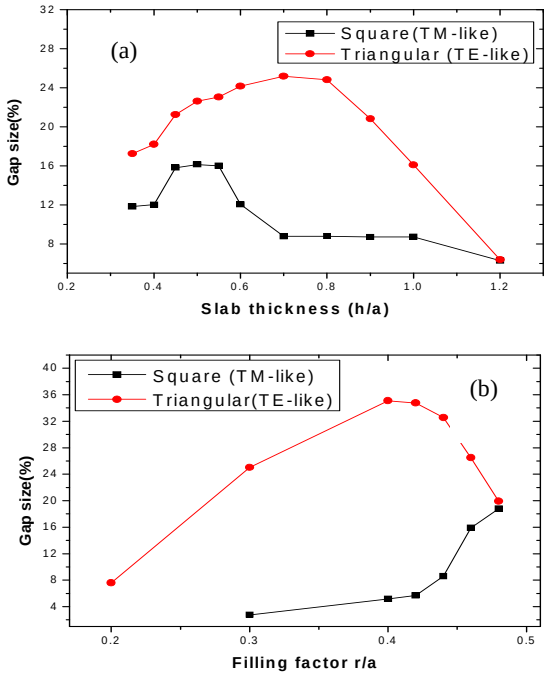

Figure2: Gap size versus (a) slab thickness (b) filling factor for both a square lattice and a triangular lattice.

References

[1]J.D.Joannopoulos, S.G. Johnson, J.N Winn and R.D Meade, "Photonic crystals molding the flow of light", Princeton University, 2008.

[2] C. Jamois, R.B. Wehrspohn, J. Schilling, F. Müller, R. Hillebrand and W. Hergert " Silicon-based photonic crystal slabs: two concepts" IEEE J. Quantum Electronics, vol. 38, NO. 7, JULY 2002.

[3]S.G. Johnson, S. Fan, P.R. Villeneuve and J.D. Joannopoulos "Guided modes in photonic crystal slabs" Phys. Rev. B, vol. 60, pp. 5751-5758, 1999.

[4] S. Kuchinsky, D.C. Allan, N.F. Borrelli, J.C Cotteverte « 3D localization in a channel waveguide in a photonic crystal with 2D periodicity" optics communications 175, 2000, pp 147-152.

[5]M. Loncar, J. Vuckovic and A. Scherer "Methods for controlling positions of guided modes of photonic-crystal waveguides" J. Opt. Soc. Am. B, Vol. 18, No. 9, September 2001.

P43- Stimulated emission in silicon's nonacristals

K. ISSA, M. HJIRI*, B. AZEZA, R M'GHAIETH and H.MAAREF

Lab. de Phys. des Semi-conducteurs et des Composants Electroniques (LA-MA-06) Faculté des Sciences de Monastir Route de l'environnement 5000, Monastir, Tunisie
* maha.hjiri@yahoo.fr

Time-resolved photoluminescence (TRPL) measurements are carried out for the porous silicon. We report the observation of optical gain or stimulated emission in porous silicon (Psi). The evidence of population inversion and amplified stimulated emission were found for Si nanocrystallites under pumping with 38ps light pulses at 380nm. These results suggest that silicon-NC-based waveguide amplifiers or silicon lasers are achievable. However, in order to obtain clear and reproducible evidence of stimulated emission, it is necessary to understand the physical mechanisms at work in the light emission process. In this paper, we report the evidence of optical gain in PSi and we discuss the effects of energy transfer mechanisms.

The photoluminescence spectra shows (figure 1) 3 pics at 510nm (2.34 eV), 580 nm (2.13eV) and at 710 nm (1.74eV). the first one shows the intraband transition in PSi ,the second, the fast transition, correspond to the spontaneous emission [1] and the third with a life time less than 1ns(figure 2) and shorter than its of spontaneous transition is attributed to the stimulated emission [2],[3]. This transition is not intrinsic because it is not a II type transition [4] as shows in figure1. So a local defaults in PSi could be at the origin of the apparition of this transition.

The evolution of PL intensity with the power pump shows that there is no shift at 710 nm.

The increases of the life time with power pump (respectively the electron number in the state where we have this transition) increase the auger effect. So we will have a competition between stimulated emission and the non-radiative Auger processes so the life time will be more and more important until a certain value where there is saturation.

The inversion of population at the origin of exists only if the value of power pump is more than a particular value.

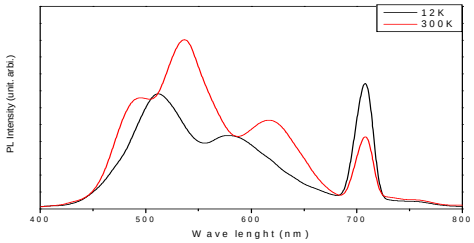

Figure 14: PL spectra of porous silicon at 300 and 12K.

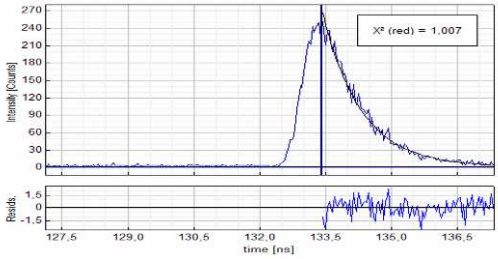

Figure 2: TRPL spectra of porous silicon at 720nm at 300K.

References:

[1] Auger Effect seen in the porous Silicon fast luminescent band.R.M'ghaieth et al. Physical Review B, Vol 60, No. 7, 99

[2] Dynamics of stimulated emission in silicon nanocrystals. L. Dal Negro et al. Applied Physics Letters Vol 82, No 26, 2003

[3]. Porous silicon formation: a quantum effect, Lehman V. et al. Applied Physics Letters, Vol 58, 856-858. 1991

[4] Stimulated emission from trap electronic states in oxide of nanocrystal Si.Wei-Qi Huang Applied Physics Letters 92, 2008

[5] Stimulated emission in plasma-enhanced chemical vapor deposited silicon nanocrystals L. Dal Negro et al. Physica E 16 (2003) 297 – 308

P44- Investigation of the electrical properties stability and metrological characteristics of ZnO/PS/c-Si photodiode (SiPZ) used as a transfer standard in the visible spectral range

O. Touayar[1], Z.Ben Achour[1], N.E.SIFI[1]
[1]Equipe de Recherché Métrologie des Rayonnements, Unité de recherche Matériaux, Mesures et Applications
[1]Institut National des Sciences Appliquées et de Technologies, INSAT, TUNISIA
Touayar.walid@planet.tn

Abstract: A PSiZ photodiode is realized in INSAT to be used as a National transfer standard for radiometric measurements. The porous silicon was used to trap the incident optical radiation and the ZnO layer is the transparent electrode[1] (see figure 1). With this detector we reach 10 mW as optical power measurements and around 7% as a reflectivity coefficient (see figure2)[2]. This photodiode was calibrated to the INM cryogenic radiometer (France) and provides a standard uncertainty of few 10^{-3} at the 1σ level[2]. With this detector we undertook a study over five years which involves the reflectivity, the serie and shunt resistance stability. The results confirm the PSiZ spectral response stability since the reflexion coefficient maximum difference is equal to 0,005 with an uncertainty of 0,002 (1σ). Moreover, the shunt and serie resistance are equal to 5,14 KΩ and 7,63 Ω respectively with 0,01 KΩ et 0,04 Ω as respective uncertainties. This photodiode does not display any ageing aspect. In consequence, we can use the PSiZ photodiode as a transfer standard.

Results : The optical and electrical studies over five years are done with a measurement sequence each six months. The optical study for different wave lengths confirm the stability of the photodiode spectral response since the reflexion coefficient maximum difference is equal to 0,005 with an experimental uncertainty of 0,002 (1σ) (see figure 2). The serie and shunt resistance are determined with a theoretical model using the I-V results in obscurity (see figure 3)[3,4]. The shunt and serie resistance are equal to 5,14 KΩ and 7,63 Ω respectively with 0,01 KΩ et 0,04 Ω as respective uncertainties.

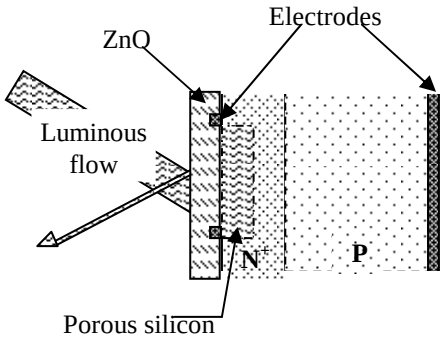

Fig. 1: The PSiZ photodiode structure.

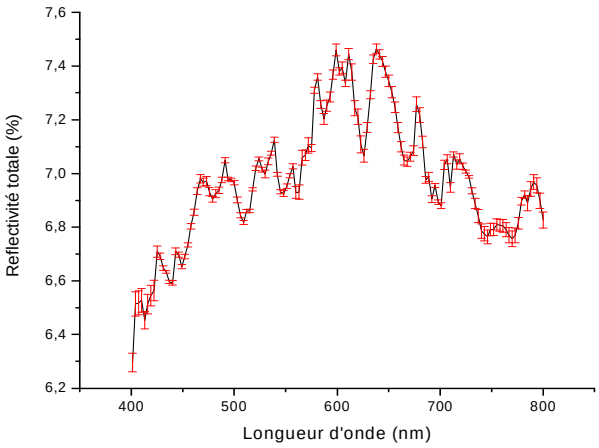

Fig. 2: PSiZ reflection coefficient Variation with the wave length

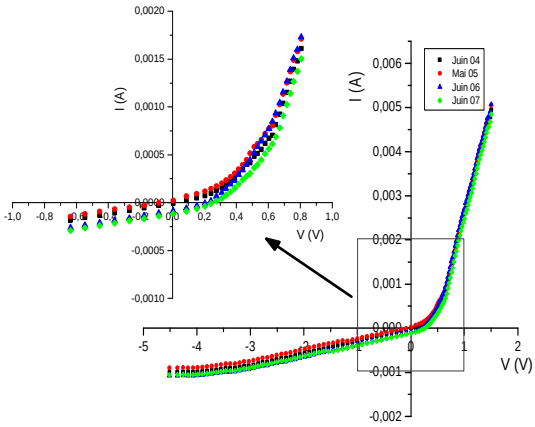

Fig. 3: The I-V response of the PSiZ photodiode in obscurity.

References: [1] Z. Ben Achour, T. Ktari, B. Ouertani, O. Touayar, B. Bessais, J. Ben Brahim, Sensors and Actuators A Physiczl, 134, 447-451, 2007.
[2] Z. Ben Achour, O. Touayar, E. Akkari, J. Bastie, B. Bessais, J. Ben Brahim, Nuclear Instruments and Methods in Physics Research A, 579, 1117-1121, 2007.
[3] Bazkir O, Samadov F, Optics and Lasers in Engineering, February 2005;43(2):131-141.
[4] Dieter K. Schroder, Semiconductor material and device characterization, Wiley-Interscience publication, USA, 1998.

P45- On-site monitoring of fish spoilage using vanadium pentoxide xerogel modified interdigitated gold electrodes

S. Helali[1], A. Abdelghani[1*], N.Jaffrezic-Renault[2], P.N. Trikalitis[3], C.E. Efstathiou[4], M.I. Prodromidis[5]

[1]Unité de Recherche de Physique des Semiconducteurs et Capteurs, IPEST, Tunisia.
[2] Laboratoire de Sciences Analytiques, Université de Claude Bernard, Lyon, France.
[3] Department of Chemistry, University of Crete, 71 003, Heraklion Crete, Greece
[4] Department of Chemistry, University of Athens, 157 71, Athens, Greece
[5] Department of Chemistry, University of Ioannina, 45 110, Ioannina, Greece

Abstract:
The development of a vanadium pentoxide xerogel (VXG)-based sensor for the detection of volatile inorganic (ammonia) and organic (dimethylamine etc.) amines is described. The xerogel film was deposited on interdigitated gold electrodes by dip-coating using an aqueous solution of VXG. The morphology of the sensing layer, its interaction with ammonia, which was used as a model analyte throughout this work, as well as the regeneration of the surface of the sensor electrodes with vapors of HCl were examined with scanning electron microscopy and FTIR spectroscopy. Signal changes, due to changes of the RC-values of the electrochemical cell (Au-VXG-Au), as a result of its interactions with ammonia vapors, were probed with a portable, homemade charge meter, the Multipulser. Finally, the proposed sensors were successfully used for on-site, real-time monitoring of fish spoilage in ambient conditions.

Introduction:
Microorganisms are the major cause of spoilage of most seafood products. However, only a few members of the microbial community, the specific spoilage organisms (SSOs), give rise to the offensive off-flavors associated with seafood spoilage. Volatile compounds such as $(CH_3)_3N$ (trimethylamine), $(CH_3)_2NH$ (dimethylamine) and NH_3 (ammonia), which are collectively known as TVB-N (Total Volatile Basic Nitrogen), are products of microbial degradation and are considered as a potential indicator of fish spoilage (index of freshness). The reference method for the determination of TVB-N, as adopted by the European community involves a rather laborious extraction - steam distillation and subsequent titration of the amines with hydrochloric acid., while other methods, which are based on instrumental approaches, such as flow injection analysis in combination with photometric detectors, and solid-phase microextraction in combination with NPD and FID chromatographic detectors have been also proposed. Although these methods provide satisfactory results and utilize instrumentation with a high degree of automation, the complexity, cost, and lengthiness of volatile analysis methods make them suitable only for specialized research and analytical laboratories. Here, we present the construction of ammonia gas sensors, which were fabricated by dip-coating of gold inderdigitated electrodes (IDEs) into aqueous solutions of vanadium pentoxide xerogel ($V_2O_5.xH_2O$, VXG). VXG is a highly reactive material (Figure.1a). The morphology of the sensing layer, its interaction with ammonia as well as the regeneration of the sensor with vapors of HCl were examined with scanning electron microscopy (Figure.1b) and FTIR spectroscopy.

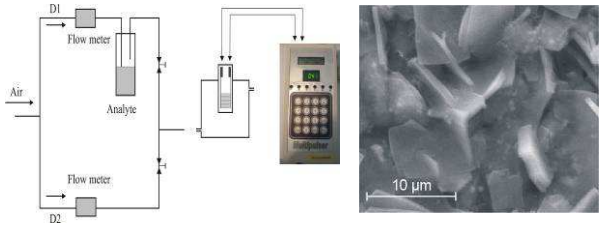

Figure 1: a) Set-up of ammonia vapor sensor.b) SEM image of the VXG films onto the IDE gold electrodes

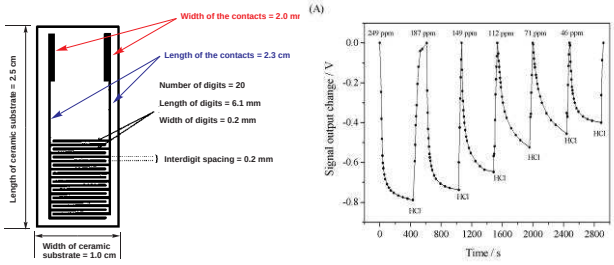

Figure2: a) Interdigitated microelectrodes. b) Signal output change of the sensor electrodes to different concentrations of ammonia;

Figure.2 shows the Multipulser signal output changes (initial signal outputs were taken as zero, and further signal changes were accordingly corrected) for different concentrations of ammonia versus time at room temperature.

Acknowledgements. This work was financially supported by a NATO Collaborative linkage grant (Contract Nr. CBP.MD.CLG.982802). Authors wish to thank Prof. L. Vonna (ICSI, Mulhouse, France) for SEM photo.

P46- Real-time scheduling for networks-on-chip using TDM virtual circuit and RTOS policies

Yahia Salah and Rached Tourki

Laboratory of Electronics and Microelectronics,
Faculty of Sciences, Monastir, 5000, TUNISIA
Yahia.Salah@fsm.rnu.tn

Abstract: In this paper, we proposed a centralized approach for messages scheduling in the Networks-on-Chip. We develop a NoC model which, together with a real-time scheduler model, called NoC_Sched, allows us to model the behavior of a complex system that has a real-time application running on a multi-processor platform. This scheduler utilize real-time scheduling algorithms using in the standards RTOS. As a result, it arrange communications paths, allocate a proper bandwidth and minimize resource usage, latency and overall time execution. In order to provide flexible and/or hard guarantee for the real-time embedded MPSoCs, we use a Time Division Multiplexing (TDM) Virtual Circuit. Each Network Interface (NI) includes a local scheduler, called NI_Sched, and a local slot table for storing an allocation of a time slot to a connection. Our on-chip communication model supports the management of different levels of quality of service (QoS). The proposed scheduling algorithms used in NoC_Sched module solve some problems within a router and network interface, and provide a global solution for the on-chip network.

Scheduling Approach: The scheduler profoundly affects the performance and the cost of the on-chip network. The optimal scheduling for the NoC is a complex problem and difficult to achieve. In this work, we try to find a feasible schedule for messages sent within time constraint between different NIs in a network. And the messages are injected in to the network periodically. A message stream (S_k) consists of several messages M_{ijk} flow from one task T_i to another task T_j: $S_k = \sum_{k=1}^{N} M_{ijk}$.

The scheduling design approach contains two essentials aspects: find a route for a message of the input S_k and find a scheduling methodology for the message M_{ijk}.

For routing, we employ the XY routing algorithm in the routing unit inside the router model and we use the breadth-first-search (BFS) algorithm to find all the minimum routes for the message, which starts from the source *src* and end to destination *dst* in a 2D-mesh network. Round robin arbitration is used in both Virtual Channel Allocation and Switch Allocation for Best Effort connections. The parameter of our generic router is fixed at 5 ports,each port with two virtual Channels, and the size of input buffer contains one 32-bit flit.

After we get a route, we should try to find a scheduling entity for each message M_{ijk} need to communicate and to turn a respence to each interface. Strategy used in NoC_Sched is always tries to schedule the earliest coming message with the shortest route and period. This strategy uses a shared memory with small size and explores a small part of the solution space. As a result, it has a small run-time.

Results: We have completed the NoC design approach in SystemC langage at the Transactional Level (TLM). Our NoC architecture are validated by a study of two real cases. These include a MPEG Decoder and a MP3 Decoder. For each benchmark, we manually mapped the tasks onto a 3x3 2D-mesh NoCs and used XY routing for the communication link routing. we have implemented the shared memory with size of 9 flits. The performance of the proposed scheduling algorithms are evaluated on both the overall execution time and the link utilization under different traffic patterns, namely random and uniform (Table 1 and Table 2). These traffic were generated by using different task mappings and injected in the network architecture to simulate the performance of the proposed approach.

Table 1 Results in Random Traffic

Application	***of msg jected in NoC***	***mprovement of verall execution time***	***provement of nk utilization***
MPEG Decoder	16	11.8%	7.8%
MP3 Decoder	12	19.7%	21.6%

Table 1 Results in Uniform Traffic

Application	***of msg jected in NoC***	***mprovement of verall execution time***	***provement of nk utilization***
MPEG Decoder	16	3.1%	5.5%
MP3 Decoder	12	11.4%	4.3%

Our proposed approach gives a quick solution and easy for implementation. The experimental results show that adding RTOS policies improves the performance considerably, but at the same time, makes the design complex. In the future work, we consider various issues of the NoC modeling.

P47- Influence of the heterojunction bipolar transistor's geometry on its microwave behaviour

A. Oudir[1], M. Mahdouani[1], R. Bourguiga[1], F. Pardo[2] and J.L. Pelouard[2]

[1] Laboratoire de Physique des Matériaux : Structures et Propriétés, Groupe physique des Composants et Dispositifs Nanométriques- Faculté des Sciences de Bizerte, 7021 Jarzouna-Bizerte, Tunisia.
amine.oudir@yahoo.fr
[2] Laboratoire de Photonique et Nanostructure-CNRS, Route de Nozay, 91190 Marcoussis, France

Abstract: The manufacturing technology of heterojunction bipolar transistors (HBT) was remarquably improved. This developpement has been illustrated by the fabrication of InP/GaAsSb/InP double heterojunction bipolar transistors (DHBT) with cutoff frequencies f_T and f_{Max} exceeding 300 GHz [1]. Better frequency performance has been obtained by using the InGaAlAs as emitter material instead of the InP. This optimization shows prospects for achieving frequency (f_T, f_{Max}) of (380 GHz, 420 GHz) [2].

In our previous studies, we have enabled highlight the low base transit time and the ballistic transport nature of carriers across the collector depletion layer for the InGaAlAs/GaAsSb/InP DHBT with strained base of 40 nm thickness [3]. Coupled with this structural optimization, a technological one has been made by reducing resistances and parasitic capacitances due to the geometry of the devices. The goals of our work are the comprehension of HBT microwave behavior for different geometries of the device, and the study of the influence of HBT dimensions on its frequency performance.

In this work, we have exploited the microwave measurements taken on the $InGa_{0.20}AlAs/GaAs_{0.38}Sb/InP$ DHBT of different sizes. The dimensions of the devices are determined by SEM measuring (figure 1).

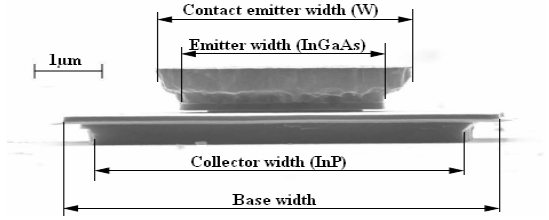

Figure 1: SEM view of $InGa_{0.20}AlAs/GaAs_{0.38}Sb/InP$ DHBT

In the first part of our work, we have modeled the physical structure of the device using a small signal equivalent circuit. First, we have determined the experimental Z-parameters by exploiting S-parameters measurements take on frequency range from 40 MHz to 50 GHz. Then, we have derived all equations of the T-topology small signal equivalent circuit with distributed base-collector capacitance and base resistance. Finally, we have extracted all the model parameters using an analytical extraction procedure that we have elaborated in [3] and applied to the InGaAlAs/GaAsSb/InP DHBT's of different sizes.

In the second part, we have established theoretical expressions of the transistor cutoff frequencies (f_T, f_{Max}). These expressions involve different geometry parameters of the transistor. These cutoff frequencies have been calculated and compared with experimental ones obtained from measurements of current gain and power gain, as shown in figure 2.

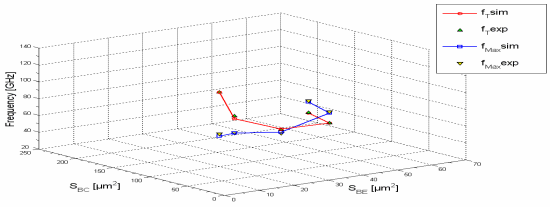

Figure 2: A 3D representation of the frequencies variation with transistor geometries

In this work, we have shown that the T-model and the extraction method are valid for different dimensions of the HBT. Moreover, we have demonstrated that the parameters affecting frequency performance are the area ratio of the base-collector and base-emitter junctions, and the ratio of the junction area and the perimeter. Finally, in order to optimize the performances of TBH, these ratios should be minimized.

References : Dvorak, M. W. Bolognesi, C. R. Pitts, O. J and Watkins, S.P. (2001) 300 GHz InP/GaAsSb/InP Double HBTs with High Current Capability and $BV_{CEO} \geq 6$ V, *IEEE Electron Device Lett.*, 22, 361-363.

Lijadi, M. (2005) Transistors bipolaires à hétérojonction : développement d'une filière InP/GaAsSb pour les applications ultrarapides, http://tel.archives.ouvertes.fr/tel-00010627/fr/

Oudir, A. Mounira, M. Bourguiga, R. Pardo F. and Pelouard J.L. (2009) Small signal modeling of Emitter-up HBT using an improved analytical approach. Application to InGaAlAs/GaAsSb/InP DHBT with strained Base. Accepted to be published in *Solid State Electronics.*

Impressum

Proceedings of 1st Humboldt Kolleg, Gammarth, Tunisia

Organizers: **Alexander von Humboldt-Stiftung, Germany**
INSAT , Centre Urbain Nord, Tunisia

Print: 80 Exemplars

Picture credits :

http://ahmadladhani.files.wordpress.com/2009/07/molecular_transistor.jpg

http://www.sciencedaily.com/images/2009/04/090430144714-large.jpg

Acknowledgement

The organizing committe gratefully thanks all sponsors of this conference, especially « The Alexander von Humboldt-Stiftung, Bonn, Germany (www.avh.de) ».

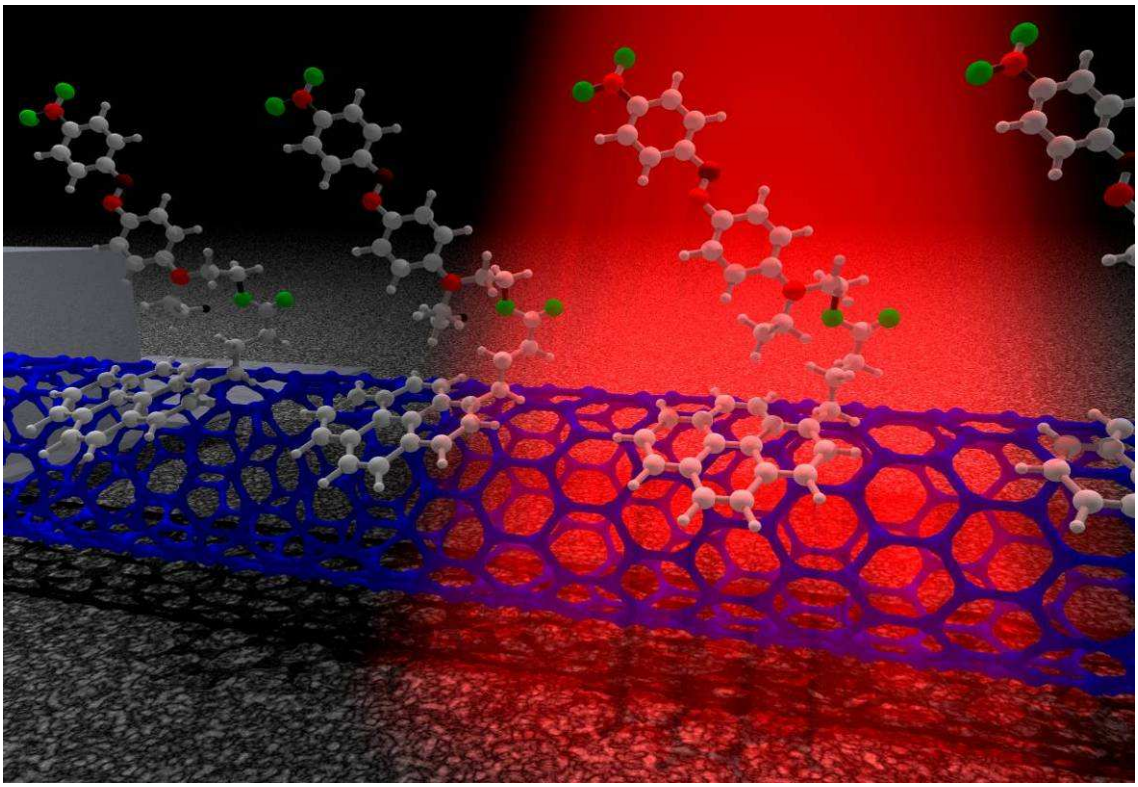

The Ministry of Higher Education and Scientific Research as well as the University of 7th November at Carthage, the National Institute of Applied Science and Technology, is acknowledged for supporting the first Humboldt Kolleg in Tunisia